

# Unveiling the origin of X-ray flares in Gamma-Ray Bursts

G. Chincarini<sup>1,11\*</sup>, J. Mao<sup>1,2,3</sup>, R. Margutti<sup>1,11</sup>, M.G. Bernardini<sup>1,4</sup>, C. Guidorzi<sup>5</sup>, F. Pasotti<sup>1</sup>, D. Giannios<sup>6</sup>, M. Della Valle<sup>7,4</sup>, A. Moretti<sup>1</sup>, P. Romano<sup>8</sup>, P. D’Avanzo<sup>1</sup>, G. Cusumano<sup>8</sup> and P. Giommi<sup>9,10</sup>

<sup>1</sup>INAF - Osservatorio Astronomico di Brera, via Bianchi 46, I-23807 Merate (LC), Italy

<sup>2</sup>Yunnan Observatory, Chinese Academy of Sciences, Kunming, Yunnan Province, 650011, China

<sup>3</sup>Key Laboratory for the Structure and Evolution of Celestial Objects, Chinese Academy of Sciences, Kunming, Yunnan Province, 650011, China

<sup>4</sup>ICRANet, p.le della Repubblica 10, I-65100 Pescara, Italy

<sup>5</sup>University of Ferrara, Physics Dept., via Saragat 1, I-44122 Ferrara, Italy

<sup>6</sup>Department of Astrophysical Sciences, Peyton Hall, Princeton University, Princeton, NJ 08544, USA

<sup>7</sup>INAF - Osservatorio di Capodimonte, Salita Moiariello 16, I-80131 Napoli, Italy

<sup>8</sup>INAF - Istituto di Astrofisica Spaziale e Fisica Cosmica, Via La Malfa 153, I-90146 Palermo, Italy

<sup>9</sup>ASI Science Data Center (ASDC), via G. Galilei, I-00044 Frascati (RM), Italy

<sup>10</sup>ASI - Unità Osservazione dell’Universo, viale Liegi 26, I-00198 Roma, Italy

<sup>11</sup>University of Milano Bicocca, Physics Dept., P.zza della Scienza 3, Milano 20126, Italy

Accepted 2010 Month day. Received 2010 Month day; in original form 2010 Month day

## ABSTRACT

We present an updated catalog of 113 X-ray flares detected by *Swift* in the  $\sim 33\%$  of the X-ray afterglows of Gamma-Ray Bursts (GRB). 43 flares have a measured redshift. For the first time the analysis is performed in 4 different X-ray energy bands, allowing us to constrain the evolution of the flare temporal properties with energy. We find that flares are narrower at higher energies: their width follows a power-law relation  $w \propto E^{-0.5}$  reminiscent of the prompt emission. Flares are asymmetric structures, with a decay time which is twice the rise time on average. Both time scales linearly evolve with time, giving rise to a constant rise-to-decay ratio: this implies that both time scales are stretched by the same factor. As a consequence, the flare width *linearly* evolves with time to larger values: this is a key point that clearly distinguishes the flare from the GRB prompt emission. The flare 0.3–10 keV peak luminosity decreases with time, following a power-law behaviour with large scatter:  $L_{pk} \propto t_{pk}^{-2.7 \pm 0.5}$ . When multiple flares are present, a global softening trend is established: each flare is on average softer than the previous one. The 0.3 – 10 keV isotropic energy distribution is a log-normal peaked at  $10^{51}$  erg, with a possible excess at low energies. The flare average spectral energy distribution (SED) is found to be a power-law with spectral energy index  $\beta \sim 1.1$ . These results confirmed that the flares are tightly linked to the prompt emission. However, after considering various models we conclude that no model is currently able to account for the entire set of observations.

**Key words:** gamma-ray: bursts – radiation mechanism: non-thermal – X-rays

## 1 INTRODUCTION

Gamma Ray Bursts (GRB) are short flashes of gamma-rays that during their early lifetime outshine any other source of gamma rays in the sky. The first event was detected in 1967 and announced in 1973 (Klebesadel et al. 1973). Since then and after about 40 years of research our knowledge has increased significantly mainly thanks to three high-energy mis-

sions, *Compton Gamma-Ray Observatory* (CGRO), *Beppo-SAX* and *Swift* that, together with related theoretical works, marked fundamental milestones in our knowledge of this phenomenon. These observations characterized the main features of these events.

The timescale of the prompt emission lasts from a few milliseconds (Vedrenne 1981) to thousands of seconds (Hurley et al. 2002). The distribution of its duration has been shown to be bimodal (Mazets et al. 1981; Norris et al. 1984; Hurley 1989; Dezalay et al. 1992; Kouveliotou et al.

\* E-mail: guido.chincarini@brera.inaf.it

1993), therefore GRBs can be classified as “short” and “long”. The time profile of the prompt emission may present either multiple spikes of very short duration or relatively broad peaks with no fast variability (Norris et al. 2005). After the discovery of the isotropic distribution of the BATSE GRBs on the sky (Meegan et al. 1992; Fishman et al. 1994; Briggs et al. 1996; Paciesas et al. 1999) and the detection of the afterglow of GRB970228 (Costa et al. 1997; Groot et al. 1997; van Paradijs et al. 1997; Paciesas et al. 1999; Djorgovski et al. 2001) it was clearly demonstrated that at least long GRBs were extragalactic and involved the emission of huge amounts of energy in a short time. After the launch of *Swift* (Gehrels et al. 2004) it was firmly established that short GRBs also have an extragalactic origin (Gehrels et al. 2005; Butler et al. 2005; Villasenor et al. 2005; Barthelmy et al. 2005b) and therefore these bursts involve the emission of a rather large amount of energy as well.

The X-Ray Telescope (XRT Burrows et al. 2005a) on board the *Swift* satellite allows the early and well sampled observations of the afterglow. The temporal behaviour of the observed light curve was completely unexpected since, according to the data gathered by *Beppo-SAX* (the record pointing of this satellite after detection was however of about 4 hours), the expectation was for a flux decaying smoothly as a power-law,  $F \sim t^{-1.5}$ . It was realized rather soon by the *Swift* team that the light curve of many GRBs was characterized by a more complex temporal behaviour (Nousek et al. 2006; O’Brien et al. 2006; Zhang et al. 2006): a steep early decay, a “plateau” and a late decay where the slope observed by *Beppo-SAX* is essentially recovered. These phases can be either all or in part present (Evans et al. 2009). The significant achievements have been accompanied by substantial theoretical effort to interpret the data. The internal - external shock model (Meszaros & Rees 1993; Rees & Meszaros 1992, 1994, see also Piran 1999, 2004 and references therein) within the fireball scenario (Cavollo & Rees 1978) explains many of the characteristics of the observed light curve and spectrum of GRBs (see e.g. Zhang et al. 2006 and reference therein; for a critical review of this model and possible alternatives see Lyutikov 2009).

Indeed one of the most intriguing discoveries of the *Swift*/XRT was the existence of flares in many of the observed GRB afterglows, that released a large emission of energy at later times than the prompt emission (Burrows et al. 2005b; Falcone et al. 2006; Chincarini et al. 2007; Falcone et al. 2007). The first detection of flares with the *Swift*/XRT occurred in X-Ray Flash (XRF) 050406 (Burrows et al. 2005b; Romano et al. 2006b) and GRB050502B (Burrows et al. 2005b; Falcone et al. 2006). In the first case the afterglow light curve exhibits a re-brightening of a factor of 6 that decayed quickly to recover the previous temporal behaviour. The flare in GRB050502B was spectacular with a re-brightening of the light curve of a factor 500; its fluence is comparable to the one of the prompt emission observed by the Burst Alert Telescope (BAT Barthelmy et al. 2005a) on board the *Swift* satellite. Further observations confirmed that flares are quite common events in the light curves of GRBs ( $\sim 33\%$  of GRB afterglows exhibit flares). The energetics involved as well as their spectral properties, in particular the hard-to-soft evolution,

are strong indications that X-ray flares have a common origin with the gamma-ray pulses. Furthermore, the presence of an underlying continuum with the same slope before and after the flaring activity excludes the possibility that flares are related to the afterglow emission by forward external shocks. Therefore their properties can provide an important clue toward the understanding of the mechanism that is at the basis of the GRB phenomenon.

Previous analysis was performed by Chincarini et al. (2007, hereafter Paper I) and Falcone et al. (2007, hereafter Paper II). These authors concluded that:

- (i) flares occur in all kind of GRBs: short and long, high energy peaked GRBs and X-ray flashes;
- (ii) the flare intensity decreases with time and the flare duration increases with time;
- (iii) a sizable fraction of flares cannot be related to the external shock mechanism;
- (iv) the temporal behaviour of flares is very similar to the one of prompt emission pulses;
- (v) the number of flares of a single event does not correlate with the number of detected prompt pulses;
- (vi) the energy emitted during a bright flare is very large and in some cases is of the order of the prompt emission observed by BAT. Their average fluence, however, is about 10% of the prompt emission fluence measured by BAT;
- (vii) the peak energy is typically in the soft X-rays,  $\leq 1$  keV;
- (viii) the hardness ratio evolves following closely the evolution of the flare luminosity with a hardening during the rise and a softening during the decay;
- (ix) a long lasting activity by the central engine is advocated.

In the present work we expand the statistics of Paper I considering a wider sample of X-ray flares. Moreover, for the first time, we constrain the evolution of the properties of the flares in different X-ray energy bands inside the 0.3 – 10 keV bandpass of the XRT. Finally, the flares are fitted with the function proposed in Norris et al. (2005): this allows us to study the asymmetry of the flare temporal profiles, to assess the rise time and the decay time evolution with time.

The paper is organized as follows. In Sec. 2 we describe the data reduction procedure and in Sec. 3 the flare sample and the fitting procedure. In Sec. 4 we describe the analysis of the temporal behaviour of flares (Sec. 4.1) and their energetic and spectral properties (Sec. 4.2). In Sec. 5 we discuss the main results of our analysis. Then conclusions follow.

Throughout the paper we follow the convention  $f_\nu(t) \propto \nu^{-\beta} t^{-\alpha}$ , where the energy spectral index  $\beta$  is related to the photon index  $\Gamma = \beta + 1$ . We have adopted the standard values of the cosmological parameters:  $H_0 = 70 \text{ km s}^{-1} \text{ Mpc}^{-1}$ ,  $\Omega_M = 0.27$  and  $\Omega_\Lambda = 0.73$ . Errors are given at  $1\sigma$  confidence level unless otherwise stated.

## 2 DATA REDUCTION

XRT data were processed with the latest version of the HEASOFT package available at the time of the discovery of the GRB explosion and corresponding calibration files: standard filtering and screening criteria were applied. In particular we used grades 0 – 2 and 0 – 12 in windowed timing (WT)

and photon counting (PC) modes, respectively. *Swift*/XRT (Burrows et al. 2005a) is designed to acquire data using different observing modes depending on source count rates to minimize the presence of pile-up (Hill et al. 2004): the first orbit contains Windowed Timing (WT) data if the source is brighter than a few counts  $s^{-1}$ , while for lower count rates the spacecraft automatically switches to the Photon Counting (PC) mode to follow the fading of the source. Generally, WT data are extracted in a  $20 \times 40$  pixel region centered at the afterglow position along the WT strip of data. For count-rates above  $\sim 150$  count  $s^{-1}$ , we expect the source to be affected by pile-up (Romano et al. 2006a): in this case the central part of the rectangular region is excluded from the analysis. The size of the exclusion region is determined from the study of the distortion of the grade 0 distribution. The study of the distortion of the mean energy associated to each photon gives consistent results. WT background data are extracted within a rectangular box which is manually chosen to be far from serendipitous background sources.

For PC observations, events are selected within four different regions: first, PC data are extracted from a circular region centered at the enhanced position provided by the XRT team. In most cases a radius of 20 pixel (1 pixel  $\sim 2.36''$ ) is used. The radius is chosen so as to contain  $\sim 90\%$  of the total flux as determined by the XRTMKARF tool. Exceptions are however present: bright (faint) sources require radii greater (smaller) than the standard 20 pixel value; at the same time, also for bright sources, a region of event extraction smaller than usual is sometimes necessary to avoid contamination from serendipitous background sources. When the PC data suffered from pile-up, we extracted the source events in an annulus whose inner radius is derived comparing the observed to the nominal Point Spread Function (PSF, Vaughan et al. 2006). The original radial distribution of radiation -and the total source flux- is then recovered using the accurate information of the instrumental PSF provided by Moretti et al. (2005). When the count-rate of the fading afterglow is lower than 0.01 count  $s^{-1}$ , the source events were extracted from a smaller region to assure a high signal-to-noise (SN) ratio. This required the introduction of a third PC extraction region: a circle with a typical 10 pixel radius. Finally, the PC background level was assessed extracting the events from an annular region centered as close as possible to the GRB location and with an inner radius greater than  $3/2$  the radius of the source region. When this was not possible, background data were selected within a circular region with size as big as possible. In both cases the background region is chosen in a source-free portion of the soft X-ray sky. This was accomplished by reading the PC cleaned event list file with the XIMAGE package and localizing any source in the field with a minimum SN equal to 2.

The background subtracted, PSF and vignetting corrected light-curves were then re-binned so as to assure a minimum SN equals to 4 for WT and PC mode data. When single-orbit data were not able to fulfill the signal-to-noise requirement, data coming from different orbits are merged to build a unique data point. Further details can be found in Margutti et al. (in prep.).

This procedure was applied 5 times to produce a  $0.3-10$  keV count-rate light curve (“tot”) together with four count-rate light curves of the same event in 4 different sub-energy bands. In particular we have: “fvs”: light curve containing

photons filtered in the observed energy interval  $0.3-1$  keV; “fms”: light curve containing photons filtered in the observed energy interval  $1-2$  keV; “fmh”: light curve containing photons filtered in the observed energy interval  $2-3$  keV; “fvh”: light curve containing photons filtered in the observed energy interval  $3-10$  keV. This assures the valuable possibility to investigate the variations of the flare temporal properties as a function of the energy of the emitted photons.

### 3 SAMPLE SELECTION AND FITTING PROCEDURE

We considered all the *Swift* GRBs observed between April 2005 and March 2008. During this period the GRBs detected were 332 (109 with redshift  $z$ ): 284 by *Swift* (104 with  $z$ ), 26 by INTEGRAL (1 with  $z$ ), 10 by IPN (1 with  $z$ ), 9 by HETE (3 with  $z$ ), and 3 by AGILE. Observations of GRB afterglows by *Swift*/XRT have been carried out in 234 cases<sup>1</sup>.

In order to have a sample as homogeneous as possible, we selected flares from all the X-ray afterglows observed by XRT with the following criteria:

- (i) the flare contains a relatively complete structure: rise, peak and decay phase;
- (ii) the flare structure can be fitted with an analytic function, thus giving a homogeneous set of parameters;
- (iii) the flare is clearly distinguishable from the underlying continuum. Small fluctuations have not been identified as flares;
- (iv) blended flares, which have more complicated structures, are included in the present statistical sample only if the various pulses are easily identified;
- (v) the flares are “early”, i.e. peak time  $< 1000$  s.

The present data set consists of 56 GRBs that have bright (i.e. peak count rate  $> 1$  count  $s^{-1}$ ) X-ray flares. Two of them, GRB051210 and GRB070724A, are short GRBs. 27 GRBs present a single flare, 15 two flares and in 14 cases we have more than two flares. The total number of flares is 113, each one analysed in the XRT energy bandpass ( $0.3-10$  keV) and, when the count-rate was high enough to properly fit the profile of the emission (30 flares), also in sub-energy bands ( $0.3-1$  keV,  $1-2$  keV,  $2-3$  keV,  $3-10$  keV) in order to detect any chromatic difference. 21 GRBs of the present sample have also redshift measurements (43 flares): this subsample has been used to investigate the flare properties in the source rest frame.

Some giant flares, such the ones detected in GRB060510B, GRB070129 and GRB070616, are not included: the initial flare in GRB060510B could be the prompt emission observed in X-rays, and the underlying continuum is hard to define; flares in GRB071029 are strongly overlapping; the flare in GRB070616 contains some fluctuations which are difficult to distinguish.

The choice of limiting the present sample only to early flares is motivated by the aim of making a direct comparison with the prompt emission pulses. Therefore, the early flares, with higher SN ratio and temporal resolution, are more suitable for this purpose. A detailed analysis of late flares and a

<sup>1</sup> For the numbers of observed GRBs provided we refer to <http://www.mpe.mpg.de/~jcg/grbgen.html>

comparison with this sample will be presented in Bernardini et al. (in prep.).

### 3.1 Fitting procedure

The flares detected by XRT generally present a rather smooth profile and only in very few cases it is possible to detect substructure indicating rapid variability, although to a rather low statistical level. Previous attempts to detect variability over very small time scales have been inconclusive. This subject, beyond the scope of the present work, will be discussed in Margutti et al. (in prep.).

To derive information about the properties of the flares, and eventually their relation to the shock physical parameters, two approaches are viable: a) to develop a model based on the assumed physical mechanism or b) to choose an empirical analytical function to fit the observed light curve and to estimate the parameters characterizing its shape. In this second case the comparison with models prescriptions can be carried out later. We choose this second empirical approach since it allows to obtain more general results that should then help in discriminating among different models and to avoid biases.

In Paper I we used a Gaussian and broken power-law functions for the combined fit flare plus underlying continuum to derive widths and peak intensities. For the rise and decaying times and slopes we used an exponential and, for a few cases, we tested the function introduced in Kobayashi et al. (1997).

In this work we derive the flare parameters using the function proposed by Norris et al. (2005, Norris05), after testing various empirical or semi-empirical profiles. The function used in Norris et al. (2005) consists of two combined exponentials defined by 5 parameters that is not differentiable at the peak time. Nevertheless it is quite flexible to reproduce a wide range of pulse shapes and width. Kobayashi et al. (1997) (but see also Daigne & Mochkovitch 1998) proposed a semi-empirical profile that would account for the variability produced by internal shocks among relativistic shells having an ad hoc distribution of the Lorentz factor. Although such an issue is beyond the scope of the present work, the function proposed is quite satisfactory. This profile is not differentiable at the peak intensity as well, since it is the sum of two functions that are used to fit the rising and decaying part separately. Kocevski et al. (2003) proposed a FRED profile using an analytic function derived from physical first principles and accounting for the spectral evolution. The derived function describes the pulses by 4 parameters and the peak time can be calculated from them. The profile is completely satisfactory and leads to clear statistical results for single pulses, as it will be discussed later on. On the other hand, when compared to the Norris05 profile it appears to be slightly more complicated and the derivation of the parameters of interest less forthcoming. For all these reasons we choose the Norris05 profile.

The Norris05 function is the inverse of the product of two exponentials and is fully determined by 4 parameters:

$$\text{Norris05}(t) = A \lambda e^{-\frac{\tau_1}{(t-t_s)} - \frac{(t-t_s)}{\tau_2}} \quad \text{for } t > t_s \quad (1)$$

where  $\mu = (\tau_1/\tau_2)^{1/2}$  and  $\lambda = e^{2\mu}$ . The intensity is at max-

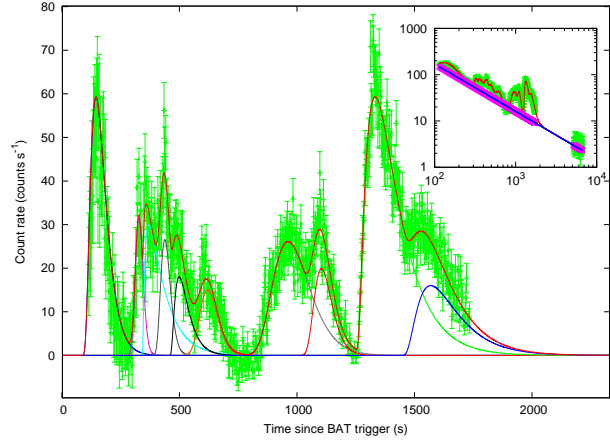


**Figure 1.** The best-fitting of the flares of GRB051117A with 11 Norris05 function (colored lines) is shown after the subtraction of the underlying continuum. *Inset:* Simultaneous fit of the same flares (red solid line) and of the underlying continuum (blue solid line). The errors on the estimate of the underlying continuum are properly accounted for (pink error bars).

imum at  $t_{pk} = \tau_{pk} + t_s = (\tau_1 \tau_2)^{1/2} + t_s$ . The pulse width is measured between the two  $1/e$  intensity points,

$$w = \Delta t_{1/e} = t_{\text{decay}} + t_{\text{rise}} = \tau_2 (1 + 4\mu)^{1/2}. \quad (2)$$

The pulse asymmetry is

$$k = \frac{t_{\text{decay}} - t_{\text{rise}}}{t_{\text{decay}} + t_{\text{rise}}} = (1 + 4\mu)^{-1/2}. \quad (3)$$

$t_{\text{decay}}$  and  $t_{\text{rise}}$  are expressed in terms of  $w$  and  $k$  as:

$$t_{\text{decay},\text{rise}} = \frac{1}{2} w (1 \pm k). \quad (4)$$

For a full description of the Norris05 function and parameters we refer to Norris et al. (2005). The results of the fitting procedure are listed in Tables 1 and 2. The errors on the derived quantities are obtained accounting for the entire covariance matrix of the fitting parameters. The flare fluence  $S$  is calculated integrating the corresponding Norris05 function over the interval between  $t_{1,90}$  and  $t_{2,90}$ , and then converted into physical units by applying a conversion factor computed by extracting the spectrum around the peak time with a minimum of 2000 photons. The spectrum has been fit using an absorbed simple power-law model within XSPEC.

We fitted simultaneously the underlying continuum and the flares by adopting a multiply broken power-law plus a number of Norris05 functions (the best-fitting of the flares of GRB051117A is shown in Fig. 1 as an example). As a measure of the quality of the fit we used the  $\chi^2$  statistics. Quite often, and especially for the 0.3 – 1 keV and 3 – 10 keV bandpasses, the fits were not satisfactory due to the low count-rate and SN ratio. However the fit could be mildly constrained by the solution of the parameters we had when fitting the whole XRT band (0.3 – 10 keV).

**Table 1.** Table of the best-fitting parameters and of the derived physical quantities. From left to right: name of the GRB, bandpass (see Sec. 2), redshift  $z$ , parameters describing the Norris05 function ( $A$ ,  $t_s$ ,  $\tau_1$ ,  $\tau_2$ ), peak time  $t_{pk}$ , width  $w$ , asymmetry  $k$ , rise time  $t_{rise}$ , decay time  $t_{decay}$ , fluence of the flare  $S$ .

GRB	band	$z$	$A$ count s $^{-1}$	$t_s$ s	$\tau_1$ s	$\tau_2$ s	$t_{pk}$ s	$w$ s	$k$	$t_{rise}$ s	$t_{decay}$ s	$S$ 10 $^{-8}$ erg cm $^{-2}$
050406	tot	-	4.6 ± 0.4	107.0 ± 90.8	903.5 ± 2404.0	11.7 ± 9.6	209.6 ± 4.0	70.1 ± 7.1	0.2 ± 0.1	29.2 ± 6.4	40.9 ± 5.5	0.9 ± 0.6
050406	fvs	-	2.7 ± 0.5	160.0 ± 59.4	429.2 ± 1341.0	8.0 ± 7.3	216.0 ± 59.4	44.0 ± 7.6	0.2 ± 0.2	18.0 ± 5.2	26.0 ± 5.7	0.2 ± 0.2
050406	fms	-	1.5 ± 0.3	169.2 ± 15.8	36.6 ± 71.0	22.6 ± 12.1	197.8 ± 6.5	55.6 ± 10.5	0.4 ± 0.2	16.5 ± 6.8	39.1 ± 9.1	0.3 ± 0.0
050406	fmh	-	-	-	-	-	-	-	-	-	-	0.0 ± 0.0
050406	fvh	-	0.7 ± 4.8	180.5 ± 27.9	0.4 ± 38.0	40.0 ± 97.4	184.3 ± 166.1	47.1 ± 25.3	0.8 ± 6.2	3.5 ± 164.3	43.6 ± 99.3	0.1 ± 0.6
050502B	tot1	-	14.6 ± 3.7	350.8 ± 39.4	656.5 ± 381.5	141.6 ± 27.0	655.7 ± 101.2	438.9 ± 86.6	0.3 ± 0.0	148.7 ± 34.3	290.2 ± 54.2	24.0 ± 7.7
050502B	tot2	-	64.2 ± 4.1	436.7 ± 26.4	1147.1 ± 397.9	53.1 ± 7.3	683.4 ± 53.1	234.9 ± 31.4	0.2 ± 0.0	90.9 ± 13.0	144.0 ± 18.7	57.0 ± 8.7
050502B	tot3	-	39.2 ± 2.8	647.4 ± 37.4	642.8 ± 611.4	21.7 ± 6.6	765.5 ± 69.4	103.5 ± 33.6	0.2 ± 0.1	40.9 ± 14.6	62.6 ± 19.3	15.0 ± 4.5
050502B	fmv1	-	4.5 ± 1.5	266.9 ± 86.5	1353.1 ± 1031.0	143.4 ± 37.5	707.4 ± 197.4	522.7 ± 139.6	0.3 ± 0.1	189.7 ± 57.1	333.0 ± 84.8	9.9 ± 4.2
050502B	fmv2	-	24.0 ± 1.8	160.0 ± 10.0	160.0 ± 190.4	60.1 ± 5.5	690.2 ± 77.4	253.0 ± 66.4	0.3 ± 0.0	96.4 ± 18.0	158.4 ± 28.0	27.0 ± 5.4
050502B	fmv3	-	18.4 ± 1.5	604.8 ± 98.0	150.0 ± 247.0	19.4 ± 10.2	780.0 ± 182.2	114.8 ± 62.2	0.3 ± 0.1	49.0 ± 14.2	69.2 ± 17.4	7.5 ± 3.5
050502B	fmv4	-	4.5 ± 1.3	425.2 ± 22.6	168.5 ± 128.9	181.0 ± 39.8	595.8 ± 73.1	398.0 ± 92.9	0.5 ± 0.1	109.0 ± 33.9	280.0 ± 62.9	3.4 ± 1.2
050502B	fms1	-	28.6 ± 1.5	448.1 ± 28.3	1061.0 ± 396.9	49.2 ± 6.6	676.6 ± 53.5	217.7 ± 29.5	0.2 ± 0.0	84.2 ± 12.5	133.5 ± 17.4	12.0 ± 1.8
050502B	fms2	-	19.7 ± 1.7	705.2 ± 111.8	75.3 ± 60.2	32.3 ± 8.2	754.5 ± 23.3	86.1 ± 22.7	0.4 ± 0.1	26.9 ± 8.7	59.2 ± 14.7	3.3 ± 0.9
050502B	fmh1	-	2.1 ± 1.1	298.6 ± 184.8	866.7 ± 1888.0	152.2 ± 133.2	661.7 ± 464.6	494.2 ± 43.9	0.3 ± 0.2	171.0 ± 158.1	323.2 ± 263.7	3.5 ± 3.1
050502B	fmh2	-	5.1 ± 1.2	471.1 ± 35.5	338.5 ± 241.1	187.3 ± 24.5	186.3 ± 138.1	0.2 ± 0.1	77.7 ± 58.1	111.5 ± 80.1	3.7 ± 2.4	
050502B	fmh3	-	4.7 ± 1.2	595.0 ± 22.4	220.4 ± 40.0	112.5 ± 14.5	323.2 ± 32.3	84.5 ± 123.1	0.1 ± 0.1	47.8 ± 15.8	77.7 ± 15.8	1.3 ± 1.4
050502B	fvh1	-	2.8 ± 2.1	277.4 ± 324.3	1671.6 ± 5039.0	92.0 ± 103.7	671.4 ± 711.5	303.6 ± 437.3	0.2 ± 0.2	150.4 ± 181.8	343.2 ± 266.0	10.0 ± 11.0
050502B	fvh2	-	4.6 ± 2.4	458.7 ± 229.6	1124.5 ± 4945.0	34.5 ± 84.4	656.5 ± 547.2	169.5 ± 360.1	0.2 ± 0.2	67.4 ± 144.9	102.2 ± 217.7	7.0 ± 12.0
050502B	fvh3	-	5.3 ± 3.1	544.4 ± 252.4	2528.7 ± 9229.0	161.4 ± 19.4	745.9 ± 462.3	114.9 ± 146.6	0.1 ± 0.1	49.4 ± 66.8	65.5 ± 80.5	5.3 ± 5.9
050607	tot	-	13.5 ± 1.5	265.3 ± 17.4	43.1 ± 50.5	44.7 ± 8.8	309.2 ± 5.7	99.2 ± 12.0	0.5 ± 0.1	27.3 ± 8.7	71.9 ± 6.0	8.3 ± 2.5
050607	fvs	-	2.9 ± 0.4	261.0 ± 26.6	78.2 ± 104.5	50.0 ± 14.0	323.5 ± 9.2	122.6 ± 15.9	0.4 ± 0.1	36.3 ± 11.6	86.3 ± 9.5	5.8 ± 2.2
050607	fms	-	5.7 ± 0.6	249.2 ± 10.6	93.1 ± 68.5	38.1 ± 8.6	308.8 ± 6.3	102.6 ± 7.9	0.4 ± 0.1	32.3 ± 4.4	70.4 ± 7.1	1.7 ± 0.5
050607	fmh	-	3.0 ± 0.6	270.4 ± 12.3	121.2 ± 21.9	58.1 ± 9.6	96.6 ± 18.6	0.6 ± 0.2	19.9 ± 10.9	76.7 ± 15.1	0.5 ± 0.2	
050607	fvh	-	2.4 ± 0.3	240.0 ± 14.5	112.5 ± 94.4	37.8 ± 9.1	314.8 ± 7.8	106.3 ± 1.1	0.4 ± 0.1	54.2 ± 5.5	72.0 ± 5.5	2.0 ± 0.7
050713A	tot1	-	181.5 ± 7.0	98.3 ± 1.1	17.9 ± 0.7	8.8 ± 0.8	110.9 ± 1.7	22.8 ± 1.7	0.4 ± 0.1	7.0 ± 0.8	15.8 ± 0.8	31.0 ± 20.0
050713A	tot2	-	25.6 ± 2.5	151.1 ± 5.6	31.0 ± 31.3	11.0 ± 3.0	169.7 ± 7.9	30.6 ± 6.9	0.4 ± 0.1	9.8 ± 3.4	20.8 ± 3.4	5.8 ± 4.1
050713A	fvs1	-	16.4 ± 1.5	90.1 ± 9.0	60.1 ± 64.4	13.7 ± 5.4	118.8 ± 13.4	41.9 ± 12.1	0.3 ± 0.2	14.1 ± 6.1	27.8 ± 6.1	17.0 ± 6.1
050713A	fvs2	-	4.8 ± 0.8	147.3 ± 16.2	49.6 ± 87.7	15.5 ± 7.8	175.4 ± 21.6	45.0 ± 18.0	0.3 ± 0.2	14.6 ± 9.0	30.4 ± 9.0	4.0 ± 2.0
050713A	fmf1	-	79.0 ± 3.5	97.0 ± 1.9	9.4 ± 1.1	13.7 ± 0.6	102.8 ± 1.7	40.4 ± 0.6	0.4 ± 0.0	23.0 ± 0.5	5.9 ± 0.8	0.0 ± 0.0
050713A	fmf2	-	10.6 ± 2.3	138.0 ± 13.2	101.6 ± 139.7	9.3 ± 3.3	177.0 ± 17.7	39.6 ± 3.1	0.3 ± 0.1	13.0 ± 2.3	23.0 ± 3.3	1.3 ± 0.5
050713A	fmh1	-	30.5 ± 2.1	91.9 ± 4.3	84.3 ± 56.3	4.5 ± 0.9	111.3 ± 6.6	19.2 ± 1.2	0.2 ± 0.0	7.4 ± 0.7	11.8 ± 0.8	2.5 ± 0.6
050713A	fmh2	-	3.6 ± 0.8	154.7 ± 8.2	15.6 ± 37.0	8.1 ± 5.0	166.0 ± 2.7	20.8 ± 5.1	0.4 ± 0.2	6.3 ± 3.2	14.5 ± 3.9	0.2 ± 0.1
050713A	fmh3	-	68.9 ± 4.0	98.8 ± 1.6	17.4 ± 10.0	5.3 ± 0.8	108.3 ± 8.5	15.3 ± 0.7	0.3 ± 0.1	5.0 ± 0.5	10.3 ± 0.6	3.8 ± 1.1
050713A	fvh2	-	4.4 ± 1.1	159.3 ± 1.7	0.7 ± 2.4	28.0 ± 8.0	163.8 ± 5.2	35.9 ± 8.4	0.8 ± 0.3	4.0 ± 5.3	32.0 ± 6.3	1.0 ± 0.4
050714B	tot1	-	-	-	-	-	-	-	-	-	-	-
050714B	fvs	-	-	-	-	-	-	-	-	-	-	-
050714B	fmh	-	-	-	-	-	-	-	-	-	-	-
050714B	fvh	-	-	-	-	-	-	-	-	-	-	-
050714B	tot1	-	12.9 ± 2.4	148.2 ± 24.3	109.8 ± 345.0	5.4 ± 5.6	172.5 ± 33.2	23.4 ± 18.4	0.2 ± 0.3	9.0 ± 9.2	14.4 ± 9.2	1.8 ± 1.5
050716	tot2	-	4.4 ± 0.6	335.0 ± 15.0	37.6 ± 49.2	46.0 ± 18.7	377.0 ± 23.5	100.3 ± 31.8	0.5 ± 0.2	26.7 ± 15.9	73.6 ± 15.9	1.9 ± 0.8
050716	fvs1	-	-	-	-	-	-	-	-	-	-	-
050716	fvs2	-	-	-	-	-	-	-	-	-	-	-
050716	fms1	-	-	-	-	-	-	-	-	-	-	-
050716	fms2	-	-	-	-	-	-	-	-	-	-	-
050716	fmh1	-	-	-	-	-	-	-	-	-	-	-
050716	fmh2	-	-	-	-	-	-	-	-	-	-	-
050716	fvh1	-	-	-	-	-	-	-	-	-	-	-
050716	fvh2	-	-	-	-	-	-	-	-	-	-	-
050726	tot1	-	7.4 ± 0.7	176.6 ± 51.2	646.8 ± 1132.0	12.5 ± 7.0	266.4 ± 3.5	68.0 ± 6.2	0.2 ± 0.1	27.8 ± 4.3	40.2 ± 5.0	1.8 ± 0.9
050726	fvs	-	3.5 ± 0.4	204.1 ± 38.2	272.2 ± 501.4	15.5 ± 9.1	269.0 ± 4.4	65.3 ± 8.3	0.2 ± 0.1	24.9 ± 5.4	40.4 ± 6.8	0.3 ± 0.2
050726	fmh	-	-	-	-	-	-	-	-	-	-	-
050726	fvh	-	-	-	-	-	-	-	-	-	-	-
050730	tot1	3.967	16.1 ± 1.7	190.5 ± 22.7	160.1 ± 27.8	10.5 ± 5.7	231.6 ± 2.6	42.9 ± 5.1	0.2 ± 0.1	16.2 ± 3.3	26.7 ± 4.3	2.9 ± 1.4
050730	tot2	3.967	23.0 ± 1.1	311.6 ± 28.9	492.1 ± 399.2	25.7 ± 6.9	424.2 ± 3.1	110.7 ± 6.3	0.2 ± 0.1	42.5 ± 5.8	68.2 ± 5.4	10.0 ± 2.7
050730	fvs1	3.967	10.5 ± 1.1	606.9 ± 35.1	282.0 ± 318.8	28.2 ± 13.6	685.8 ± 5.7	98.4 ± 13.8	0.3 ± 0.1	35.1 ± 7.1	63.3 ± 11.8	3.7 ± 1.7
050730	fvs2	3.967	2.9 ± 0.5	317.0 ± 31.5	234.0 ± 228.6	53.0 ± 18.4	429.5 ± 7.2	164.6 ± 16.9	0.3 ± 0.1	109.2 ± 15.9	25.0 ± 8.8	0.0 ± 0.0
050730	fvs3	3.967	5.2 ± 0.5	481.0 ± 173.5	996.0 ± 2588.0	54.6 ± 60.1	714.1 ± 10.3	232.2 ± 61.9	0.2 ± 0.2	88.8 ± 14.0	143.4 ± 59.4	2.6 ± 2.3
050730	fmv1	3.967	6.6 ± 1.0	186.9 ± 34.3	231.6 ± 53.7	9.7 ± 7.4	234.7 ± 3.5	44.1 ± 7.6	0.2 ± 0.2	17.2 ± 4.2	26.9 ± 6.2	0.4 ± 0.3
050730	fmv2	3.967	9.0 ± 0.6	274.6 ± 59.5	1022.3 ± 1255.0	22.1 ± 9.1	425.0 ± 4.0	117.4 ± 8.6	0.2 ± 0.1	47.6 ± 5.2	69.8 ± 7.2	1.6 ± 0.6
050730	fmv3	3.967	4.3 ± 0.5	579.6 ± 52.6	342.2 ± 561.3	30.7 ± 17.1	682.2 ± 7.1	116.4 ± 18.7	0.3 ± 0.1	42.8 ± 9.4	73.6 ± 15.2	0.7 ± 0.4
050730	fmh1	3.967	3.7 ± 0.5	192.0 ± 49.7	229.7 ± 50.0	4.5 ± 1.1	232.8 ± 7.9	28.0 ± 5.3	0.2 ± 0.1	16.7 ± 4.4	30.3 ± 3.3	0.3 ± 0.3
050730	fmh2	3.967	3.0 ± 0.5	239.3 ± 60.1	493.0 ± 297.0	8.2 ± 17.3	678.0 ± 17.1	224.8 ± 5.5	0.1 ± 0.1	11.0 ± 30.8	33.8 ± 22.8	0.3 ± 0.6
050730	fvh1	3.967	5.1 ± 1.1	198.8 ± 39.7	203.7 ± 806.2	4.4 ± 5.4	229.8 ± 2.9	23.5 ± 4.8	0.2 ± 0.2	9.5 ± 3.7	14.0 ± 3.5	1.1 ± 1.1
050730	fvh2	3.967	4.7 ± 0.4	198.6 ± 207.8	4623.6 ± 1257.0	11.4 ± 10.0	427.9 ± 4.0	102.8 ± 7.0	0.1 ± 0.1	45.7 ± 7.0	57.1 ± 6.9	3.8 ± 2.8
050730	fvh3	3.967	2.1 ± 3.4	615.1 ± 508.5	1026.6 ± 2379.0	3.3 ± 18.4	673.7 ± 0.0	28.2 ± 46.1	0.1 ± 0.8	12.4 ± 31.9	15.8 ± 14.6	0.3 ± 1.1
050822	tot1	-	64.0 ± 5.9	25.2 ± 15.1	6020.4 ± 1687.0	4.4 ± 4.0	136.7 ± 4.9	53.3 ± 5.2	0.1 ± 0.1	24.5 ± 3.4	28.8 ± 3.2	18.0 ± 14.0
050822	tot2	-	15.1 ± 2.4	137.8 ± 19.3	339.0 ± 1915.0	3.1 ± 4.4	239.6 ± 9.8	35.4 ± 6.2	0.1 ± 0.2	16.2 ± 4.7	19.2 ± 3.4	2.7 ± 3.6
050822	fms1	-	4.0 ± 0.5	30.4 ± 1.5	107.8 ± 11.7	569.7 ± 2666.0	34.2 ± 2.6	439.5 ± 10.0	0.6 ± 0.2			

**Table 1.** Continued

GRB	band	$z$	$A$	$t_s$	$\tau_1$	$\tau_2$	$t_{pk}$	$w$	$k$	$t_{rise}$	$t_{decay}$	S	
			count $s^{-1}$	s	s	s	s	s	s	s	s	$10^{-8} \text{ erg cm}^{-2}$	
051117A	fmh4	-	3.2 ± 5.0	24.9 ± 3807.0	132105.0 ± 4.01E06	1.3 ± 15.1	435.4 ± --	45.8 ± 61.1	0.0 ± 0.3	22.3 ± 23.3	23.5 ± 37.9	0.4 ± 2.4	
051117A	fmh5	-	2.2 ± 1.1	453.6 ± 55.4	50.8 ± 254.6	37.3 ± 101.4	497.1 ± 15.5	88.8 ± 112.8	0.4 ± 0.7	25.7 ± 17.9	63.0 ± 105.8	0.5 ± 1.1	
051117A	fmh6	-	1.3 ± 3.8	-439.2 ± 8219.0	324995.0 ± 8.60E06	3.4 ± 37.1	612.7 ± --	119.7 ± 196.5	0.0 ± 0.3	58.2 ± 80.4	61.6 ± 116.3	0.4 ± 1.3	
051117A	fmh7	-	3.3 ± 0.3	584.1 ± 478.1	6358.8 ± 26200.0	21.4 ± 32.4	953.4 ± 20.9	179.2 ± 31.8	0.1 ± 0.2	78.9 ± 11.6	100.3 ± 29.9	1.4 ± 1.6	
051117A	fmh8	-	2.1 ± 1.4	674.7 ± 2579.0	38928.0 ± 654500.0	4.7 ± 21.7	1100.6 ± --	89.1 ± 67.0	0.1 ± 0.3	42.2 ± 43.5	46.9 ± 24.2	0.4 ± 1.3	
051117A	fmh9	-	7.4 ± 0.4	1234.4 ± 15.0	132.4 ± 79.1	68.3 ± 11.6	1329.5 ± 5.0	175.1 ± 11.9	0.4 ± 0.1	53.4 ± 5.0	121.7 ± 12.4	4.4 ± 1.0	
051117A	fmh10	-	2.0 ± 0.3	120.4 ± 19.3	10.0 ± 1.2	120.4 ± 15.8	154.6 ± 10.4	241.1 ± 10.2	0.5 ± 0.2	33.0 ± 19.5	110.1 ± 10.2	1.4 ± 0.8	
051117A	fvh1	-	21.5 ± 1.6	102.9 ± 12.4	10.0 ± 13.4	52.5 ± 7.0	125.9 ± 3.1	87.0 ± 11.3	0.6 ± 0.1	17.3 ± 8.1	69.8 ± 4.7	14.0 ± 3.2	
051117A	fvh2	-	5.4 ± 1.0	292.6 ± 16.3	32.7 ± 8.9	14.8 ± 14.8	314.6 ± 4.5	39.0 ± 11.7	0.4 ± 0.3	12.1 ± 4.7	26.9 ± 12.4	1.6 ± 1.3	
051117A	fvh3	-	5.4 ± 1.2	339.1 ± 5.9	2.7 ± 5.9	69.2 ± 29.1	352.7 ± 8.1	92.4 ± 25.5	0.7 ± 0.2	11.7 ± 9.5	80.9 ± 25.7	3.9 ± 1.8	
051117A	fvh4	-	4.0 ± 1.0	59.2 ± 5.7	132105.0 ± 1906.0	1.1 ± 0.0	434.9 ± 3.1	40.1 ± 0.7	0.0 ± 0.0	19.5 ± 0.3	20.6 ± 0.3	1.1 ± 0.3	
051117A	fvh5	-	4.0 ± 1.0	472.8 ± 6.9	5.0 ± 1.6	25.5 ± 13.0	484.3 ± 4.9	42.8 ± 18.2	0.6 ± 0.3	8.6 ± 5.7	34.2 ± 10.2	1.6 ± 0.8	
051117A	fvh6	-	2.3 ± 4.4	160.4 ± 97.3	494814.0 ± 65960.0	2.0 ± 0.4	618.3 ± 7.6	106.8 ± 10.2	0.0 ± 0.0	51.1 ± 3.1	54.6 ± 10.2	1.4 ± 0.3	
051117A	fvh7	-	1.3 ± 0.3	541.2 ± 532.4	9784.2 ± 40220.0	17.4 ± 25.1	948.4 ± --	167.2 ± 22.8	0.1 ± 0.1	75.1 ± 8.6	92.1 ± 22.4	4.9 ± 5.5	
051117A	fvh8	-	2.2 ± 1.2	668.5 ± 2513.0	36788.3 ± 598200.0	5.0 ± 22.5	1096.9 ± --	92.6 ± 65.8	0.1 ± 0.3	43.8 ± 43.6	48.8 ± 22.8	1.4 ± 3.9	
051117A	fvh9	-	8.3 ± 0.4	1248.6 ± 9.0	80.2 ± 36.6	78.3 ± 11.9	1327.9 ± 4.5	175.9 ± 9.7	0.4 ± 0.1	48.8 ± 4.3	127.1 ± 9.9	16.0 ± 2.7	
051117A	fvh10	-	2.5 ± 0.3	1470.0 ± 40.7	129.0 ± 187.3	69.7 ± 29.1	1564.8 ± 12.5	176.9 ± 21.8	0.4 ± 0.2	53.6 ± 14.7	123.3 ± 21.1	4.6 ± 1.9	
051210	tot1	-	6.2 ± 1.5	3.34 ± 17.1	48.8 ± 153.0	6.5 ± 6.5	131.2 ± 34.0	22.6 ± 23.4	0.3 ± 0.2	8.0 ± 9.7	14.6 ± 14.3	0.7 ± 0.6	
051210	tot2	-	3.8 ± 1.1	155.0 ± 19.0	13.0 ± 19.0	13.0 ± 19.0	139.0 ± 18.6	15.5 ± 10.5	0.7 ± 0.7	10.7 ± 9.9	14.7 ± 13.3	0.5 ± 0.6	
051210	fv1	-	10.2 ± 1.0	102.9 ± 102.1	277.8 ± 2547.0	4.0 ± 11.3	136.1 ± 189.2	23.3 ± 72.3	0.2 ± 0.4	9.7 ± 32.4	13.6 ± 40.3	0.1 ± 0.1	
051210	fv2	-	1.1 ± 13.6	165.2 ± 31.6	0.2 ± 27.8	11.0 ± 30.5	166.5 ± 11.9	13.4 ± 19.2	0.8 ± 11.6	1.2 ± 9.4	12.2 ± 100.0	0.0 ± 0.4	
051210	fm1	-	2.4 ± 0.8	90.4 ± 94.9	277.2 ± 1830.0	6.9 ± 14.3	134.2 ± 17.8	35.5 ± 79.3	0.2 ± 0.3	14.3 ± 35.0	21.2 ± 45.0	0.1 ± 0.2	
051210	fm2	-	1.5 ± 12180.0	172.6 ± 1.9E06	5.5 ± 1.9E06	3.9 ± 39500.0	177.2 ± 1.5E06	9.4 ± 70699.0	0.4 ± 3158.7	2.7 ± 351919.0	6.7 ± 356101.0	0.0 ± 140.0	
051210	fmh1	-	--	--	--	--	--	--	--	--	--	--	
051210	fmh2	-	--	--	--	--	--	--	--	--	--	--	
051210	fmh3	-	--	--	--	--	--	--	--	--	--	--	
051210	fmh4	-	--	--	--	--	--	--	--	--	--	--	
051210	fmh5	-	--	--	--	--	--	--	--	--	--	--	
051210	fmh6	-	--	--	--	--	--	--	--	--	--	--	
051210	fmh7	-	--	--	--	--	--	--	--	--	--	--	
051210	fmh8	-	--	--	--	--	--	--	--	--	--	--	
051210	fmh9	-	--	--	--	--	--	--	--	--	--	--	
051210	fmh10	-	--	--	--	--	--	--	--	--	--	--	
051210	fvh1	-	2.9 ± 0.9	47.1 ± 607.5	12680.3 ± 273600.0	0.6 ± 3.9	120.6 ± 1125.8	13.6 ± 102.2	0.0 ± 0.2	6.5 ± 40.8	7.1 ± 52.4	0.4 ± 0.6	
051210	fvh2	-	1.2 ± 0.5	134.4 ± 67.3	165.8 ± 1207.0	5.3 ± 12.5	163.0 ± 131.6	25.5 ± 63.9	0.2 ± 0.4	10.1 ± 27.8	15.4 ± 36.7	0.3 ± 0.6	
051227	tot1	-	8.9 ± 2.0	108.3 ± 4.7	2.5 ± 7.6	14.9 ± 8.9	114.4 ± 3.6	24.1 ± 6.5	0.6 ± 0.3	4.6 ± 4.5	19.5 ± 6.4	1.3 ± 0.8	
051227	fvs	-	--	--	--	--	--	--	--	--	--	--	
051227	fms	-	--	--	--	--	--	--	--	--	--	--	
051227	fmh	-	3.3 ± 14.0	110.2 ± 4.6	21.8 ± 13.0	110.6 ± 48.9	22.3 ± 93.8	1.0 ± 4.4	0.4 ± 51.6	22.2 ± 42.6	0.7 ± 0.7		
051227	fvh	-	--	--	--	--	--	--	--	--	--	--	
060111A	tot1	-	75.0 ± 4.8	-130.7 ± 349.8	9690.5 ± 45240.0	5.2 ± 8.2	94.7 ± 2.8	69.0 ± 3.7	0.1 ± 0.1	31.9 ± 4.1	37.1 ± 4.9	28.033.0	
060111A	tot2	-	40.6 ± 2.8	114.7 ± 14.1	157.1 ± 128.9	17.4 ± 4.7	167.0 ± 1.7	62.8 ± 3.2	0.3 ± 0.1	22.7 ± 2.1	40.1 ± 3.4	15.03.9	
060111A	tot3	-	135.4 ± 2.7	-0.9 ± 88.3	12706.6 ± 12290.0	6.5 ± 2.3	285.4 ± --	86.2 ± 2.7	0.1 ± 0.0	39.9 ± 0.9	46.3 ± 2.3	60.019.0	
060111A	tot4	-	32.8 ± 3.9	312.3 ± 2.6	7.6 ± 3.8	84.6 ± 6.5	337.6 ± 4.2	125.4 ± 9.4	0.7 ± 0.0	20.4 ± 4.1	105.0 ± 7.1	23.03.6	
060111A	fmh1	-	20.1 ± 0.8	131.0 ± 4.4	1.7 ± 0.0	102.0 ± 0.5	65.2 ± 0.5	63.5 ± 0.5	0.3 ± 0.0	31.0 ± 0.0	32.0 ± 0.0	31.0 ± 0.0	
060111A	fmh2	-	19.3 ± 0.8	114.1 ± 18.5	135.7 ± 167.2	10.5 ± 1.0	67.7 ± 1.0	72.4 ± 2.9	0.3 ± 0.0	25.5 ± 6.0	47.7 ± 9.3	9.54.1	
060111A	fmh3	-	28.6 ± 1.0	104.7 ± 80.1	219.0 ± 3103.0	14.6 ± 7.7	283.8 ± 1.0	103.4 ± 7.8	0.1 ± 0.1	44.4 ± 3.0	59.0 ± 7.2	21.010.0	
060111A	fmh4	-	7.9 ± 2.3	313.7 ± 3.9	1.5 ± 3.5	123.9 ± 37.3	149.0 ± 29.9	0.8 ± 0.2	12.5 ± 11.8	136.4 ± 31.7	9.33.9		
060111A	fmh5	-	33.1 ± 2.7	-169.3 ± 498.2	1223.7 ± 68640.0	5.6 ± 10.0	91.7 ± --	76.5 ± 5.7	0.1 ± 0.1	35.4 ± 7.0	41.0 ± 4.2	4.66.1	
060111A	fmh6	-	18.4 ± 1.5	141.1 ± 3.4	18.2 ± 11.1	26.1 ± 5.5	54.3 ± 4.3	0.5 ± 0.1	14.1 ± 1.8	40.2 ± 4.6	23.06.6		
060111A	fmh7	-	59.3 ± 5.6	154.2 ± 25.3	32.5 ± 2.3	250.6 ± 3.6	84.3 ± 7.6	33.3 ± 5.7	0.1 ± 0.0	18.5 ± 3.4	32.0 ± 7.8	1.06.2	
060111A	fmh8	-	9.4 ± 0.4	-636.2 ± 7.5	252320.0 ± 25040.0	2.0 ± 0.0	81.3 ± 2.9	76.6 ± 0.5	0.0 ± 0.0	39.3 ± 0.3	42.0	2.40.3	
060111A	fmh9	-	4.6 ± 0.6	110.4 ± 27.2	10.1 ± 306.6	13.9 ± 6.6	161.8 ± 3.5	55.2 ± 6.0	0.3 ± 0.1	20.7 ± 4.4	34.5 ± 4.5	0.70.3	
060111A	fmh10	-	2.3 ± 2.8	45.8 ± 90.2	4881.6 ± 17910.0	1.1 ± 1.2	381.2 ± 94.1	117.5 ± 16.7	0.1 ± 0.1	8.2 ± 10.5	37.1 ± 10.2	4.64.5	
060204B	tot1	-	133.0 ± 6.2	39.8 ± 40.0	2853.6 ± 4256.0	2.2 ± 1.0	118.7 ± 73.6	26.4 ± 13.6	0.1 ± 0.0	12.1 ± 6.4	14.3 ± 7.2	18.07.9	
060204B	tot2	-	23.3 ± 2.0	271.9 ± 17.4	17.3 ± 182.8	16.1 ± 5.2	32.47 ± 34.0	60.5 ± 21.2	0.3 ± 0.1	22.2 ± 8.9	38.3 ± 12.6	8.63.0	
060204B	fv1	-	16.4 ± 1.5	85.0 ± 24.7	266.0 ± 48.4	5.6 ± 2.8	123.4 ± 44.0	29.8 ± 17.4	0.2 ± 0.1	12.1 ± 7.9	17.7 ± 9.7	4.12.0	
060204B	fv2	-	6.4 ± 1.4	283.6 ± 18.1	91.9 ± 131.4	24.6 ± 12.8	331.2 ± 40.4	72.7 ± 37.4	0.3 ± 0.1	24.0 ± 14.2	48.6 ± 24.1	2.51.3	
060204B	fm1	-	50.6 ± 3.5	160.1 ± 12.2	30.3 ± 16.9	21.1 ± 7.7	120.0 ± 15.7	126.0 ± 18.7	0.1 ± 0.0	24.2 ± 9.4	35.0 ± 13.2	1.03.0	
060204B	fm2	-	13.0 ± 3.6	30.2 ± 2.6	16.2 ± 8.0	2.3 ± 3.4	31.8 ± 7.8	43.4 ± 9.9	0.5 ± 0.1	10.5 ± 5.7	34.7 ± 10.7	1.10.3	
060204B	fmh1	-	2.7 ± 0.8	10.2 ± 2.8	50.1 ± 9.9	11.6 ± 5.4	117.4 ± 14.2	24.0 ± 2.2	0.1 ± 0.1	10.7 ± 15.2	13.3 ± 17.1	2.01.9	
060204B	fvh1	-	41.9 ± 2.8	45.8 ± 90.2	4881.6 ± 17910.0	1.1 ± 1.2	117.5 ± 16.7	17.4 ± 21.9	0.1 ± 0.1	8.2 ± 10.5	9.2 ± 11.4	6.35.7	
060210	fv1	-	84.7 ± 3.4	145.6 ± 10.2	24.8 ± 114.1	14.5 ± 2.5	196.5 ± 1.0	60.7 ± 2.1	0.2 ± 0.0	23.1 ± 1.5	37.6 ± 2.1	23.04.0	
060210	fv2	-	3.91	358.4 ± 1.2	30.9 ± 2.0	30.9 ± 1.7	37.0 ± 0.0	60.1 ± 0.5	0.1 ± 0.1	14.8 ± 1.6	42.4 ± 2.2	19.02.4	
060210	fv2	-	3.91	157.5 ± 1.0	123.3 ± 23.8	32.95 ± 312.4	19.9 ± 7.4	204.2 ± 33.7	82.7 ± 22.0	0.2 ± 0.1	31.4 ± 11.0	51.3 ± 11.0	6.02.0
060210	fvs	-	3.91	15.7 ± 0.8	303.5 ± 19.0	19.0 ± 2.4	33.1 ± 8.1	38.2 ± 26.5	107.6 ± 20.4	0.3 ± 0.1	37.3 ± 10.2	70.3 ± 10.2	6.91.8
060210	fms	-	3.91	34.5 ± 1.6	128.5 ± 15.5	35.8 ± 4.4	130.6 ± 3.0	13.6 ± 3.0	0.2 ± 0.1	24.7 ± 5.3	38.3 ± 5.3	3.90.9	
060210	fmh1	-	16.1 ± 0.9	167.4 ± 8.6	22.6 ± 22.1	39.5 ± 8.0	197.2 ± 4.3	79.2 ± 7.8	0.5 ± 0.1	19.9 ± 5.3	59.4 ± 5.8	4.51.6	
060210	fmh2	-	0.4 ± 0.6	162.1 ± 13.5	49.8 ± 4.6	48.9 ± 10.7	211.4 ± 5.9	109.8 ± 10.0	0.4 ± 0.1	30.4 ± 6.8	79.		

**Table 1.** Continued

GRB	band	$z$	$A$	$t_s$	$\tau_1$	$\tau_2$	$t_{pk}$	$w$	$k$	$t_{rise}$	$t_{decay}$	$S$
			count $s^{-1}$	s	s	s	s	s	s	s	s	$10^{-8} \text{ erg cm}^{-2}$
060707	fwh	3.425	- ± -	- ± -	- ± -	- ± -	- ± -	- ± -	- ± -	- ± -	- ± -	0.0 ± 0.0
060707	rvb	3.425	2.1 ± 54.1	152.9 ± 3154.0	18.3 ± 2585.0	31.5 ± 144.5	176.9 ± 1521.0	63.4 ± 460.9	0.5 ± 13.7	15.9 ± 800.0	47.5 ± 661.5	1.0 ± 15.0
060714	tot1	2.7	11.8 ± 4.6	103.9 ± 3.2	3.1 ± 2.8	33.1 ± 1.9	49.9 ± 1.5	0.7 ± 0.1	8.0 ± 3.0	4.6 ± 2.0	33.0 ± 4.3	1.0 ± 1.3
060714	tot2	2.711	89.6 ± 12.1	55.4 ± 75.7	2936.6 ± 54480.0	5.2 ± 0.0	132.1 ± 1.8	8.2 ± 4.1	0.4 ± 0.0	4.0 ± 2.1	4.2 ± 1.1	0.9 ± 2.4
060714	tot3	2.711	121.8 ± 12.6	131.5 ± 4.2	12.8 ± 12.3	5.2 ± 1.0	130.7 ± 1.4	14.0 ± 1.9	0.4 ± 0.1	4.4 ± 1.1	9.6 ± 1.0	0.4 ± 2.4
060714	tot4	2.711	120.6 ± 4.9	151.5 ± 4.7	127.6 ± 76.1	4.5 ± 0.8	175.4 ± 0.5	21.1 ± 0.8	0.2 ± 0.0	8.3 ± 0.6	12.8 ± 0.5	11.0 ± 2.0
060714	fvs1	2.711	20.8 ± 4.2	106.3 ± 67.7	0.0 ± 2.6	46.5 ± 9.6	107.5 ± 20.1	48.8 ± 89.1	1.0 ± 1.9	1.2 ± 48.4	47.7 ± 40.9	3.6 ± 1.5
060714	fvs2	2.711	14.7 ± 44.6	-17.5 ± 6486.0	23001.6 ± 3.34E06	1.0 ± 60.5	134.2 ± -	24.7 ± 223.9	0.0 ± 2.1	11.8 ± 81.7	12.8 ± 142.2	1.0 ± 24.0
060714	fvs3	2.711	17.7 ± 168.1	-10.5 ± 2898.0	53122.2 ± 3.08E06	0.5 ± 10.5	149.2 ± 137.7	17.5 ± 38.3	0.0 ± 0.5	8.5 ± 14.5	9.0 ± 24.0	1.0 ± 13.0
060714	fvs4	2.711	25.7 ± 3.6	153.5 ± 5.4	25.3 ± 17.8	14.6 ± 2.7	172.7 ± 2.2	36.6 ± 2.9	0.4 ± 0.1	11.0 ± 1.7	25.6 ± 2.2	5.9 ± 1.4
060714	fms1	2.711	41.2 ± 2.4	100.9 ± 9.5	6.0 ± 11.6	32.2 ± 4.4	114.5 ± 3.4	53.2 ± 10.7	0.6 ± 0.2	10.5 ± 7.3	42.7 ± 3.7	4.7 ± 1.1
060714	fms2	2.711	27.7 ± 7.2	29.9 ± 8.8	3573.0 ± 60060.0	0.3 ± 0.1	131.6 ± 1.9	10.9 ± 4.3	0.0 ± 0.0	5.3 ± 2.2	4.0 ± 0.5	0.0 ± 0.5
060714	fms3	2.711	41.2 ± 4.5	130.9 ± 10.5	15.6 ± 19.8	5.2 ± 1.8	141.4 ± 1.7	14.1 ± 1.7	0.1 ± 0.1	8.0 ± 1.1	10.0 ± 1.4	1.4 ± 0.5
060714	fms4	2.711	53.2 ± 3.2	144.5 ± 10.2	25.6 ± 24.8	3.1 ± 1.1	173.4 ± 0.6	20.6 ± 1.1	0.2 ± 0.1	8.5 ± 0.9	12.0 ± 0.7	2.0 ± 0.6
060714	fmh1	2.711	20.0 ± 2.3	106.1 ± 3.1	0.7 ± 1.6	27.1 ± 3.0	110.4 ± 2.3	34.6 ± 6.9	0.8 ± 0.2	3.8 ± 4.0	30.0 ± 3.5	2.3 ± 0.5
060714	fmh2	2.711	23.8 ± 3.1	39.4 ± 2.5	23248.4 ± 1418.0	0.3 ± 0.0	131.6 ± 0.6	9.8 ± 0.2	0.0 ± 0.0	4.8 ± 0.1	5.1 ± 0.1	0.7 ± 0.1
060714	fmh3	2.711	24.5 ± 3.7	134.5 ± 2.4	4.8 ± 7.9	4.4 ± 1.5	139.0 ± 0.9	9.9 ± 1.6	0.4 ± 0.2	2.8 ± 1.1	7.1 ± 1.1	0.8 ± 0.3
060714	fmh4	2.711	21.6 ± 2.3	143.5 ± 23.4	445.7 ± 970.7	2.2 ± 1.4	174.7 ± 1.1	16.7 ± 1.6	0.1 ± 0.1	7.3 ± 1.3	9.4 ± 0.8	1.0 ± 0.6
060714	fvh1	2.711	37.4 ± 4.5	84.6 ± 117.5	104.9 ± 130.0	6.3 ± 20.4	110.3 ± 1.2	26.1 ± 15.1	0.2 ± 0.9	9.9 ± 16.4	16.2 ± 7.3	12.0 ± 26.0
060714	fvh2	2.711	33.6 ± 11.5	38.5 ± 69.1	32384.7 ± 49000.0	0.3 ± 0.0	130.7 ± 0.6	9.8 ± 3.8	0.0 ± 0.0	4.8 ± 1.9	5.1 ± 1.9	3.9 ± 1.7
060714	fvh3	2.711	42.6 ± 9.5	131.8 ± 8.8	4.5 ± 6.0	134.4 ± 0.9	10.5 ± 2.9	0.5 ± 0.2	2.9 ± 0.8	7.6 ± 2.7	5.5 ± 2.9	0.0 ± 0.5
060714	fvh4	2.711	24.0 ± 2.5	141.0 ± 1.5	572.7 ± 1492.0	1.4 ± 1.1	174.5 ± 1.2	16.0 ± 0.3	0.1 ± 0.1	7.0 ± 2.2	9.0 ± 1.7	4.0 ± 2.7
060714	fvh5	-	8.2 ± 79.8	188.0 ± 35.0	14.1 ± 7.6	14.4 ± 22.5	192.3 ± 89.2	3.1 ± 5.4	3.0 ± 8.2	18.0 ± 62.1	21.8 ± 18.0	0.0 ± 0.0
060719	fvs	-	-	-	-	-	-	-	-	-	-	0.0 ± 0.0
060719	fms	-	8.1 ± 142.0	188.0 ± 55.1	1.4 ± 126.3	10.9 ± 23.2	191.9 ± 115.5	17.0 ± 193.6	0.6 ± 8.6	3.1 ± 107.9	13.0 ± 85.8	0.4 ± 7.0
060719	fmh	-	-	-	-	-	-	-	-	-	-	0.0 ± 0.0
060719	fvh	-	-	-	-	-	-	-	-	-	-	0.0 ± 0.0
060729	tot	0.54	272.9 ± 13.6	163.4 ± 1.1	7.2 ± 2.2	24.5 ± 1.9	176.7 ± 1.0	43.7 ± 2.5	0.6 ± 0.0	9.6 ± 1.0	34.1 ± 2.0	93.0 ± 10.0
060729	fvs	0.54	88.2 ± 6.4	159.5 ± 4.6	30.6 ± 17.1	23.0 ± 3.0	185.7 ± 2.0	54.6 ± 3.3	0.4 ± 0.1	15.8 ± 2.1	33.8 ± 2.4	21.0 ± 5.0
060729	fms	0.54	142.7 ± 11.9	16.0 ± 2.2	8.8 ± 5.9	14.9 ± 2.7	175.4 ± 1.2	30.1 ± 3.0	0.5 ± 0.1	7.6 ± 1.4	22.5 ± 2.5	38.0 ± 10.0
060729	fmh	0.54	29.2 ± 5.4	164.9 ± 3.7	6.2 ± 10.1	11.2 ± 4.0	173.3 ± 2.1	22.3 ± 3.7	0.5 ± 0.2	5.5 ± 2.4	16.7 ± 3.0	6.1 ± 2.6
060804	tot	-	-	-	-	-	-	-	-	-	-	0.0 ± 0.0
060804	fvs	-	1.7 ± 0.4	419.1 ± 7.2	8.2 ± 21.2	93.7 ± 36.5	446.8 ± 25.1	138.5 ± 30.2	0.7 ± 0.3	22.4 ± 20.5	116.1 ± 26.4	2.1 ± 1.0
060804	fms	-	-	-	-	-	-	-	-	-	-	0.0 ± 0.0
060804	fmh	-	-	-	-	-	-	-	-	-	-	0.0 ± 0.0
060804	fvh	-	-	-	-	-	-	-	-	-	-	0.0 ± 0.0
060814	tot	0.84	123.7 ± 7.8	11.9 ± 5.7	9.0 ± 4.7	20.4 ± 2.7	130.3 ± 1.3	39.0 ± 2.5	0.5 ± 0.1	9.3 ± 1.3	29.7 ± 2.3	31.0 ± 4.8
060814	fvs	0.84	- ± -	-	-	-	-	-	-	-	-	0.0 ± 0.0
060814	fms	0.84	42.7 ± 3.5	110.4 ± 4.4	20.7 ± 16.5	20.4 ± 4.8	136.9 ± 2.2	45.7 ± 1.3	0.4 ± 0.1	12.7 ± 2.2	33.1 ± 4.0	4.9 ± 1.3
060814	fmh	0.84	10.0 ± 1.7	100.9 ± 1.5	8.0 ± 0.7	9.0 ± 1.0	130.4 ± 1.4	30.3 ± 1.4	0.3 ± 0.1	12.0 ± 2.2	33.0 ± 4.0	3.1 ± 1.4
060814	fvh	0.84	86.5 ± 20.0	12.9 ± 1.1	0.2 ± 1.1	18.6 ± 2.9	127.1 ± 4.3	23.5 ± 7.4	0.4 ± 0.3	1.9 ± 3.7	20.5 ± 3.7	18.0 ± 6.9
060904	tot1	-	16.0 ± 1.3	186.5 ± 48.3	762.9 ± 917.2	10.5 ± 7.2	308.6 ± 4.6	99.6 ± 7.2	0.2 ± 0.1	40.0 ± 5.1	59.0 ± 5.1	7.0 ± 2.5
060904	tot2	-	4.8 ± 3.3	661.2 ± 10.4	0.7 ± 9.2	78.7 ± 24.1	668.9 ± 36.2	92.8 ± 64.0	0.8 ± 0.7	7.0 ± 39.4	85.7 ± 28.1	2.2 ± 1.7
060904	fvs1	-	-	-	-	-	-	-	-	-	-	0.0 ± 0.0
060904	fvs2	-	-	-	-	-	-	-	-	-	-	0.0 ± 0.0
060904	fms1	-	7.4 ± 0.8	199.0 ± 50.2	579.4 ± 1183.0	12.9 ± 6.4	297.9 ± 4.0	72.5 ± 6.3	0.2 ± 0.1	29.8 ± 4.3	42.7 ± 4.7	0.9 ± 0.4
060904	fms2	-	2.6 ± 5.1	661.7 ± 76.1	0.1 ± 10.9	61.1 ± 22.9	66.4 ± 38.1	66.6 ± 192.8	0.9 ± 2.9	2.8 ± 104.6	63.8 ± 88.8	0.3 ± 0.7
060904	fmh1	-	-	-	-	-	-	-	-	-	-	0.0 ± 0.0
060904	fmh2	-	-	-	-	-	-	-	-	-	-	0.0 ± 0.0
060904	fvh1	-	-	-	-	-	-	-	-	-	-	0.0 ± 0.0
060904	fvh2	-	-	-	-	-	-	-	-	-	-	0.0 ± 0.0
060904	fvh3	-	-	-	-	-	-	-	-	-	-	0.0 ± 0.0
060904	fvh4	-	-	-	-	-	-	-	-	-	-	0.0 ± 0.0
060904	fvh5	-	-	-	-	-	-	-	-	-	-	0.0 ± 0.0
060904	fvh6	-	-	-	-	-	-	-	-	-	-	0.0 ± 0.0
060904	fvh7	-	-	-	-	-	-	-	-	-	-	0.0 ± 0.0
060904	fvh8	-	-	-	-	-	-	-	-	-	-	0.0 ± 0.0
060904	fvh9	-	-	-	-	-	-	-	-	-	-	0.0 ± 0.0
060929	tot	67.1 ± 1.6	432.0 ± 6.0	173.1 ± 34.0	52.0 ± 2.5	29.5 ± 0.8	170.7 ± 6.0	78.5 ± 0.9	0.4 ± 0.0	24.5 ± 0.5	54.0 ± 0.6	200.0 ± 12.0
060929	fms	7.03	51.5 ± 1.8	119.8 ± 4.4	133.5 ± 32.0	37.5 ± 2.8	190.5 ± 1.9	109.6 ± 2.5	0.3 ± 0.0	36.0 ± 1.4	73.5 ± 2.2	48.0 ± 5.2
060929	fmh	7.03	176.4 ± 3.7	115.9 ± 2.1	153.2 ± 18.3	24.2 ± 0.8	176.7 ± 0.7	80.5 ± 0.9	0.3 ± 0.0	28.1 ± 0.6	52.3 ± 0.6	33.0 ± 2.7
060929	fmh	7.03	77.7 ± 3.0	122.7 ± 2.7	100.4 ± 21.3	20.0 ± 1.1	167.5 ± 1.0	63.0 ± 1.3	0.3 ± 0.0	21.5 ± 0.8	41.5 ± 0.9	17.0 ± 1.7
060904	tot1	0.703	38.1 ± 0.6	476.0 ± 187.8	84.0 ± 145.1	570.8 ± 34.7	197.1 ± 11.0	0.4 ± 0.7	56.5 ± 77.7	140.6 ± 100.7	1.0 ± 0.7	0.5 ± 0.7
060904	fvs1	0.836	0.8 ± 2.0	78.0 ± 29.6	0.3 ± 15.1	55.3 ± 43.5	79.3 ± 7.6	62.6 ± 15.7	0.2 ± 2.7	37.3 ± 9.3	59.0 ± 67.7	0.1 ± 0.2
060904	fvs2	0.836	0.4 ± 0.2	418.8 ± 258.3	228.3 ± 168.0	62.2 ± 156.0	53.8 ± 0.5	183.0 ± 142.1	0.3 ± 0.7	60.4 ± 68.2	122.6 ± 132.7	0.1 ± 0.1
060904	fms1	0.836	0.3 ± 0.2	63.77 ± 336.4	333.7 ± 244.0	61.0 ± 137.6	78.0 ± 44.6	67.7 ± 143.0	0.3 ± 0.7	67.7 ± 76.4	128.7 ± 106.6	0.1 ± 0.2
060904	fms2	0.836	5.8 ± 2.7	407.6 ± 17.5	14.9 ± 97.4	5.0 ± 8.7	148.3 ± 27.8	42.9 ± 16.0	0.3 ± 0.1	48.9 ± 8.6	100.9 ± 11.8	48.0 ± 3.6
060904	fms3	0.836	6.6 ± 1.5	433.6 ± 3.6	1.8 ± 4.5	29.9 ± 14.3	44.0 ± 10.4	0.3 ± 0.0	48.9 ± 3.6	27.2 ± 9.5	3.4 ± 1.2	0.0 ± 0.0
060904	fms4	0.836	0.6 ± 0.2	124.0 ± 34.4	4.7 ± 155.4	32.9 ± 11.2	173.5 ± 16.7	16.8 ± 3.2	0.1 ± 0.4	74.2 ± 24.4	91.2 ± 29.1	0.4 ± 0.8
060904	fms5	0.836	0.6 ± 0.5	33.0 ± 5.0	1.8 ± 11.8	58.4 ± 8.4	17.0 ± 3.6	0.3 ± 0.0	47.4 ± 1.2	95.3 ± 6.0	7.0 ± 0.0	
060904	fms6	0.836	3.8 ± 3.4	35.3 ± 13.7	0.1 ± 4.4	47.4 ± 2.8	52.9 ± 4.3	12.7 ± 9.0	0.3 ± 0.0	43.3 ± 7.1	84.7 ± 10.1	4.2 ± 0.7
060904	fms7	0.836	0.8 ± 1.3	378.5 ± 67.4	23.2 ± 29.0	19.4 ± 15.6	43.7 ± 6.7	51.9 ± 51.5	0.3 ± 0.2	36.7 ± 5.6	78.0 ± 8.0	18.0 ± 2.6
060904	fms8	0.836	0.5 ± 0.2	1275.3 ± 112.5	31.8 ± 157.4	166.9 ± 119.1	134.8 ± 21.4	6.1 ± 0.5	54.8 ± 111.3	221.7 ± 179.3	1.3 ± 1.0	
060904	fms9	0.836	13.2 ± 1.1	312.9 ± 1.6	3.5 ± 3.2	57.6 ± 2.9	32.71 ± 7.5	81.2 ± 37.6	0.7 ± 0.1	11.8 ± 5.7	69.4 ± 33.4	3.9 ± 1.9
060904	fms10	0.836	5.8 ± 2.7	407.6 ± 17.5	14.9 ± 97.4	5.0 ± 8.7	140.3 ± 27.8	0.6 ± 0.5	54.7 ± 26.6	17.2 ± 9.5	3.3 ± 1.6	0.0 ± 0.0
060904	fms11	0.836	3.8 ± 1.1	185.4 ± 8.7	4.9 ± 22.5	26.0 ± 3.8	181.3 ± 1.3	43.4 ± 3.4	0.6 ± 0.1	8.7 ± 1.4	34.7 ± 3.3	21.0 ± 3.5
060904	fms12	0.836	8.8 ± 0.6	204.6 ± 19.0	120.9 ± 86.0	49.6 ± 8.9	28.2 ± 34.2	133.6 ± 27.8	0.4 ± 0.1	42.0 ± 11.4	91.6 ± 17.2	2.0 ± 0.5
060904	fms13	0.836	2.8 ± 1.4	186.1 ± 23.0	25.1 ± 179.2	3.6 ± 6.0	195.6 ± 41.6	12.1 ± 2.5	0.3 ± 0.5	4.3 ± 11.1	7.9 ± 14.8	1.0 ± 0.2
060904	fms14	0.836	2.9 ± 2.0	197.7 ± 30.6	125.4							

**Table 1.** Continued

GRB	band	$z$	$A$ count s $^{-1}$	$t_s$ s	$\tau_1$ s	$\tau_2$ s	$t_{pk}$ s	$w$ s	$k$ s	$t_{rise}$ s	$t_{decay}$ s	$S$ $10^{-8} \text{ erg cm}^{-2}$
070518	tot1	-	23.2 ± 2.1	97.8 ± 2.1	3.5 ± 4.3	16.7 ± 5.3	105.4 ± 5.3	28.2 ± 9.3	0.6 ± 0.1	5.7 ± 3.0	22.5 ± 7.0	2.6 ± 0.8
070518	tot2	-	7.4 ± 1.3	130.0 ± 5.4	8.6 ± 13.4	36.0 ± 37.0	148.5 ± 17.3	61.9 ± 55.5	0.6 ± 0.2	13.0 ± 11.3	48.9 ± 45.8	1.8 ± 1.5
070518	tot3	-	22.2 ± 1.7	151.8 ± 11.5	179.1 ± 174.3	7.6 ± 2.4	188.6 ± 22.1	34.2 ± 11.6	0.2 ± 0.1	13.3 ± 5.0	20.9 ± 6.7	2.9 ± 0.9
070518	fvs1	-	6.9 ± 1.0	59.2 ± 84.0	669.8 ± 3299.0	4.3 ± 7.4	112.7 ± 163.0	30.6 ± 54.4	0.1 ± 0.2	13.1 ± 24.6	17.4 ± 30.0	0.8 ± 1.0
070518	fvs2	-	5.8 ± 6.9	133.8 ± 4.2	0.1 ± 3.8	14.3 ± 17.7	135.2 ± 19.5	16.9 ± 37.6	0.8 ± 1.6	1.3 ± 16.1	15.6 ± 24.6	0.4 ± 0.7
070518	fvs3	-	11.7 ± 0.9	105.1 ± 76.4	1255.3 ± 3372.0	5.6 ± 4.8	189.2 ± 141.1	43.9 ± 40.5	0.1 ± 0.1	19.1 ± 18.6	24.8 ± 22.0	1.8 ± 1.3
070518	fms1	-	10.9 ± 1.3	93.7 ± 7.0	205.5 ± 32.7	10.1 ± 4.3	108.0 ± 13.8	26.0 ± 12.4	0.4 ± 0.1	8.0 ± 5.0	18.0 ± 7.9	0.4 ± 0.2
070518	fms2	-	6.0 ± 1.2	136.9 ± 3.9	4.5 ± 10.4	15.5 ± 9.8	145.6 ± 13.3	27.9 ± 17.8	0.6 ± 0.2	6.2 ± 5.6	21.7 ± 13.2	0.3 ± 0.2
070518	fms3	-	6.0 ± 1.2	109.7 ± 6.6	38.5 ± 45.2	8.6 ± 2.9	148.1 ± 12.9	26.7 ± 7.7	0.2 ± 0.1	8.0 ± 6.0	17.7 ± 6.0	0.1 ± 0.1
070518	fuh1	-	3.8 ± 0.8	75.6 ± 59.1	670.0 ± 3810.0	1.4 ± 1.5	106.2 ± 108.5	13.1 ± 25.3	0.1 ± 0.2	5.9 ± 11.9	7.3 ± 13.5	0.1 ± 0.2
070518	fuh2	-	0.3 ± 0.4	131.9 ± 23.0	5.7 ± 92.3	6.2 ± 34.0	137.9 ± 55.6	13.6 ± 74.2	0.5 ± 1.5	3.7 ± 25.4	9.9 ± 51.8	0.0 ± 0.0
070518	fuh3	-	1.0 ± 0.3	112.6 ± 324.7	1255.5 ± 16610.0	4.5 ± 20.1	187.5 ± 615.5	36.8 ± 173.1	0.1 ± 0.4	16.2 ± 79.6	20.6 ± 94.1	0.1 ± 0.3
070518	fh1	-	4.7 ± 1.1	94.5 ± 9.4	16.8 ± 62.8	2.5 ± 2.2	100.9 ± 15.5	8.3 ± 9.1	0.3 ± 0.3	2.9 ± 4.0	5.4 ± 5.3	0.2 ± 0.2
070518	fh2	-	1.5 ± 5.6	136.5 ± 276.0	0.0 ± 3.5	17.1 ± 17.0	136.6 ± 328.5	17.4 ± 349.8	1.0 ± 19.7	0.2 ± 174.7	17.2 ± 175.5	0.1 ± 0.5
070518	fh3	-	0.8 ± 0.3	168.5 ± 53.3	40.0 ± 233.9	18.0 ± 24.5	195.3 ± 96.9	47.5 ± 78.2	0.4 ± 0.5	14.8 ± 32.5	32.8 ± 47.9	0.4 ± 0.5
070518	tot	-	75.8 ± 2.1	147.4 ± 3.7	76.0 ± 20.2	32.1 ± 2.6	194.4 ± 1.3	80.8 ± 1.3	0.2 ± 0.1	27.0 ± 1.3	59.1 ± 2.2	30.0 ± 3.7
070518	fvs	-	19.4 ± 4.7	104.9 ± 15.6	392.0 ± 190.5	20.7 ± 1.7	210.0 ± 1.7	11.5 ± 2.0	0.3 ± 0.0	42.2 ± 2.4	70.4 ± 4.2	15.0 ± 1.0
070520B	fms	-	10.9 ± 1.2	130.2 ± 4.8	1.4 ± 31.9	27.8 ± 2.5	193.6 ± 1.4	82.5 ± 2.5	0.3 ± 0.0	27.4 ± 1.4	45.1 ± 2.0	5.7 ± 0.8
070520B	fuh	-	11.2 ± 0.8	168.8 ± 1.6	6.9 ± 3.7	33.5 ± 3.9	182.0 ± 2.0	56.2 ± 3.7	0.6 ± 0.1	11.4 ± 1.9	44.8 ± 3.3	1.9 ± 0.3
070520B	fvh	-	11.8 ± 0.8	165.7 ± 2.2	9.6 ± 5.4	28.9 ± 3.5	182.4 ± 1.9	52.5 ± 3.4	0.6 ± 0.1	11.8 ± 1.9	40.7 ± 2.9	5.4 ± 0.9
070621	tot1	-	26.1 ± 3.6	123.1 ± 25.2	219.0 ± 676.8	2.7 ± 2.6	147.5 ± 1.5	16.5 ± 2.6	0.2 ± 0.2	6.9 ± 1.9	9.6 ± 1.8	3.0 ± 2.4
070621	tot2	-	7.0 ± 1.4	168.9 ± 14.0	42.2 ± 68.8	17.9 ± 9.0	196.4 ± 4.1	47.9 ± 10.6	0.4 ± 0.2	15.0 ± 5.1	32.9 ± 8.4	2.8 ± 1.4
070621	fvs1	-	-	-	-	-	-	-	-	-	-	0.0 ± 0.0
070621	fvs2	-	-	-	-	-	-	-	-	-	-	0.0 ± 0.0
070621	fvs3	-	-	-	-	-	-	-	-	-	-	0.0 ± 0.0
070621	fvs4	-	-	-	-	-	-	-	-	-	-	0.0 ± 0.0
070621	fvs5	-	-	-	-	-	-	-	-	-	-	0.0 ± 0.0
070621	fvs6	-	-	-	-	-	-	-	-	-	-	0.0 ± 0.0
070621	fvs7	-	-	-	-	-	-	-	-	-	-	0.0 ± 0.0
070621	fvs8	-	-	-	-	-	-	-	-	-	-	0.0 ± 0.0
070621	fvs9	-	-	-	-	-	-	-	-	-	-	0.0 ± 0.0
070621	fvs10	-	-	-	-	-	-	-	-	-	-	0.0 ± 0.0
070621	fvs11	-	-	-	-	-	-	-	-	-	-	0.0 ± 0.0
070621	fvs12	-	-	-	-	-	-	-	-	-	-	0.0 ± 0.0
070621	fvs13	-	-	-	-	-	-	-	-	-	-	0.0 ± 0.0
070621	fvs14	-	-	-	-	-	-	-	-	-	-	0.0 ± 0.0
070621	fvs15	-	-	-	-	-	-	-	-	-	-	0.0 ± 0.0
070621	fvs16	-	-	-	-	-	-	-	-	-	-	0.0 ± 0.0
070621	fvs17	-	-	-	-	-	-	-	-	-	-	0.0 ± 0.0
070621	fvs18	-	-	-	-	-	-	-	-	-	-	0.0 ± 0.0
070621	fvs19	-	-	-	-	-	-	-	-	-	-	0.0 ± 0.0
070621	fvs20	-	-	-	-	-	-	-	-	-	-	0.0 ± 0.0
070621	fvs21	-	-	-	-	-	-	-	-	-	-	0.0 ± 0.0
070621	fvs22	-	-	-	-	-	-	-	-	-	-	0.0 ± 0.0
070621	fvs23	-	-	-	-	-	-	-	-	-	-	0.0 ± 0.0
070621	fvs24	-	-	-	-	-	-	-	-	-	-	0.0 ± 0.0
070621	fvs25	-	-	-	-	-	-	-	-	-	-	0.0 ± 0.0
070621	fvs26	-	-	-	-	-	-	-	-	-	-	0.0 ± 0.0
070621	fvs27	-	-	-	-	-	-	-	-	-	-	0.0 ± 0.0
070621	fvs28	-	-	-	-	-	-	-	-	-	-	0.0 ± 0.0
070621	fvs29	-	-	-	-	-	-	-	-	-	-	0.0 ± 0.0
070621	fvs30	-	-	-	-	-	-	-	-	-	-	0.0 ± 0.0
070621	fvs31	-	-	-	-	-	-	-	-	-	-	0.0 ± 0.0
070621	fvs32	-	-	-	-	-	-	-	-	-	-	0.0 ± 0.0
070621	fvs33	-	-	-	-	-	-	-	-	-	-	0.0 ± 0.0
070621	fvs34	-	-	-	-	-	-	-	-	-	-	0.0 ± 0.0
070621	fvs35	-	-	-	-	-	-	-	-	-	-	0.0 ± 0.0
070621	fvs36	-	-	-	-	-	-	-	-	-	-	0.0 ± 0.0
070621	fvs37	-	-	-	-	-	-	-	-	-	-	0.0 ± 0.0
070621	fvs38	-	-	-	-	-	-	-	-	-	-	0.0 ± 0.0
070621	fvs39	-	-	-	-	-	-	-	-	-	-	0.0 ± 0.0
070621	fvs40	-	-	-	-	-	-	-	-	-	-	0.0 ± 0.0
070621	fvs41	-	-	-	-	-	-	-	-	-	-	0.0 ± 0.0
070621	fvs42	-	-	-	-	-	-	-	-	-	-	0.0 ± 0.0
070621	fvs43	-	-	-	-	-	-	-	-	-	-	0.0 ± 0.0
070621	fvs44	-	-	-	-	-	-	-	-	-	-	0.0 ± 0.0
070621	fvs45	-	-	-	-	-	-	-	-	-	-	0.0 ± 0.0
070621	fvs46	-	-	-	-	-	-	-	-	-	-	0.0 ± 0.0
070621	fvs47	-	-	-	-	-	-	-	-	-	-	0.0 ± 0.0
070621	fvs48	-	-	-	-	-	-	-	-	-	-	0.0 ± 0.0
070621	fvs49	-	-	-	-	-	-	-	-	-	-	0.0 ± 0.0
070621	fvs50	-	-	-	-	-	-	-	-	-	-	0.0 ± 0.0
070621	fvs51	-	-	-	-	-	-	-	-	-	-	0.0 ± 0.0
070621	fvs52	-	-	-	-	-	-	-	-	-	-	0.0 ± 0.0
070621	fvs53	-	-	-	-	-	-	-	-	-	-	0.0 ± 0.0
070621	fvs54	-	-	-	-	-	-	-	-	-	-	0.0 ± 0.0
070621	fuh1	-	-	-	-	-	-	-	-	-	-	0.0 ± 0.0
070621	fuh2	-	-	-	-	-	-	-	-	-	-	0.0 ± 0.0
070621	fuh3	-	-	-	-	-	-	-	-	-	-	0.0 ± 0.0
070621	fh1	-	-	-	-	-	-	-	-	-	-	0.0 ± 0.0
070621	fh2	-	-	-	-	-	-	-	-	-	-	0.0 ± 0.0
070621	fh3	-	-	-	-	-	-	-	-	-	-	0.0 ± 0.0
070621	tot	-	34.6 ± 2.4	-70.2 ± 23.0	23655.5 ± 60090.0	3.4 ± 3.0	212.0 ± 5.4	61.7 ± 3.6	0.1 ± 0.0	29.2 ± 1.6	32.6 ± 2.9	9.5 ± 6.8
070621	fvs	-	6.9 ± 0.7	72.7 ± 9.8	1329.1 ± 2699.0	14.0 ± 8.1	209.2 ± 5.5	88.6 ± 10.2	0.2 ± 0.1	37.3 ± 7.7	51.3 ± 5.1	2.2 ± 1.2
070621	fms	-	15.6 ± 1.9	-150.8 ± 352.8	47428.0 ± 146100.0	2.8 ± 3.2	212.8 ± 0.0	63.7 ± 6.4	0.0 ± 0.0	30.5 ± 2.0	33.3 ± 4.6	2.5 ± 2.2
070621	fuh	-	4.9 ± 1.7	-236.9 ± 761.1	48567.3 ± 48100.0	2.4 ± 5.5	212.1 ± 25.6	65.5 ± 20.9	0.0 ± 0.1	31.5 ± 7.9	33.9 ± 13.1	1.0 ± 1.5
070621	fvh	-	7.3 ± 3.9	-129.6 ± 784.4	84003.4 ± 667800.0	1.4 ± 4.6	210.9 ± 9.7	43.4 ± 23.0	0.0 ± 0.1	21.0 ± 9.2	22.4 ± 13.8	2.0 ± 4.4
070621	fms1	-	10.9 ± 2.0	153.0 ± 8.8	188.1 ± 128.3	8.0 ± 1.7	192.1 ± 1.0	35.7 ± 1.8	0.2 ± 0.0	29.0 ± 1.2	32.6 ± 2.9	9.5 ± 6.8
070621	fms2	-	16.4 ± 2.3	164.4 ± 12.7	46.2 ± 75.7	32.0 ± 37.6	202.9 ± 5.5	77.0 ± 47.6	0.4 ± 0.2	22.5 ± 6.0	54.5 ± 42.4	19.0 ± 17.0
070621	fms3	-	2.9 ± 12.5	162.0 ± 20.0	20.9 ± 20.0	3.6 ± 3.5	248.1 ± 1.0	21.1 ± 8.0	0.5 ± 0.1	32.5 ± 9.2	52.2 ± 30.0	15.0 ± 15.0
070621	fms4	-	2.9 ± 0.7	242.8 ± 2.3	5.1 ± 4.2	32.3 ± 7.2	255.6 ± 2.2	5.9 ± 6.3	0.6 ± 0.1	9.8 ± 2.4	42.1 ± 6.3	5.4 ± 1.3
070621	fms5	-	21.1 ± 3.0	352.7 ± 5.9	62.4 ± 15.5	145.0 ± 10.0	447.8 ± 4.4	276.1 ± 10.0	0.5 ± 0.0	210.6 ± 9.0	19.0 ± 1.9	0.0 ± 0.0
070621	fms6	-	2.6 ± 4.5	40.2 ± 157.2	851.5 ± 3345.0	15.9 ± 19.8						

**Table 2.** Table of the best-fitting parameters and of the derived physical quantities of the underlying continuum. From left to right: name of the GRB, bandpass (see Sec. 2), parameters describing the fitting function (power law or broken power law): normalization  $N$ , power law indices  $\alpha_1$  and  $\alpha_2$ , break time  $t_{br}$ , boundaries of the flare  $T_{90}$ ,  $\chi^2/dof$  of the simultaneous fit of the flares and of the underlying continuum.

GRB	band	$N$ count s $^{-1}$	$\alpha_1$	$\alpha_2$	$t_{br}$ s	$t_{1,90}$ s	$t_{2,90}$ s	$\chi^2/dof$
050406	tot	229.3 ± 160.0	1.1 ± 0.1	—	—	174.9	262.0	0.7
050406	fvs	664.9 ± 808.2	1.4 ± 0.2	—	—	196.5	254.0	1.3
050406	fms	257.1 ± 439.9	1.4 ± 0.3	—	—	177.9	262.7	0.8
050406	fmh	—	—	—	—	—	—	—
050406	fvh	151.1 ± 265.9	1.4 ± 0.3	—	—	180.6	296.2	0.9
050502B	tot1	42.0 ± 34.0	0.9 ± 0.1	—	—	479.4	1073.9	1.2
050502B	tot2	42.0 ± 34.0	0.9 ± 0.1	—	—	578.7	865.3	1.2
050502B	tot3	42.0 ± 34.0	0.9 ± 0.1	—	—	718.0	844.9	1.2
050502B	fvs1	127.5 ± 241.9	1.2 ± 0.3	—	—	488.5	1142.5	0.9
050502B	fvs2	127.5 ± 241.9	1.2 ± 0.3	—	—	579.1	889.5	0.9
050502B	fvs3	127.5 ± 241.9	1.2 ± 0.3	—	—	723.4	865.7	0.9
050502B	fms1	6.7 ± 14.5	0.8 ± 0.3	—	—	475.1	1035.1	1.2
050502B	fms2	6.7 ± 14.5	0.8 ± 0.3	—	—	577.6	851.3	1.2
050502B	fms3	6.7 ± 14.5	0.8 ± 0.3	—	—	722.7	844.1	1.2
050502B	fmh1	55.8 ± 126.5	1.1 ± 0.4	—	—	460.6	1112.4	0.9
050502B	fmh2	55.8 ± 126.5	1.1 ± 0.4	—	—	584.0	811.5	0.9
050502B	fmh3	55.8 ± 126.5	1.1 ± 0.4	—	—	713.8	814.7	0.9
050502B	fvh1	67.1 ± 1303.0	1.1 ± 2.6	—	—	495.1	990.4	0.9
050502B	fvh2	67.1 ± 1303.0	1.1 ± 2.6	—	—	578.2	785.9	0.9
050502B	fvh3	67.1 ± 1303.0	1.1 ± 2.6	—	—	688.7	825.8	0.9
050607	tot	3580.0 ± 1787.0	1.5 ± 0.1	—	—	276.5	437.2	2.3
050607	fvs	982.2 ± 750.8	1.5 ± 0.1	—	—	281.8	449.2	1.1
050607	fms	1483.2 ± 994.9	1.5 ± 0.1	—	—	271.5	408.4	1.3
050607	fmh	50606.7 ± 45000.0	2.2 ± 0.2	—	—	280.0	440.5	0.7
050607	fvh	1107.5 ± 635.3	1.5 ± 0.1	—	—	274.9	417.3	0.6
050713A	tot1	6.00E10 ± 1.69E11	4.6 ± 0.6	2.3 ± 0.1	97.5 ± 6.9	102.9	133.2	2.0
050713A	tot2	6.00E10 ± 1.69E11	4.6 ± 0.6	2.3 ± 0.1	97.5 ± 6.9	158.4	198.6	2.0
050713A	fvs1	1.00E10 ± 5.44E10	4.6 ± 1.2	1.6 ± 0.8	131.3 ± 39.8	102.5	156.4	1.2
050713A	fvs2	1.00E10 ± 5.44E10	4.6 ± 1.2	1.6 ± 0.8	131.3 ± 39.8	158.6	216.8	1.2
050713A	fms1	1.00E10 ± 2.86E10	4.4 ± 0.6	0.9 ± 0.4	165.3 ± 24.3	103.9	138.8	1.4
050713A	fms2	1.00E10 ± 2.86E10	4.4 ± 0.6	0.9 ± 0.4	165.3 ± 24.3	159.9	188.1	1.4
050713A	fmh1	1.00E10 ± 5.44E10	4.7 ± 1.2	2.2 ± 0.3	97.5 ± 12.9	103.1	125.9	1.1
050713A	fmh2	1.00E10 ± 5.44E10	4.7 ± 1.2	2.2 ± 0.3	97.5 ± 12.9	160.2	177.8	1.1
050713A	fvh1	1.00E11 ± 5.47E11	5.2 ± 1.2	1.7 ± 0.4	120.8 ± 18.5	102.5	122.7	1.5
050713A	fvh2	1.00E11 ± 5.47E11	5.2 ± 1.2	1.7 ± 0.4	120.8 ± 18.5	159.6	235.3	1.5
050714B	tot	—	—	—	—	—	—	—
050714B	fvs	—	—	—	—	—	—	—
050714B	fms	11.7 ± 8.4	0.8 ± 0.1	—	—	310.6	466.1	1.6
050714B	fmh	—	—	—	—	—	—	—
050714B	fvh	—	—	—	—	—	—	—
050716	tot1	1688.7 ± 1334.0	0.8 ± 0.2	2.1 ± 0.2	205.3 ± 12.8	162.0	190.7	0.9
050716	tot2	1688.7 ± 1334.0	0.8 ± 0.2	2.1 ± 0.2	205.3 ± 12.8	346.5	487.8	0.9
050716	fvs1	—	—	—	—	—	—	—
050716	fvs2	—	—	—	—	—	—	—
050716	fms1	190.4 ± 204.9	318.7 ± 0.6	0.3 ± 2.0	0.3 ± 203.7	158.8	190.4	0.9
050716	fms2	474.5 ± 204.9	318.7 ± 0.6	0.3 ± 2.0	0.3 ± 203.7	339.5	474.5	0.9
050716	fmh1	—	—	—	—	—	—	—
050716	fmh2	—	—	—	—	—	—	—
050716	fvh1	—	—	—	—	—	—	—
050726	tot	876.9 ± 268.8	0.9 ± 0.1	—	—	234.0	317.0	0.9
050726	fvs	—	—	—	—	—	—	—
050726	fms	219.4 ± 117.9	0.9 ± 0.1	—	—	240.0	321.6	0.9
050726	fmh	—	—	—	—	—	—	—
050726	fvh	—	—	—	—	—	—	—
050730	tot1	1.00E07 ± 1.19E07	2.5 ± 0.2	0.1 ± 0.1	226.4 ± 11.3	212.7	266.5	1.5
050730	tot2	1.00E07 ± 1.19E07	2.5 ± 0.2	0.1 ± 0.1	226.4 ± 11.3	375.2	511.0	1.5
050730	tot3	1.00E07 ± 1.19E07	2.5 ± 0.2	0.1 ± 0.1	226.4 ± 11.3	645.2	769.1	1.5
050730	fvs1	1.00E07 ± 3.13E07	2.8 ± 0.6	0.1 ± 0.0	226.4 ± 0.0	—	—	—
050730	fvs2	1.00E07 ± 3.13E07	2.8 ± 0.6	0.1 ± 0.0	226.4 ± 0.0	365.5	576.6	1.4
050730	fvs3	1.00E07 ± 3.13E07	2.8 ± 0.6	0.1 ± 0.0	226.4 ± 0.0	611.0	899.1	1.4
050730	fms1	1.00E07 ± 1.60E07	2.7 ± 0.3	0.5 ± 0.2	209.7 ± 17.0	214.9	268.6	1.1
050730	fms2	1.00E07 ± 1.60E07	2.7 ± 0.3	0.5 ± 0.2	209.7 ± 17.0	370.1	511.4	1.1
050730	fms3	1.00E07 ± 1.60E07	2.7 ± 0.3	0.5 ± 0.2	209.7 ± 17.0	632.7	777.7	1.1
050730	fmh1	1.00E07 ± 2.63E07	2.9 ± 0.5	0.0 ± 0.2	243.2 ± 22.5	214.3	247.1	1.1
050730	fmh2	1.00E07 ± 2.63E07	2.9 ± 0.5	0.0 ± 0.2	243.2 ± 22.5	383.9	481.6	1.1
050730	fmh3	1.00E07 ± 2.63E07	2.9 ± 0.5	0.0 ± 0.2	243.2 ± 22.5	665.7	695.8	1.1
050730	fvh1	1.00E07 ± 2.00E07	2.8 ± 0.4	0.1 ± 0.1	239.3 ± 18.1	218.7	247.3	1.1
050730	fvh2	1.00E07 ± 2.00E07	2.8 ± 0.4	0.1 ± 0.1	239.3 ± 18.1	374.9	497.0	1.1
050730	fvh3	1.00E07 ± 2.00E07	2.8 ± 0.4	0.1 ± 0.1	239.3 ± 18.1	659.2	693.1	1.1
050822	tot1	5.00E06 ± 4.39E06	2.4 ± 0.2	—	—	108.3	171.2	2.3
050822	tot2	5.00E06 ± 4.39E06	2.4 ± 0.2	—	—	220.4	263.2	2.3
050822	tot3	5.00E06 ± 4.39E06	2.4 ± 0.2	—	—	410.5	569.7	2.3
050822	fvs1	300000.0 ± 499500.0	2.1 ± 0.3	—	—	114.6	188.9	2.2
050822	fvs2	300000.0 ± 499500.0	2.1 ± 0.3	—	—	210.9	320.5	2.2
050822	fvs3	300000.0 ± 499500.0	2.1 ± 0.3	—	—	412.4	588.2	2.2
050822	fms1	299990.0 ± 414600.0	2.2 ± 0.2	—	—	102.8	174.5	1.4
050822	fms2	299990.0 ± 414600.0	2.2 ± 0.2	—	—	219.8	263.9	1.4
050822	fms3	299990.0 ± 414600.0	2.2 ± 0.2	—	—	406.9	530.0	1.4
050822	fmh1	299990.0 ± 2.27E06	2.3 ± 1.3	—	—	98.2	166.0	1.0
050822	fmh2	299990.0 ± 2.27E06	2.3 ± 1.3	—	—	221.3	260.7	1.0
050822	fmh3	299990.0 ± 2.27E06	2.3 ± 1.3	—	—	—	—	—
050822	fvh1	—	—	—	—	—	—	—
050822	fvh2	—	—	—	—	—	—	—
050822	fvh3	—	—	—	—	—	—	—
050908	tot	3.54E06 ± 9.54E06	2.8 ± 0.5	1.0 ± 0.1	280.3 ± 58.5	365.0	631.9	1.2
050908	fvs	3.54E06 ± 8.64E06	3.0 ± 0.5	1.0 ± 0.1	280.6 ± 61.9	365.0	597.1	1.3
050908	fms	3.54E06 ± 1.48E07	3.0 ± 0.8	1.0 ± 0.1	280.5 ± 72.6	366.1	539.4	1.1
050908	fmh	—	—	—	—	—	—	—
050908	fvh	—	—	—	—	—	—	—
050922B	tot1	4.00E11 ± 2.93E11	3.9 ± 0.1	—	—	636.4	1057.7	2.0
050922B	tot2	4.00E11 ± 2.93E11	3.9 ± 0.1	—	—	783.4	886.7	2.0
050922B	tot3	4.00E11 ± 2.93E11	3.9 ± 0.1	—	—	890.9	1088.9	2.0
050922B	fvs1	6.00E09 ± 3.50E09	3.3 ± 0.1	—	—	668.6	791.5	1.3
050922B	fvs2	6.00E09 ± 3.50E09	3.3 ± 0.1	—	—	730.8	1105.4	1.3
050922B	fvs3	6.00E09 ± 3.50E09	3.3 ± 0.1	—	—	1002.1	1130.5	1.3
050922B	fms1	6.00E09 ± 3.73E09	3.3 ± 0.1	—	—	626.8	910.6	1.7
050922B	fms2	6.00E09 ± 3.73E09	3.3 ± 0.1	—	—	772.6	883.1	1.7
050922B	fms3	6.00E09 ± 3.73E09	3.3 ± 0.1	—	—	891.5	1104.4	1.7
050922B	fmh1	1.00E10 ± 2.55E10	3.7 ± 0.4	—	—	630.4	667.0	1.1
050922B	fmh2	1.00E10 ± 2.55E10	3.7 ± 0.4	—	—	650.7	1115.1	1.1

**Table 2.** Continued

GRB	band	N count s <sup>-1</sup>	$\alpha_1$	$\alpha_2$	$t_{br}$ s	$t_{1,90}$ s	$t_{2,90}$ s	$\chi^2/dof$
050922B	fmh3	$1.00E10 \pm 2.55E10$	$3.7 \pm 0.4$	—	—	1018.4	1152.6	1.1
050922B	fvh1	$4.00E11 \pm 1.19E12$	$4.3 \pm 0.5$	—	—	652.0	661.0	0.8
050922B	fvh2	$4.00E11 \pm 1.19E12$	$4.3 \pm 0.5$	—	—	645.9	1091.4	0.8
050922B	fvh3	$4.00E11 \pm 1.19E12$	$4.3 \pm 0.5$	—	—	927.0	1001.1	0.8
051117A	tot1	$18983.1 \pm 2563.0$	$1.0 \pm 0.0$	—	—	106.8	231.3	1.0
051117A	tot2	$18983.1 \pm 2563.0$	$1.0 \pm 0.0$	—	—	303.3	358.5	1.0
051117A	tot3	$18983.1 \pm 2563.0$	$1.0 \pm 0.0$	—	—	345.0	522.4	1.0
051117A	tot4	$18983.1 \pm 2563.0$	$1.0 \pm 0.0$	—	—	409.2	481.1	1.0
051117A	tot5	$18983.1 \pm 2563.0$	$1.0 \pm 0.0$	—	—	469.2	584.6	1.0
051117A	tot6	$18983.1 \pm 2563.0$	$1.0 \pm 0.0$	—	—	563.8	694.7	1.0
051117A	tot7	$18983.1 \pm 2563.0$	$1.0 \pm 0.0$	—	—	856.3	1130.3	1.0
051117A	tot8	$18983.1 \pm 2563.0$	$1.0 \pm 0.0$	—	—	1053.3	1187.5	1.0
051117A	tot9	$18983.1 \pm 2563.0$	$1.0 \pm 0.0$	—	—	1268.2	1566.4	1.0
051117A	tot10	$18983.1 \pm 2563.0$	$1.0 \pm 0.0$	—	—	1479.3	1829.2	1.0
051117A	fvs1	$4739.2 \pm 634.1$	$1.0 \pm 0.0$	—	—	155.0	222.4	0.9
051117A	fvs2	$4739.2 \pm 634.1$	$1.0 \pm 0.0$	—	—	315.3	347.4	0.9
051117A	fvs3	$4739.2 \pm 634.1$	$1.0 \pm 0.0$	—	—	346.5	645.5	0.9
051117A	fvs4	$4739.2 \pm 634.1$	$1.0 \pm 0.0$	—	—	412.8	480.6	0.9
051117A	fvs5	$4739.2 \pm 634.1$	$1.0 \pm 0.0$	—	—	452.0	565.0	0.9
051117A	fvs6	$4739.2 \pm 634.1$	$1.0 \pm 0.0$	—	—	566.4	710.0	0.9
051117A	fvs7	$4739.2 \pm 634.1$	$1.0 \pm 0.0$	—	—	842.4	1285.6	0.9
051117A	fvs8	$4739.2 \pm 634.1$	$1.0 \pm 0.0$	—	—	1037.5	1211.6	0.9
051117A	fvs9	$4739.2 \pm 634.1$	$1.0 \pm 0.0$	—	—	1273.3	1663.7	0.9
051117A	fvs10	$4739.2 \pm 634.1$	$1.0 \pm 0.0$	—	—	1475.1	2426.7	0.9
051117A	fms1	$7777.9 \pm 956.5$	$1.0 \pm 0.0$	—	—	107.5	218.5	0.9
051117A	fms2	$7777.9 \pm 956.5$	$1.0 \pm 0.0$	—	—	298.5	373.5	0.9
051117A	fms3	$7777.9 \pm 956.5$	$1.0 \pm 0.0$	—	—	350.7	499.5	0.9
051117A	fms4	$7777.9 \pm 956.5$	$1.0 \pm 0.0$	—	—	408.2	472.3	0.9
051117A	fms5	$7777.9 \pm 956.5$	$1.0 \pm 0.0$	—	—	466.9	541.9	0.9
051117A	fms6	$7777.9 \pm 956.5$	$1.0 \pm 0.0$	—	—	548.4	683.2	0.9
051117A	fms7	$7777.9 \pm 956.5$	$1.0 \pm 0.0$	—	—	868.2	1091.5	0.9
051117A	fms8	$7777.9 \pm 956.5$	$1.0 \pm 0.0$	—	—	1051.8	1172.6	0.9
051117A	fms9	$7777.9 \pm 956.5$	$1.0 \pm 0.0$	—	—	1267.8	1537.9	0.9
051117A	fms10	$7777.9 \pm 956.5$	$1.0 \pm 0.0$	—	—	1473.9	1763.3	0.9
051117A	fmh1	$1629.2 \pm 382.8$	$1.0 \pm 0.0$	—	—	86.5	207.0	1.0
051117A	fmh2	$1629.2 \pm 382.8$	$1.0 \pm 0.0$	—	—	306.1	334.8	1.0
051117A	fmh3	$1629.2 \pm 382.8$	$1.0 \pm 0.0$	—	—	335.2	473.1	1.0
051117A	fmh4	$1629.2 \pm 382.8$	$1.0 \pm 0.0$	—	—	409.7	462.9	1.0
051117A	fmh5	$1629.2 \pm 382.8$	$1.0 \pm 0.0$	—	—	467.9	586.3	1.0
051117A	fmh6	$1629.2 \pm 382.8$	$1.0 \pm 0.0$	—	—	545.5	684.5	1.0
051117A	fmh7	$1629.2 \pm 382.8$	$1.0 \pm 0.0$	—	—	861.7	1075.3	1.0
051117A	fmh8	$1629.2 \pm 382.8$	$1.0 \pm 0.0$	—	—	1051.6	1155.1	1.0
051117A	fmh9	$1629.2 \pm 382.8$	$1.0 \pm 0.0$	—	—	1268.2	1502.0	1.0
051117A	fmh10	$1629.2 \pm 382.8$	$1.0 \pm 0.0$	—	—	1474.8	1831.3	1.0
051117A	fvh1	$1625.7 \pm 466.7$	$1.0 \pm 0.0$	—	—	106.7	244.3	0.9
051117A	fvh2	$1625.7 \pm 466.7$	$1.0 \pm 0.0$	—	—	300.8	351.4	0.9
051117A	fvh3	$1625.7 \pm 466.7$	$1.0 \pm 0.0$	—	—	340.2	511.3	0.9
051117A	fvh4	$1625.7 \pm 466.7$	$1.0 \pm 0.0$	—	—	412.4	458.9	0.9
051117A	fvh5	$1625.7 \pm 466.7$	$1.0 \pm 0.0$	—	—	474.8	539.9	0.9
051117A	fvh6	$1625.7 \pm 466.7$	$1.0 \pm 0.0$	—	—	553.6	677.1	0.9
051117A	fvh7	$1625.7 \pm 466.7$	$1.0 \pm 0.0$	—	—	861.0	1060.6	0.9
051117A	fvh8	$1625.7 \pm 466.7$	$1.0 \pm 0.0$	—	—	1046.5	1154.1	0.9
051117A	fvh9	$1625.7 \pm 466.7$	$1.0 \pm 0.0$	—	—	1272.5	1512.0	0.9
051117A	fvh10	$1625.7 \pm 466.7$	$1.0 \pm 0.0$	—	—	1501.6	1754.8	0.9
051210	tot1	$1.05E06 \pm 524900.0$	$2.5 \pm 0.1$	—	—	122.0	150.5	1.3
051210	tot2	$1.05E06 \pm 524900.0$	$2.5 \pm 0.1$	—	—	158.8	190.9	1.3
051210	fvs1	$561414.0 \pm 630200.0$	$2.7 \pm 0.2$	—	—	124.8	153.3	1.2
051210	fvs2	$561414.0 \pm 630200.0$	$2.7 \pm 0.2$	—	—	165.3	194.3	1.2
051210	fms1	$209178.0 \pm 176100.0$	$2.4 \pm 0.2$	—	—	116.4	164.4	1.7
051210	fms2	$209178.0 \pm 176100.0$	$2.4 \pm 0.2$	—	—	174.1	186.8	1.7
051210	fmh1	$207974.0 \pm 297600.0$	$2.6 \pm 0.3$	—	—	—	—	—
051210	fmh2	$207974.0 \pm 297600.0$	$2.6 \pm 0.3$	—	—	—	—	—
051210	fvh1	$1.05E06 \pm 1.39E06$	$2.8 \pm 0.3$	—	—	123.1	138.9	0.9
051210	fvh2	$1.05E06 \pm 1.39E06$	$2.8 \pm 0.3$	—	—	152.0	184.0	0.9
051227	tot	$3163.2 \pm 6882.0$	$1.3 \pm 0.4$	—	—	109.2	148.0	0.9
051227	fvs	$— \pm —$	$— \pm —$	—	—	—	—	—
051227	fms	$35.7 \pm 108.5$	$0.6 \pm 0.6$	—	—	110.3	146.7	0.7
051227	fmh	$3163.2 \pm 24840.0$	$1.7 \pm 1.7$	—	—	110.2	163.2	0.4
051227	fvh	$— \pm —$	$— \pm —$	—	—	—	—	—
060111A	tot1	$106.4 \pm 29.8$	$0.8 \pm 0.0$	$— \pm —$	$— \pm —$	57.7	138.9	1.2
060111A	tot2	$106.4 \pm 29.8$	$0.8 \pm 0.0$	$— \pm —$	$— \pm —$	140.9	219.4	1.2
060111A	tot3	$106.4 \pm 29.8$	$0.8 \pm 0.0$	$— \pm —$	$— \pm —$	239.1	340.7	1.2
060111A	tot4	$106.4 \pm 29.8$	$0.8 \pm 0.0$	$— \pm —$	$— \pm —$	315.2	528.0	1.2
060111A	fvs1	$24.9 \pm 12.8$	$0.8 \pm 0.1$	$— \pm —$	$— \pm —$	66.8	140.9	1.0
060111A	fvs2	$24.9 \pm 12.8$	$0.8 \pm 0.1$	$— \pm —$	$— \pm —$	135.9	232.1	1.0
060111A	fvs3	$24.9 \pm 12.8$	$0.8 \pm 0.1$	$— \pm —$	$— \pm —$	232.4	355.7	1.0
060111A	fvs4	$24.9 \pm 12.8$	$0.8 \pm 0.1$	$— \pm —$	$— \pm —$	314.2	683.4	1.0
060111A	fms1	$35.2 \pm 13.2$	$0.8 \pm 0.0$	$— \pm —$	$— \pm —$	50.5	140.6	1.0
060111A	fms2	$35.2 \pm 13.2$	$0.8 \pm 0.0$	$— \pm —$	$— \pm —$	146.7	226.3	1.0
060111A	fms3	$35.2 \pm 13.2$	$0.8 \pm 0.0$	$— \pm —$	$— \pm —$	239.7	334.5	1.0
060111A	fms4	$35.2 \pm 13.2$	$0.8 \pm 0.0$	$— \pm —$	$— \pm —$	315.6	501.9	1.0
060111A	fmh1	$6.4 \pm 3.7$	$0.8 \pm 0.1$	$— \pm —$	$— \pm —$	38.2	127.2	1.1
060111A	fmh2	$6.4 \pm 3.7$	$0.8 \pm 0.1$	$— \pm —$	$— \pm —$	137.7	207.2	1.1
060111A	fmh3	$6.4 \pm 3.7$	$0.8 \pm 0.1$	$— \pm —$	$— \pm —$	246.4	329.9	1.1
060111A	fmh4	$6.4 \pm 3.7$	$0.8 \pm 0.1$	$— \pm —$	$— \pm —$	313.3	508.3	1.1
060111A	fvh1	$9.0 \pm 5.5$	$0.8 \pm 0.1$	$— \pm —$	$— \pm —$	50.5	139.6	1.1
060111A	fvh2	$9.0 \pm 5.5$	$0.8 \pm 0.1$	$— \pm —$	$— \pm —$	138.1	238.2	1.1
060111A	fvh3	$9.0 \pm 5.5$	$0.8 \pm 0.1$	$— \pm —$	$— \pm —$	247.7	344.5	1.1
060111A	fvh4	$9.0 \pm 5.5$	$0.8 \pm 0.1$	$— \pm —$	$— \pm —$	319.5	539.7	1.1
060115	tot	$648687.0 \pm 373000.0$	$2.2 \pm 0.1$	$— \pm —$	$— \pm —$	375.1	505.0	0.8
060115	fvs	$648656.0 \pm 688100.0$	$2.3 \pm 0.2$	$— \pm —$	$— \pm —$	376.5	518.9	0.9
060115	fms	$648353.0 \pm 742000.0$	$2.3 \pm 0.2$	$— \pm —$	$— \pm —$	375.8	488.3	0.9
060115	fmh	$648353.0 \pm 1.67E06$	$2.5 \pm 0.4$	$— \pm —$	$— \pm —$	378.8	478.8	0.8
060115	fvh	$648003.0 \pm 797200.0$	$2.4 \pm 0.2$	$— \pm —$	$— \pm —$	364.4	494.6	0.5
060204B	tot1	$1.00E07 \pm 1.85E07$	$2.7 \pm 0.3$	$0.7 \pm 1.2$	$300.9 \pm 106.5$	104.8	135.6	2.0
060204B	tot2	$1.00E07 \pm 1.85E07$	$2.7 \pm 0.3$	$0.7 \pm 1.2$	$300.9 \pm 106.5$	299.1	374.7	2.0
060204B	fvs1	$1.95E08 \pm 3.30E08$	$3.5 \pm 0.3$	$0.6 \pm 8.9$	$303.2 \pm 510.2$	109.3	145.7	1.0
060204B	fvs2	$1.95E08 \pm 3.30E08$	$3.5 \pm 0.3$	$0.6 \pm 8.9$	$303.2 \pm 510.2$	302.8	401.9	1.0
060204B	fms1	$1.95E08 \pm 7.62E08$	$3.5 \pm 0.8$	$1.8 \pm 0.4$	$209.2 \pm 33.5$	105.9	137.0	1.2
060204B	fms2	$1.95E08 \pm 7.62E08$ </						

**Table 2.** Continued

GRB	band	N count s <sup>-1</sup>	$\alpha_1$	$\alpha_2$	$t_{br}$ s	$t_{1,90}$ s	$t_{2,90}$ s	$\chi^2/dof$
060210	fvs1	1.50E06 ± 2.89E06	2.4 ± 0.4	0.2 ± 0.5	215.9 ± 47.3	168.1	269.6	1.5
060210	fvs2	1.50E06 ± 2.89E06	2.4 ± 0.4	0.2 ± 0.5	215.9 ± 47.3	340.0	475.6	1.5
060210	fms1	4.01E07 ± 6.34E07	3.0 ± 0.3	0.8 ± 0.2	192.9 ± 21.2	169.9	245.9	1.7
060210	fms2	4.01E07 ± 6.34E07	3.0 ± 0.3	0.8 ± 0.2	192.9 ± 21.2	356.0	430.2	1.7
060210	fmh1	1.50E08 ± 3.59E08	3.5 ± 0.5	0.9 ± 0.4	205.5 ± 31.0	169.3	237.2	1.3
060210	fmh2	1.50E08 ± 3.59E08	3.5 ± 0.5	0.9 ± 0.4	205.5 ± 31.0	358.3	417.5	1.3
060210	fvh1	1.00E10 ± 2.65E10	4.3 ± 0.6	0.4 ± 0.4	213.9 ± 25.9	172.7	230.6	2.3
060210	fvh2	1.00E10 ± 2.65E10	4.3 ± 0.6	0.4 ± 0.4	213.9 ± 25.9	362.2	394.5	2.3
060312	tot	999992.0 ± 1.24E06	2.6 ± 0.3	0.8 ± 0.1	258.7 ± 61.5	83.7	135.7	4.6
060312	fvs	—	—	—	—	—	—	—
060312	fms	—	—	—	—	—	—	—
060312	fmh	—	—	—	—	—	—	—
060312	fvh	1.00E06 ± 1.23E07	3.0 ± 3.0	1.6 ± 0.5	127.4 ± 181.4	85.3	132.5	3.2
060413	tot	3815.8 ± 2132.0	1.2 ± 0.1	—	—	562.8	823.8	1.0
060413	fvs	—	—	—	—	—	—	—
060413	fms	23829.9 ± 38850.0	1.8 ± 0.3	—	—	516.2	908.3	0.9
060413	fmh	1414.6 ± 1836.0	1.3 ± 0.2	—	—	544.7	840.5	1.0
060413	fvh	598.8 ± 459.5	1.0 ± 0.1	—	—	558.5	830.4	1.0
060418	tot	1.00E12 ± 1.46E12	4.9 ± 0.3	1.9 ± 0.0	108.5 ± 2.3	123.3	165.2	1.9
060418	fvs	5.00E10 ± 8.95E10	4.5 ± 0.4	0.7 ± 0.0	171.3 ± 11.0	119.9	207.4	1.6
060418	fms	1.00E13 ± 1.29E13	5.6 ± 0.3	1.4 ± 0.0	134.6 ± 3.6	122.0	167.8	1.5
060418	fmh	1.00E12 ± 3.56E12	5.4 ± 0.8	1.7 ± 0.1	108.3 ± 4.2	122.9	148.5	1.0
060418	fvh	1.00E11 ± 5.73E11	5.0 ± 1.3	1.5 ± 0.1	105.7 ± 6.2	123.7	149.0	1.7
060512	tot	1.00E07 ± 2.09E07	2.9 ± 0.4	1.1 ± 0.0	190.8 ± 24.4	174.6	290.2	0.8
060512	fvs	1.00E07 ± 2.36E07	3.0 ± 0.5	1.1 ± 0.1	292.2 ± 76.4	176.7	329.3	0.8
060512	fms	1.00E07 ± 6.53E08	3.4 ± 13.9	1.1 ± 0.0	118.1 ± 31.1	176.8	283.5	0.7
060512	fmh	—	—	—	—	—	—	—
060512	fvh	—	—	—	—	—	—	—
060526	tot1	3155.0 ± 1134.0	1.4 ± 0.1	-0.4 ± 0.1	1142.4 ± 231.1	240.0	268.4	1.0
060526	tot2	3155.0 ± 1134.0	1.4 ± 0.1	-0.4 ± 0.1	1142.4 ± 231.1	261.6	313.0	1.0
060526	tot3	3155.0 ± 1134.0	1.4 ± 0.1	-0.4 ± 0.1	1142.4 ± 231.1	289.3	354.6	1.0
060526	tot4	3155.0 ± 1134.0	1.4 ± 0.1	-0.4 ± 0.1	1142.4 ± 231.1	318.0	440.4	1.0
060526	fvs1	475.2 ± 203.9	1.2 ± 0.1	-0.4 ± 0.2	1287.8 ± 587.6	242.5	269.9	1.0
060526	fvs2	475.2 ± 203.9	1.2 ± 0.1	-0.4 ± 0.2	1287.8 ± 587.6	262.1	336.3	1.0
060526	fvs3	475.2 ± 203.9	1.2 ± 0.1	-0.4 ± 0.2	1287.8 ± 587.6	291.4	367.0	1.0
060526	fvs4	475.2 ± 203.9	1.2 ± 0.1	-0.4 ± 0.2	1287.8 ± 587.6	319.0	460.6	1.0
060526	fms1	449.9 ± 209.9	1.2 ± 0.1	-0.3 ± 0.1	1320.1 ± 401.4	240.6	275.8	0.9
060526	fms2	449.9 ± 209.9	1.2 ± 0.1	-0.3 ± 0.1	1320.1 ± 401.4	266.8	292.2	0.9
060526	fms3	449.9 ± 209.9	1.2 ± 0.1	-0.3 ± 0.1	1320.1 ± 401.4	279.0	346.2	0.9
060526	fms4	449.9 ± 209.9	1.2 ± 0.1	-0.3 ± 0.1	1320.1 ± 401.4	330.8	452.5	0.9
060526	fmh1	199.9 ± 140.4	1.2 ± 0.1	0.7 ± 0.9	3763.6 ± 1053.0	240.4	264.6	1.4
060526	fmh2	199.9 ± 140.4	1.2 ± 0.1	0.7 ± 0.9	3763.6 ± 1053.0	258.5	283.4	1.4
060526	fmh3	199.9 ± 140.4	1.2 ± 0.1	0.7 ± 0.9	3763.6 ± 1053.0	283.6	324.4	1.4
060526	fmh4	199.9 ± 140.4	1.2 ± 0.1	0.7 ± 0.9	3763.6 ± 1053.0	318.4	396.6	1.4
060526	fvh1	233.8 ± 169.5	1.3 ± 0.1	-0.3 ± 1.0	1838.2 ± 2601.0	240.4	263.4	1.3
060526	fvh2	233.8 ± 169.5	1.3 ± 0.1	-0.3 ± 1.0	1838.2 ± 2601.0	258.3	300.4	1.3
060526	fvh3	233.8 ± 169.5	1.3 ± 0.1	-0.3 ± 1.0	1838.2 ± 2601.0	318.7	432.7	1.3
060602B	tot	58.9 ± 24.5	0.8 ± 0.1	—	—	123.8	324.4	1.3
060602B	fvs	—	—	—	—	—	—	—
060602B	fms	—	—	—	—	—	—	—
060602B	fmh	56.8 ± 29.5	1.0 ± 0.1	—	—	113.9	506.4	0.5
060602B	fvh	20.5 ± 8.0	0.8 ± 0.1	—	—	132.8	300.8	0.9
060604	tot1	5.00E08 ± 6.00E08	3.4 ± 0.2	—	—	126.1	167.0	2.5
060604	tot2	5.00E08 ± 6.00E08	3.4 ± 0.2	—	—	164.9	198.5	2.5
060604	fvs1	5.04E06 ± 1.15E07	2.6 ± 0.5	—	—	125.5	181.2	1.8
060604	fvs2	5.04E06 ± 1.15E07	2.6 ± 0.5	—	—	163.9	217.7	1.8
060604	fms1	2.94E10 ± 4.87E10	4.4 ± 0.3	—	—	125.9	170.9	1.3
060604	fms2	2.94E10 ± 4.87E10	4.4 ± 0.3	—	—	165.7	189.3	1.3
060604	fmh1	2.94E10 ± 2.34E11	4.7 ± 1.7	—	—	124.7	162.6	1.3
060604	fmh2	2.94E10 ± 2.34E11	4.7 ± 1.7	—	—	165.1	185.9	1.3
060604	fvh1	2.94E10 ± 1.23E11	4.7 ± 0.9	—	—	127.8	155.5	1.4
060604	fvh2	2.94E10 ± 1.23E11	4.7 ± 0.9	—	—	164.9	178.3	1.4
060607A	tot1	7766.3 ± 1447.0	1.1 ± 0.0	—	—	93.5	117.1	2.2
060607A	tot2	7766.3 ± 1447.0	1.1 ± 0.0	—	—	225.8	321.3	2.2
060607A	fvs1	1811.6 ± 1042.0	1.1 ± 0.1	—	—	102.1	132.7	1.3
060607A	fvs2	1811.6 ± 1042.0	1.1 ± 0.1	—	—	226.7	346.1	1.3
060607A	fms1	3012.3 ± 856.7	1.1 ± 0.1	—	—	93.8	117.1	1.7
060607A	fms2	3012.3 ± 856.7	1.1 ± 0.1	—	—	228.8	309.9	1.7
060607A	fmh1	17454.0 ± 389700.0	2.4 ± 0.5	—	—	93.5	114.1	1.2
060607A	fmh2	17454.0 ± 389700.0	2.4 ± 0.5	—	—	225.6	314.5	1.2
060607A	fvh1	161.4 ± 75.0	0.8 ± 0.1	—	—	93.0	111.1	1.5
060607A	fvh2	161.4 ± 75.0	0.8 ± 0.1	—	—	223.7	299.0	1.5
060707	tot	7946.7 ± 3807.0	1.5 ± 0.1	—	—	177.8	215.7	1.5
060707	fvs	—	—	—	—	—	—	—
060707	fms	7953.2 ± 7553.0	1.7 ± 0.2	—	—	176.0	264.6	1.3
060707	fmh	—	—	—	—	—	—	—
060707	fvh	7947.1 ± 13170.0	1.8 ± 0.3	—	—	161.2	222.3	1.2
060714	tot1	15.4 ± 13.9	0.4 ± 0.1	—	—	105.0	189.9	1.1
060714	tot2	15.4 ± 13.9	0.4 ± 0.1	—	—	127.5	136.9	1.1
060714	tot3	15.4 ± 13.9	0.4 ± 0.1	—	—	134.6	153.7	1.1
060714	tot4	15.4 ± 13.9	0.4 ± 0.1	—	—	165.8	191.4	1.1
060714	fvs1	11.6 ± 6.2	0.6 ± 0.1	—	—	106.3	217.7	0.8
060714	fvs2	11.6 ± 6.2	0.6 ± 0.1	—	—	120.6	149.2	0.8
060714	fvs3	11.6 ± 6.2	0.6 ± 0.1	—	—	139.3	159.7	0.8
060714	fvs4	11.6 ± 6.2	0.6 ± 0.1	—	—	160.1	209.3	0.8
060714	fms1	12.7 ± 6.6	0.6 ± 0.1	—	—	103.1	188.6	1.0
060714	fms2	12.7 ± 6.6	0.6 ± 0.1	—	—	125.5	138.2	1.0
060714	fms3	12.7 ± 6.6	0.6 ± 0.1	—	—	134.6	154.4	1.0
060714	fms4	12.7 ± 6.6	0.6 ± 0.1	—	—	163.7	188.3	1.0
060714	fmh1	0.8 ± 1.8	0.3 ± 0.3	—	—	106.4	176.9	1.0
060714	fmh2	0.8 ± 1.8	0.3 ± 0.3	—	—	126.0	137.5	1.0
060714	fmh3	0.8 ± 1.8	0.3 ± 0.3	—	—	135.9	149.1	1.0
060714	fmh4	0.8 ± 1.8	0.3 ± 0.3	—	—	166.2	186.5	1.0
060714	fvh1	0.4 ± 0.8	0.2 ± 0.3	—	—	98.8	130.9	1.2
060714	fvh2	0.4 ± 0.8	0.2 ± 0.3	—	—	125.2	136.6	1.2
060714	fvh3	0.4 ± 0.8	0.2 ± 0.3	—	—	133.2	146.7	1.2
060714	fvh4	0.4 ± 0.8	0.2 ± 0.3	—	—	166.4	185.3	1.2
060719	tot	0.0 ± 1258.1	2392.0 ± 1.3	0.3 ± —	—	188.5	225.3	1.8
060719	fvs	—	—	—	—	—	—	—
060719	fms	9.0 ± 1258.0	2947.0 ± 1.5	0.4 ± —	—	188.5	217.0	1.2
060719	fmh	—	—	—	—	—	—	—
060719	fvh	—	—	—	—	—	—	—
060719	fvs1	8.4 ± 0.3	4.4 ± 0.5	197.3 ± 12.8	166.8	215.4	1.3	
060719	fms1	7.0E21 ± 1.18E22	8.9 ± 0.3	6.0 ± 1.0	195.9 ± 30.0	166.9	208.8	1.2

**Table 2.** Continued

GRB	band	N count s <sup>-1</sup>	$\alpha_1$	$\alpha_2$	$t_{br}$ s	$t_{1,90}$ s	$t_{2,90}$ s	$\chi^2/dof$	
060729	fmh	$1.0E29 \pm 3.88E29$	$12.6 \pm 0.8$	$3.7 \pm 1.9$	$188.4 \pm 18.8$	166.9	199.3	1.1	
060729	fvh	$- \pm -$	$- \pm -$	$- \pm -$	$- \pm -$	-	-	-	
060804	tot	$7.0 \pm 17.6$	$4.8 \pm 0.5$	$0.0 \pm -$	$- \pm -$	422.2	662.1	0.8	
060804	fvs	$- \pm -$	$- \pm -$	$- \pm -$	$- \pm -$	-	-	-	
060804	fms	$- \pm -$	$- \pm -$	$- \pm -$	$- \pm -$	-	-	-	
060804	fmh	$1.3 \pm 0.8$	$0.4 \pm 0.1$	$- \pm -$	$- \pm -$	389.1	583.8	0.6	
060804	fvh	$3.6 \pm 1.7$	$0.5 \pm 0.1$	$- \pm -$	$- \pm -$	419.1	671.8	0.5	
060814	tot	$661685.0 \pm 138000.0$	$1.7 \pm 0.0$	$3.2 \pm 0.1$	$257.9 \pm 8.5$	122.5	179.0	1.0	
060814	fvs	$- \pm -$	$- \pm -$	$- \pm -$	$- \pm -$	-	-	-	
060814	fms	$103319.0 \pm 32560.0$	$1.5 \pm 0.1$	$3.4 \pm 0.1$	$247.4 \pm 8.6$	122.4	186.7	1.1	
060814	fmh	$314849.0 \pm 127000.0$	$1.9 \pm 0.1$	$3.7 \pm 0.3$	$238.9 \pm 13.4$	123.3	164.8	1.1	
060814	fvh	$3.55E06 \pm 1.39E06$	$2.3 \pm 0.1$	$3.6 \pm 0.3$	$258.6 \pm 23.8$	121.5	168.6	1.4	
060904A	tot1	$1.00E09 \pm 4.42E08$	$3.5 \pm 0.1$	$1.0 \pm 0.0$	$307.9 \pm 17.5$	272.0	360.8	4.2	
060904A	tot2	$1.00E09 \pm 4.42E08$	$3.5 \pm 0.1$	$1.0 \pm 0.0$	$307.9 \pm 17.5$	661.5	840.2	4.2	
060904A	fvs1	$- \pm -$	$- \pm -$	$- \pm -$	$- \pm -$	-	-	-	
060904A	fvs2	$- \pm -$	$- \pm -$	$- \pm -$	$- \pm -$	-	-	-	
060904A	fms1	$1.00E09 \pm 4.90E08$	$3.7 \pm 0.1$	$1.0 \pm 0.0$	$291.9 \pm 16.2$	273.2	330.0	2.3	
060904A	fms2	$1.00E09 \pm 4.90E08$	$3.7 \pm 0.1$	$1.0 \pm 0.0$	$291.9 \pm 16.2$	633.9	661.0	2.3	
060904A	fmh1	$- \pm -$	$- \pm -$	$- \pm -$	$- \pm -$	-	-	-	
060904A	fmh2	$- \pm -$	$- \pm -$	$- \pm -$	$- \pm -$	-	-	-	
060904A	fvh1	$- \pm -$	$- \pm -$	$- \pm -$	$- \pm -$	-	-	-	
060904A	fvh2	$- \pm -$	$- \pm -$	$- \pm -$	$- \pm -$	-	-	-	
060904B	tot	$178.3 \pm 48.7$	$0.8 \pm 0.0$	$1.3 \pm 0.1$	$5017.0 \pm 1400.0$	142.5	246.6	2.0	
060904B	fvs	$75.6 \pm 32.3$	$0.9 \pm 0.1$	$1.4 \pm 0.2$	$16858.2 \pm 11000.0$	148.9	291.7	1.4	
060904B	fms	$54.5 \pm 18.8$	$0.7 \pm 0.1$	$1.4 \pm 0.1$	$5304.9 \pm 1404.0$	144.3	246.4	1.1	
060904B	fmh	$19.0 \pm 11.6$	$0.8 \pm 0.1$	$3.0 \pm 0.5$	$8654.5 \pm 1347.0$	142.4	224.5	1.3	
060904B	fvh	$0.0 \pm 0.1$	$-0.8 \pm 1.0$	$1.3 \pm 0.1$	$218.6 \pm 78.5$	141.9	207.5	1.1	
060908	tot1	$158.1 \pm 65.7$	$0.7 \pm 0.1$	$- \pm -$	$- \pm -$	503.2	745.3	0.8	
060908	tot2	$158.1 \pm 65.7$	$0.7 \pm 0.1$	$- \pm -$	$- \pm -$	747.0	967.7	0.8	
060908	fvs1	$36.0 \pm 19.8$	$0.6 \pm 0.1$	$- \pm -$	$- \pm -$	504.3	794.0	0.5	
060908	fvs2	$36.0 \pm 19.8$	$0.6 \pm 0.1$	$- \pm -$	$- \pm -$	789.8	953.4	0.5	
060908	fms1	$72.9 \pm 74.1$	$0.8 \pm 0.2$	$- \pm -$	$- \pm -$	462.8	741.7	1.0	
060908	fms2	$72.9 \pm 74.1$	$0.8 \pm 0.2$	$- \pm -$	$- \pm -$	697.2	979.5	1.0	
060908	fmh1	$- \pm -$	$- \pm -$	$- \pm -$	$- \pm -$	-	-	-	
060908	fmh2	$- \pm -$	$- \pm -$	$- \pm -$	$- \pm -$	-	-	-	
060908	fvh2	$- \pm -$	$- \pm -$	$- \pm -$	$- \pm -$	-	-	-	
060929	tot	$9.3 \pm 9.0$	$0.7 \pm 0.1$	$-$	$-$	470.7	664.4	2.4	
060929	fvs	$2.5 \pm 3.3$	$0.6 \pm 0.2$	$-$	$-$	473.0	698.2	1.2	
060929	fms	$7.5 \pm 8.7$	$0.8 \pm 0.2$	$-$	$-$	475.4	657.0	1.4	
060929	fmh	$0.1 \pm 0.3$	$0.3 \pm 0.4$	$-$	$-$	465.6	631.1	1.4	
060929	fvh	$0.0 \pm 0.1$	$0.0 \pm 0.5$	$-$	$-$	474.0	622.3	1.7	
061202	tot1	$100020.0 \pm 415700.0$	$1.7 \pm 0.8$	$-$	$-$	129.0	161.4	1.6	
061202	tot2	$100020.0 \pm 415700.0$	$1.7 \pm 0.8$	$-$	$-$	155.9	190.2	1.6	
061202	fvs1	$899983.0 \pm 1.96E06$	$2.6 \pm 0.4$	$-$	$-$	134.9	155.0	1.3	
061202	fvs2	$899983.0 \pm 1.96E06$	$2.6 \pm 0.4$	$-$	$-$	160.7	180.4	1.3	
061202	fms1	$394502.0 \pm 1.34E06$	$2.1 \pm 0.6$	$-$	$-$	129.8	184.7	0.8	
061202	fms2	$394502.0 \pm 1.34E06$	$2.1 \pm 0.6$	$-$	$-$	165.0	185.8	0.8	
061202	fmh1	$794502.0 \pm 4.99E06$	$2.4 \pm 1.1$	$-$	$-$	128.5	168.0	1.3	
061202	fmh2	$794502.0 \pm 4.99E06$	$2.4 \pm 1.1$	$-$	$-$	170.6	183.3	1.3	
061202	fvh1	$326399.0 \pm 1.27E06$	$2.2 \pm 0.7$	$-$	$-$	128.0	161.0	1.9	
061202	fvh2	$326399.0 \pm 1.27E06$	$2.2 \pm 0.7$	$-$	$-$	170.6	178.2	1.9	
070107	tot1	$724.3 \pm 258.5$	$0.9 \pm 0.1$	$-$	$-$	314.4	371.5	1.1	
070107	tot2	$724.3 \pm 258.5$	$0.9 \pm 0.1$	$-$	$-$	343.7	493.4	1.1	
070107	tot3	$724.3 \pm 258.5$	$0.9 \pm 0.1$	$-$	$-$	390.8	399.8	1.1	
070107	tot4	$724.3 \pm 258.5$	$0.9 \pm 0.1$	$-$	$-$	427.6	480.7	1.1	
070107	tot5	$724.3 \pm 258.5$	$0.9 \pm 0.1$	$-$	$-$	1288.1	1614.8	1.1	
070107	fvs1	$44.8 \pm 23.1$	$0.7 \pm 0.1$	$-$	$-$	314.8	422.3	0.8	
070107	fvs2	$44.8 \pm 23.1$	$0.7 \pm 0.1$	$-$	$-$	347.3	524.5	0.8	
070107	fvs3	$44.8 \pm 23.1$	$0.7 \pm 0.1$	$-$	$-$	386.0	407.3	0.8	
070107	fvs4	$44.8 \pm 23.1$	$0.7 \pm 0.1$	$-$	$-$	414.6	490.2	0.8	
070107	fvs5	$44.8 \pm 23.1$	$0.7 \pm 0.1$	$-$	$-$	1285.4	1802.8	0.8	
070107	fms1	$714.2 \pm 330.0$	$1.0 \pm 0.1$	$-$	$-$	314.2	465.1	1.4	
070107	fms2	$714.2 \pm 330.0$	$1.0 \pm 0.1$	$-$	$-$	344.0	453.1	1.4	
070107	fms3	$714.2 \pm 330.0$	$1.0 \pm 0.1$	$-$	$-$	411.2	428.5	1.4	
070107	fms4	$714.2 \pm 330.0$	$1.0 \pm 0.1$	$-$	$-$	434.3	508.9	1.4	
070107	fms5	$714.2 \pm 330.0$	$1.0 \pm 0.1$	$-$	$-$	1259.0	1869.4	1.4	
070107	fmh1	$14.5 \pm 8.6$	$0.5 \pm 0.1$	$-$	$-$	309.6	465.3	1.1	
070107	fmh2	$14.5 \pm 8.6$	$0.5 \pm 0.1$	$-$	$-$	353.6	429.0	1.1	
070107	fmh3	$14.5 \pm 8.6$	$0.5 \pm 0.1$	$-$	$-$	384.6	434.1	1.1	
070107	fmh4	$14.5 \pm 8.6$	$0.5 \pm 0.1$	$-$	$-$	431.1	471.2	1.1	
070107	fmh5	$14.5 \pm 8.6$	$0.5 \pm 0.1$	$-$	$-$	1274.0	1906.1	1.1	
070107	fvh1	$37.2 \pm 21.2$	$0.6 \pm 0.1$	$-$	$-$	299.9	430.3	0.9	
070107	fvh2	$37.2 \pm 21.2$	$0.6 \pm 0.1$	$-$	$-$	319.2	327.9	0.9	
070107	fvh3	$37.2 \pm 21.2$	$0.6 \pm 0.1$	$-$	$-$	385.0	409.4	0.9	
070107	fvh4	$37.2 \pm 21.2$	$0.6 \pm 0.1$	$-$	$-$	427.4	479.1	0.9	
070107	fvh5	$37.2 \pm 21.2$	$0.6 \pm 0.1$	$-$	$-$	1140.0	1604.7	0.9	
070220	tot	$188.3 \pm 88.7$	$0.7 \pm 0.1$	$-$	$-$	532.8	566.3	1.2	
070220	fvs	$- \pm -$	$- \pm -$	$-$	$-$	-	-	-	
070220	fms	$66.7 \pm 54.9$	$0.7 \pm 0.1$	$-$	$-$	528.7	576.3	1.1	
070220	fmh	$34.5 \pm 25.9$	$0.7 \pm 0.1$	$-$	$-$	541.6	569.3	0.5	
070220	fvh	$- \pm -$	$- \pm -$	$-$	$-$	-	-	-	
070306	tot	$1.00E14 \pm 1.52E14$	$5.4 \pm 0.3$	$-$	$-$	171.6	240.9	1.0	
070306	fvs	$- \pm -$	$- \pm -$	$-$	$-$	-	-	-	
070306	fms	$1.00E14 \pm 1.47E14$	$5.5 \pm 0.3$	$-$	$-$	171.9	236.0	0.8	
070306	fmh	$1.00E14 \pm 3.49E14$	$5.8 \pm 0.7$	$-$	$-$	172.4	228.0	1.4	
070306	fvh	$1.00E14 \pm 3.14E14$	$5.7 \pm 0.6$	$-$	$-$	168.9	239.9	0.8	
070318	tot1	$3358.6 \pm 202.8$	$1.1 \pm 0.0$	$-$	$-$	186.6	223.7	1.3	
070318	tot2	$3358.6 \pm 202.8$	$1.1 \pm 0.0$	$-$	$-$	232.0	427.2	1.3	
070318	fvs1	$9990.9 \pm 14470.0$	$1.7 \pm 0.3$	$1.0 \pm 0.0$	$151.3 \pm 44.0$	197.9	230.0	1.0	
070318	fvs2	$9990.9 \pm 14470.0$	$1.7 \pm 0.3$	$1.0 \pm 0.0$	$151.3 \pm 44.0$	234.4	506.1	1.0	
070318	fms1	$934.2 \pm 95.8$	$1.1 \pm 0.0$	$-$	$-$	187.2	242.1	1.4	
070318	fms2	$934.2 \pm 95.8$	$1.1 \pm 0.0$	$-$	$-$	233.7	410.7	1.4	
070318	fmh1	$866.8 \pm 259.6$	$1.2 \pm 0.1$	$-$	$-$	190.6	206.4	0.9	
070318	fmh2	$866.8 \pm 259.6$	$1.2 \pm 0.1$	$-$	$-$	226.9	425.0	0.9	
070318	fvh1	$1914.0 \pm 413.4$	$1.2 \pm 0.0$	$-$	$-$	187.7	196.3	1.0	
070318	fvh2	$1914.0 \pm 413.4$	$1.2 \pm 0.0$	$-$	$-$	251.9	412.3	1.0	
070330	tot	$89.2 \pm 20.4$	$0.9 \pm 0.0$	$-$	$-$	-	172.7	292.4	1.0
070330	fvs	$10.7 \pm 7.4$	$0.8 \pm 0.1$	$-$	$-$	180.8	348.1	1.1	
070330	fms	$24.7 \pm 8.2$	$0.9 \pm 0.0$	$-$	$-$	176.4	267.3	0.9	
070330	fmh	$28.5 \pm 9.9$	$1.0 \pm 0.0$	$-$	$-$	174.7	268.8	0.	

**Table 2.** Continued

GRB	band	N count s <sup>-1</sup>	$\alpha_1$	$\alpha_2$	$t_{br}$ s	$t_{1,90}$ s	$t_{2,90}$ s	$\chi^2/dof$
070419B	fvh	200070.0 ± 89830.0	1.8 ± 0.1	--	--	199.1	306.0	2.3
070518	tot1	5000.0 ± 6861.0	1.3 ± 0.3	--	--	99.0	143.5	0.7
070518	tot2	5000.0 ± 6861.0	1.3 ± 0.3	--	--	133.9	233.9	0.7
070518	tot3	5000.0 ± 6861.0	1.3 ± 0.3	--	--	173.1	215.4	0.7
070518	fvs1	103.6 ± 110.6	0.7 ± 0.2	--	--	97.0	134.9	0.8
070518	fvs2	103.6 ± 110.6	0.7 ± 0.2	--	--	133.8	171.7	0.8
070518	fvs3	103.6 ± 110.6	0.7 ± 0.2	--	--	166.1	221.0	0.8
070518	fms1	554857.0 ± 3.60E06	2.6 ± 1.5	--	--	98.7	134.4	1.2
070518	fms2	554857.0 ± 3.60E06	2.6 ± 1.5	--	--	138.2	191.3	1.2
070518	fms3	554857.0 ± 3.60E06	2.6 ± 1.5	--	--	174.5	209.2	1.2
070518	fmh1	152.0 ± 339.1	1.1 ± 0.5	--	--	99.4	114.8	1.1
070518	fmh2	152.0 ± 339.1	1.1 ± 0.5	--	--	133.6	152.8	1.1
070518	fmh3	152.0 ± 339.1	1.1 ± 0.5	--	--	168.7	212.5	1.1
070518	fvh1	169.9 ± 244.5	1.1 ± 0.3	--	--	97.6	107.7	0.6
070518	fvh2	169.9 ± 244.5	1.1 ± 0.3	--	--	136.5	176.5	0.6
070518	fvh3	169.9 ± 244.5	1.1 ± 0.3	--	--	178.2	242.5	0.6
070520B	tot	92241.3 ± 71040.0	1.7 ± 0.2	--	--	163.3	277.0	1.9
070520B	fvs	27336.2 ± 37500.0	1.7 ± 0.3	--	--	161.9	299.0	1.1
070520B	fms	60385.7 ± 55590.0	1.9 ± 0.2	--	--	161.9	269.2	1.3
070520B	fmh	3911.6 ± 5665.0	1.6 ± 0.3	--	--	169.3	260.0	1.1
070520B	fvh	9244.9 ± 9104.0	1.7 ± 0.2	--	--	168.9	253.5	1.0
070621	tot1	4.00E10 ± 5.16E10	4.2 ± 0.3	--	--	139.6	159.2	1.0
070621	tot2	4.00E10 ± 5.16E10	4.2 ± 0.3	--	--	179.2	242.4	1.0
070621	fvs1	-- ± --	-- ± --	--	--	--	--	--
070621	fvs2	-- ± --	-- ± --	--	--	--	--	--
070621	fms1	2.00E10 ± 4.29E10	4.2 ± 0.4	--	--	142.5	159.0	1.2
070621	fms2	2.00E10 ± 4.29E10	4.2 ± 0.4	--	--	176.8	244.6	1.2
070621	fmh1	2.00E10 ± 3.04E10	4.4 ± 0.3	--	--	137.2	156.9	1.0
070621	fmh2	2.00E10 ± 3.04E10	4.4 ± 0.3	--	--	189.1	215.3	1.0
070621	fvh1	2.00E10 ± 5.71E10	4.4 ± 0.6	--	--	139.7	151.6	1.1
070621	fvh2	2.00E10 ± 5.71E10	4.4 ± 0.6	--	--	--	--	--
070704	tot	6344.2 ± 1238.0	1.3 ± 0.0	--	--	280.0	438.6	1.9
070704	fvs	59.1 ± 78.7	1.0 ± 0.2	--	--	281.1	453.2	0.7
070704	fms	1991.6 ± 556.5	1.3 ± 0.0	--	--	284.0	449.8	1.4
070704	fmh	1527.9 ± 494.1	1.3 ± 0.1	--	--	280.0	424.5	1.3
070704	fvh	2395.6 ± 629.3	1.3 ± 0.0	--	--	277.9	428.3	1.5
070721B	tot1	6.00E08 ± 1.09E09	3.6 ± 0.4	0.6 ± 0.1	165.3 ± 9.1	256.2	531.0	1.0
070721B	tot2	6.00E08 ± 1.09E09	3.6 ± 0.4	0.6 ± 0.1	165.3 ± 9.1	304.5	316.5	1.0
070721B	tot3	6.00E08 ± 1.09E09	3.6 ± 0.4	0.6 ± 0.1	165.3 ± 9.1	335.5	372.2	1.0
070721B	tot4	6.00E08 ± 1.09E09	3.6 ± 0.4	0.6 ± 0.1	165.3 ± 9.1	598.7	956.6	1.0
070721B	fvs1	6.00E08 ± 1.32E09	3.8 ± 0.5	0.6 ± 0.1	162.9 ± 10.1	245.8	584.0	0.9
070721B	fvs2	6.00E08 ± 1.32E09	3.8 ± 0.5	0.6 ± 0.1	162.9 ± 10.1	305.3	322.4	0.9
070721B	fvs3	6.00E08 ± 1.32E09	3.8 ± 0.5	0.6 ± 0.1	162.9 ± 10.1	341.8	375.2	0.9
070721B	fvs4	6.00E08 ± 1.32E09	3.8 ± 0.5	0.6 ± 0.1	162.9 ± 10.1	617.6	937.2	0.9
070721B	fms1	6.00E08 ± 1.39E09	3.8 ± 0.5	0.5 ± 0.1	167.4 ± 11.0	255.7	288.6	1.0
070721B	fms2	6.00E08 ± 1.39E09	3.8 ± 0.5	0.5 ± 0.1	167.4 ± 11.0	304.2	329.0	1.0
070721B	fms3	6.00E08 ± 1.39E09	3.8 ± 0.5	0.5 ± 0.1	167.4 ± 11.0	334.0	409.7	1.0
070721B	fms4	6.00E08 ± 1.39E09	3.8 ± 0.5	0.5 ± 0.1	167.4 ± 11.0	625.0	1053.0	1.0
070721B	fmh1	6.00E08 ± 2.07E09	4.0 ± 0.7	0.3 ± 0.2	158.9 ± 13.6	259.1	302.2	0.5
070721B	fmh2	6.00E08 ± 2.07E09	4.0 ± 0.7	0.3 ± 0.2	158.9 ± 13.6	302.0	319.2	0.5
070721B	fmh3	6.00E08 ± 2.07E09	4.0 ± 0.7	0.3 ± 0.2	158.9 ± 13.6	334.3	392.8	0.5
070721B	fmh4	6.00E08 ± 2.07E09	4.0 ± 0.7	0.3 ± 0.2	158.9 ± 13.6	620.7	800.2	0.5
070721B	fvh1	6.00E08 ± 2.46E09	4.0 ± 0.9	0.3 ± 0.2	152.9 ± 12.6	255.6	312.1	0.9
070721B	fvh2	6.00E08 ± 2.46E09	4.0 ± 0.9	0.3 ± 0.2	152.9 ± 12.6	304.0	315.3	0.9
070721B	fvh3	6.00E08 ± 2.46E09	4.0 ± 0.9	0.3 ± 0.2	152.9 ± 12.6	334.5	369.0	0.9
070721B	fvh4	6.00E08 ± 2.46E09	4.0 ± 0.9	0.3 ± 0.2	152.9 ± 12.6	634.2	688.4	0.9
070724A	tot1	5.00E06 ± 4.20E06	3.0 ± 0.2	--	--	87.1	125.4	1.4
070724A	tot2	5.00E06 ± 4.20E06	3.0 ± 0.2	--	--	153.5	272.1	1.4
070724A	fvs1	-- ± --	-- ± --	--	--	--	--	--
070724A	fvs2	-- ± --	-- ± --	--	--	--	--	--
070724A	fms1	5.00E06 ± 2.69E08	3.4 ± 12.0	--	--	76.8	121.2	1.7
070724A	fms2	5.00E06 ± 2.69E08	3.4 ± 12.0	--	--	151.2	272.2	1.7
070724A	fmh1	-- ± --	-- ± --	--	--	--	--	--
070724A	fmh2	-- ± --	-- ± --	--	--	--	--	--
070724A	fvh1	-- ± --	-- ± --	--	--	--	--	--
070724A	fvh2	-- ± --	-- ± --	--	--	--	--	--
071021	tot	1.00E10 ± 5.89E09	3.9 ± 0.1	--	--	160.5	273.2	1.9
071021	fvs	1.00E10 ± 1.33E10	4.1 ± 0.3	--	--	164.8	274.8	1.3
071021	fms	1.00E11 ± 1.08E11	4.5 ± 0.2	--	--	163.2	275.3	1.4
071021	fmh	1.00E11 ± 3.31E11	4.8 ± 0.7	--	--	160.1	270.4	0.9
071021	fvh	1.00E11 ± 3.65E11	4.7 ± 0.7	--	--	162.7	269.5	1.9
071031	tot1	5.00E07 ± 5.50E07	2.7 ± 0.2	--	--	118.0	192.0	1.5
071031	tot2	5.00E07 ± 5.50E07	2.7 ± 0.2	--	--	190.3	260.1	1.5
071031	tot3	5.00E07 ± 5.50E07	2.7 ± 0.2	--	--	244.7	327.9	1.5
071031	tot4	5.00E07 ± 5.50E07	2.7 ± 0.2	--	--	373.4	789.3	1.5
071031	fvs1	700000.0 ± 1.06E06	2.2 ± 0.3	--	--	114.8	222.3	1.1
071031	fvs2	700000.0 ± 1.06E06	2.2 ± 0.3	--	--	191.1	269.4	1.1
071031	fvs3	700000.0 ± 1.06E06	2.2 ± 0.3	--	--	244.8	312.6	1.1
071031	fvs4	700000.0 ± 1.06E06	2.2 ± 0.3	--	--	386.0	793.9	1.1
071031	fms1	5.00E07 ± 6.36E07	2.9 ± 0.3	--	--	119.6	192.1	1.3
071031	fms2	5.00E07 ± 6.36E07	2.9 ± 0.3	--	--	189.3	242.5	1.3
071031	fms3	5.00E07 ± 6.36E07	2.9 ± 0.3	--	--	243.0	309.1	1.3
071031	fms4	5.00E07 ± 6.36E07	2.9 ± 0.3	--	--	383.6	633.5	1.3
071031	fmh1	299877.06 ± 91300.0	2.2 ± 0.4	--	--	108.3	175.7	0.9
071031	fmh2	299877.06 ± 91300.0	2.2 ± 0.4	--	--	188.4	218.6	0.9
071031	fmh3	299877.06 ± 91300.0	2.2 ± 0.4	--	--	244.1	273.8	0.9
071031	fmh4	299877.06 ± 91300.0	2.2 ± 0.4	--	--	377.9	690.7	0.9
071031	fvh1	450000.0 ± 1.71E06	2.2 ± 0.7	--	--	99.8	173.5	1.0
071031	fvh2	450000.0 ± 1.71E06	2.2 ± 0.7	--	--	186.1	237.9	1.0
071031	fvh3	450000.0 ± 1.71E06	2.2 ± 0.7	--	--	247.0	283.8	1.0
071031	fvh4	450000.0 ± 1.71E06	2.2 ± 0.7	--	--	349.8	803.1	1.0
071118	tot	744.0 ± 307.3	1.0 ± 0.1	--	--	456.7	791.6	1.1
071118	fvs	784.4 ± 794.8	1.2 ± 0.2	--	--	416.7	891.6	0.6
071118	fms	387.0 ± 237.3	1.0 ± 0.1	--	--	503.5	761.7	1.0
071118	fmh	-- ± --	-- ± --	--	--	--	--	--
071118	fvh	-- ± --	-- ± --	--	--	--	--	--
080210	tot	59647.31 ± 19500.0	1.8 ± 0.4	--	--	174.6	224.2	1.1
080210	fvs	293949.08 ± 26800.0	2.2 ± 0.5	--	--	176.8	226.4	1.0
080210	fms	64891.1 ± 20320.0	1.6 ± 0.6	--	--	176.3	213.0	0.8
080210	fmh	39.8 ± 163.8	0.8 ± 0.7	--	--	178.2	223.6	0.4
080210	fvh	40.8 ± 131.4	0.7 ± 0.6	--	--	177.9	219.3	0.3
080212	tot1	7.01E12 ± 7.75E12	5.2 ± 0.2	1.1 ± 0.0	171.5 ± 5.0	176.7	284.8	1.6
080212	tot2	7.01E12 ± 7.75E12	5.2 ± 0.2	1.1 ± 0.0	171.5 ± 5.0	220.4	321.7	1.6
080212	tot3	7.01E12 ± 7.75E12	5.2 ± 0.2	1.1 ± 0.0	171.5 ± 5.0	273.6	365.5	1.6
080212	fvs1	3.08E12 ± 5.98E12	5.3 ± 0.4	1.1 ± 0.1	200.1 ± 14.5	178.1	262.0	1.1
080212	fvs2	3.08E12 ± 5.98E12	5.3 ± 0.4	1.1 ± 0.1	200.1 ± 14.5	222.2	351.0	1.1

**Table 2.** Continued

GRB	band	N count s <sup>-1</sup>	$\alpha_1$	$\alpha_2$	$t_{br}$ s	$t_{1,90}$ s	$t_{2,90}$ s	$\chi^2/dof$
080212	fvs3	3.08E12 ± 5.98E12	5.3 ± 0.4	1.1 ± 0.1	200.1 ± 14.5	274.6	392.6	1.1
080212	fms1	7.01E12 ± 1.09E13	5.4 ± 0.3	1.1 ± 0.0	182.4 ± 7.6	176.4	266.9	1.7
080212	fms2	7.01E12 ± 1.09E13	5.4 ± 0.3	1.1 ± 0.0	182.4 ± 7.6	219.9	309.0	1.7
080212	fms3	7.01E12 ± 1.09E13	5.4 ± 0.3	1.1 ± 0.0	182.4 ± 7.6	273.9	353.3	1.7
080212	fmh1	7.01E12 ± 3.00E13	5.8 ± 0.9	1.1 ± 0.0	157.5 ± 8.3	181.6	233.9	1.0
080212	fmh2	7.01E12 ± 3.00E13	5.8 ± 0.9	1.1 ± 0.0	157.5 ± 8.3	218.7	306.2	1.0
080212	fmh3	7.01E12 ± 3.00E13	5.8 ± 0.9	1.1 ± 0.0	157.5 ± 8.3	272.9	350.8	1.0
080212	fvh1	5.01E13 ± 3.64E14	6.3 ± 1.5	0.7 ± 0.3	150.4 ± 10.3	189.3	193.8	1.1
080212	fvh2	5.01E13 ± 3.64E14	6.3 ± 1.5	0.7 ± 0.3	150.4 ± 10.3	220.0	273.5	1.1
080212	fvh3	5.01E13 ± 3.64E14	6.3 ± 1.5	0.7 ± 0.3	150.4 ± 10.3	270.8	352.0	1.1
080310	tot1	118000.0 ± 37000.0	1.7 ± 0.1	---	---	477.5	719.6	---
080310	tot2	118000.0 ± 37000.0	1.7 ± 0.1	---	---	544.6	615.1	---
080310	fvs1	102000.0 ± 38000.0	1.9 ± 0.1	---	---	475.2	728.9	---
080310	fvs2	102000.0 ± 38000.0	1.9 ± 0.1	---	---	547.2	661.2	---
080310	fms1	31000.0 ± 13000.0	1.8 ± 0.1	---	---	480.0	659.9	---
080310	fms2	31000.0 ± 13000.0	1.8 ± 0.1	---	---	543.0	623.7	---
080310	fmh1	3200.0 ± 2200.0	1.5 ± 0.1	---	---	478.3	661.2	---
080310	fmh2	3200.0 ± 2200.0	1.5 ± 0.1	---	---	541.5	608.5	---
080310	fvh1	5300.0 ± 4500.0	1.6 ± 0.2	---	---	489.5	662.4	---
080310	fvh2	5300.0 ± 4500.0	1.6 ± 0.2	---	---	543.4	599.0	---
080319D	tot1	5.84E06 ± 6.93E06	2.6 ± 0.2	---	---	267.6	417.1	1.3
080319D	tot2	5.84E06 ± 6.93E06	2.6 ± 0.2	---	---	417.7	556.9	1.3
080319D	fvs1	66003.6 ± 254400.0	2.1 ± 0.7	---	---	263.7	442.6	0.8
080319D	fvs2	66003.6 ± 254400.0	2.1 ± 0.7	---	---	432.4	611.6	0.8
080319D	fms1	5.84E06 ± 1.09E07	2.8 ± 0.3	---	---	260.1	422.9	0.9
080319D	fms2	5.84E06 ± 1.09E07	2.8 ± 0.3	---	---	417.6	592.0	0.9
080319D	fmh1	5.84E06 ± 3.03E07	2.9 ± 1.0	---	---	273.2	367.5	0.5
080319D	fmh2	5.84E06 ± 3.03E07	2.9 ± 1.0	---	---	360.5	539.6	0.5
080319D	fvh1	3.69E06 ± 1.25E07	2.8 ± 0.6	---	---	234.0	458.8	0.5
080319D	fvh2	3.69E06 ± 1.25E07	2.8 ± 0.6	---	---	443.9	677.2	0.5
080320	tot1	5999.3 ± 6857.0	1.4 ± 0.2	---	---	204.9	225.4	1.2
080320	tot2	5999.3 ± 6857.0	1.4 ± 0.2	---	---	281.4	429.3	1.2
080320	tot3	5999.3 ± 6857.0	1.4 ± 0.2	---	---	696.5	1176.5	1.2
080320	fvs1	5989.9 ± 6759.0	1.6 ± 0.2	---	---	195.6	228.1	1.0
080320	fvs2	5989.9 ± 6759.0	1.6 ± 0.2	---	---	285.3	493.8	1.0
080320	fvs3	5989.9 ± 6759.0	1.6 ± 0.2	---	---	693.7	1179.8	1.0
080320	fms1	5973.0 ± 9371.0	1.6 ± 0.3	---	---	—	—	—
080320	fms2	5973.0 ± 9371.0	1.6 ± 0.3	---	---	279.8	409.0	0.9
080320	fms3	5973.0 ± 9371.0	1.6 ± 0.3	---	---	728.8	1382.7	0.9
080320	fmh1	6022.8 ± 13870.0	1.7 ± 0.3	---	---	—	—	—
080320	fmh2	6022.8 ± 13870.0	1.7 ± 0.3	---	---	278.4	398.9	0.8
080320	fmh3	6022.8 ± 13870.0	1.7 ± 0.3	---	---	662.6	989.3	0.8
080320	fvh1	6002.6 ± 8083.0	1.6 ± 0.2	---	---	—	—	—
080320	fvh2	6002.6 ± 8083.0	1.6 ± 0.2	---	---	278.0	476.1	0.5
080320	fvh3	6002.6 ± 8083.0	1.6 ± 0.2	---	---	804.0	1054.0	0.5

## 4 ANALYSIS

### 4.1 Flares shape parameters

In the following we revisit with this new sample the results obtained in Paper I and Paper II. In addition to a more detailed analysis of the flares temporal behaviour, the major contribution of the present work is the analysis of the flares in 4 XRT sub-energy bandpasses (see Sec. 2). When not specified, we consider the parameters of the flares obtained fitting the 0.3 – 10 keV band light curve. The phenomenology of the flares is presented in the observer frame unless otherwise stated.

#### 4.1.1 Width versus $t_{pk}$

The first property of flares that we want to investigate is their temporal variability. Based on the fits described in Sec. 3.1, we calculate the ratio between the width and the peak time:  $w/t_{pk}$ . The median value of the distribution is 0.23 and the standard deviation is 0.14 (see Fig. 3, Inset). This value is in agreement with the result of Paper I, since the width obtained with the Norris05 profile corresponds to the one measured at  $\sim 37\%$  of the maximum, and if we consider the width measured at 37% of the maximum on a Gaussian profile, it results to be  $w_{\text{Gauss}} = 2.83 \sigma_{\text{Gauss}}$ .

What is evident in Fig. 2 is that the flare width increases linearly with time with a best fit  $w \sim 0.2 t_{pk}$ . This correlation is quite strong, with a Spearman rank coefficient  $\rho = 0.7115$  (number of points  $N = 109$ , null hypothesis probability  $\text{nhp} < 2.2 \times 10^{-16}$ ), and it is confirmed also in the source rest frame, thus excluding an effect due to the red-

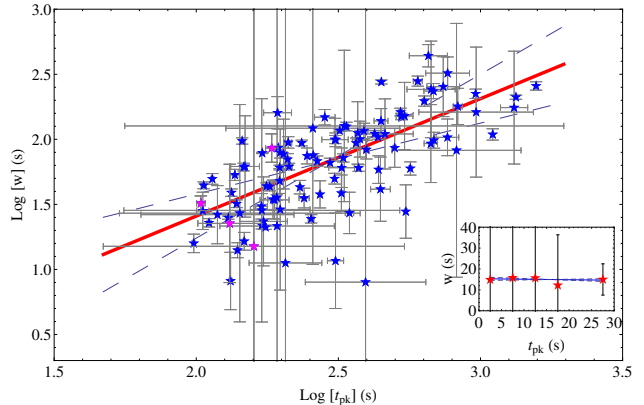


**Figure 2.** Plot of the observed width as a function of the observed peak time for the sample of the X-ray flares (blue and pink dots correspond to flare belonging to long and short GRBs respectively). Red solid line: best-fitting  $w = 10^{(-0.4 \pm 0.9)t_{pk}^{(0.9 \pm 0.4)}}$ . Inset: median of the width of pulses with peak time within different intervals for BATSE sample from Norris et al. (2005) (red points), showing that  $w$  remains constant with time during the prompt emission.

shift. This is remarkably different from what has been found for the prompt emission pulses observed by BATSE: the width remains constant throughout the GRB time history (Ramirez-Ruiz & Fenimore 2000, see also Fig. 2, inset). By comparing the BATSE broad pulses from the Norris et al. (2005) sample with X-ray flares, this different trend is evi-

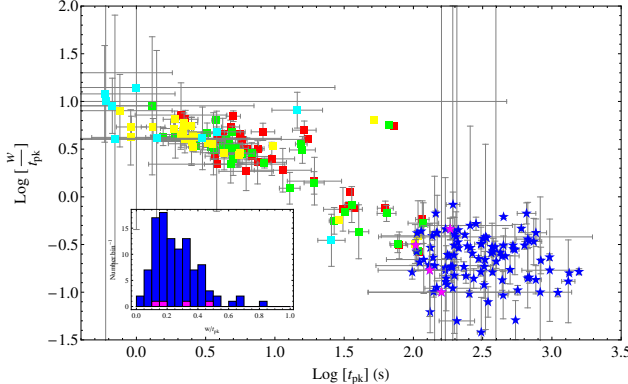


**Figure 3.** Plot of the ratio  $w/t_{pk}$  of X-ray flares (blue and pink dots correspond to flare belonging to long and short GRBs respectively) compared with the one of the BATSE pulses in 4 sub-energy bandpasses in the Norris et al. (2005) sample (colored dots). Their different behaviour is evident: while the BATSE pulse ratio  $w/t_{pk}$  decreases with time in all the energy bands, for the flares it remains constant up to late times. *Inset:* distribution of the ratio  $w/t_{pk}$  of X-ray flares (blue and pink rectangles correspond to flare belonging to long and short GRBs respectively). The distribution is centered on  $w/t_{pk} = 0.23$  with  $\sigma = 0.14$

dent: while the  $w/t_{pk}$  of the BATSE pulses decreases with time in all the 4 sub-energy bandpasses, for XRT flares it tends to be constant up to late times (see Fig. 3). It is important to note, however, that apart from the different trend the ratio  $w/t_{pk}$  of the flares joints smoothly with the one observed in the BATSE broad pulses, thus pointing to a continuous transition from one class to the other.

#### 4.1.2 Width versus Energy

We considered the sub-sample of flares that have been fit in all the 4 sub-energy bandpasses that have also a redshift measurement to investigate the existence of a correlation between width and energy band. This analysis has been carried out in the source rest frame. We defined therefore the effective rest frame energy in the observed energy band  $[h\nu_1; h\nu_2]$  as:

$$E_{\text{eff}} = (1+z) \frac{\int_{h\nu_1}^{h\nu_2} h\nu f(\nu) \text{RM}(\nu) d(h\nu)}{\int_{h\nu_1}^{h\nu_2} f(\nu) \text{RM}(\nu) d(h\nu)}, \quad (5)$$

where  $\text{RM}(\nu)$  is the response matrix of the XRT and  $f(\nu)$  is the spectrum,  $f(\nu) \propto \nu^{-\beta}$  with  $\beta \simeq 1$ . By correlating the width measured in the source rest frame ( $w_{\text{RF}} = w/(1+z)$ ) with the rest frame effective energy of each sub-energy band we find:  $w_{\text{RF}} \propto E_{\text{eff}}^{-0.5}$  (see Fig 4). We conclude that flares are broader at lower energies. It is interesting to observe, at this point, that while flares are very clearly detected at X-ray frequencies they are almost undetectable over the optical light curve (see e.g. Kröhler et al. 2009, however with the exception of the optical flare of GRB080129, Greiner et al. 2009). Whether or not this is a consequence of the present correlation it is unknown and a new analysis is in progress to establish that.

Fenimore et al. (1995) reported in the analysis of BATSE pulses an inverse correlation between the width of a

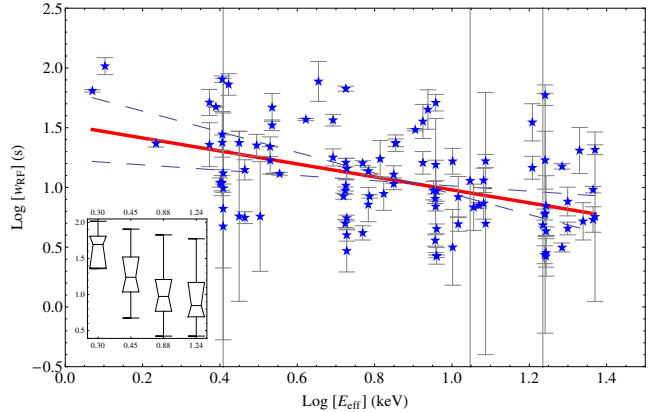


**Figure 4.** Plot of the rest frame width as a function of the rest frame effective energy for the X-ray flares fitted in all the 4 sub-energy bandpasses (blue dots). Red solid line: best-fitting  $w_{\text{RF}} = 10^{(1.5 \pm 0.3)} E_{\text{eff}}^{(-0.5 \pm 0.3)}$ . *Inset:* Boxplot of the same quantities.

peak and the energy band in which the observation is made,  $w \propto E^{-0.4}$ , confirmed later on by Norris et al. (1996), and by Borgonovo et al. (2007) that extended this analysis also to the prompt emission pulses detected by the *BeppoSAX* satellite in the X-ray and gamma-ray bands.

#### 4.1.3 Asymmetry and rise and decay times

Another characterizing property of the flare temporal behaviour is their asymmetry. Flares are asymmetric with a median value of 0.35 and standard deviation of 0.2. Furthermore, the asymmetry  $k$  does not correlate with the width  $w$ , thus indicating that flares profiles are extremely self-similar. As a direct comparison, the distribution of asymmetry values from the 4 bandpass BATSE sample of Norris et al. (2005) is characterized by a median of 0.49 and standard deviation of 0.26. The two distributions are portrayed in the inset of Fig. 5. Kocevski et al. (2003) found a distribution of  $t_{\text{rise}}/t_{\text{decay}}$  values centered on 0.47 for a sample of separable BATSE pulses<sup>2</sup>, in good agreement with our results. Flares and prompt pulses share very similar values of asymmetry. Despite their similarity, the flare distribution of  $t_{\text{rise}}/t_{\text{decay}}$  is more symmetric while the prompt pulses distribution is skewed to lower values. This feature can be understood considering the results that will be discussed in detail in Margutti et al. (in prep.): these authors found that both the evolution of the rise and the evolution of the decay times with energy band can be described by a power-law, with a steeper decaying power-law index associated to the rise time evolution. This means that in a softer energy band (like the X-ray when compared to the prompt gamma-ray photons) the pulses will be allowed to have a larger  $t_{\text{rise}}/t_{\text{decay}}$  ratio.

Fig. 5 further demonstrates the presence of a strong correlation between the rise and decay times:  $t_{\text{decay}} \propto t_{\text{rise}}$ , with  $\rho = 0.7856$  ( $N = 113$ ,  $n_{\text{hp}} < 2.2 \times 10^{-16}$ ). The correlation smoothly joins the prompt and the flare emission, from the gamma-ray to the soft X-rays, from the trigger to

<sup>2</sup> Note, however, that in Kocevski et al. (2003) the rise and decay times were defined at the profile half maximum.

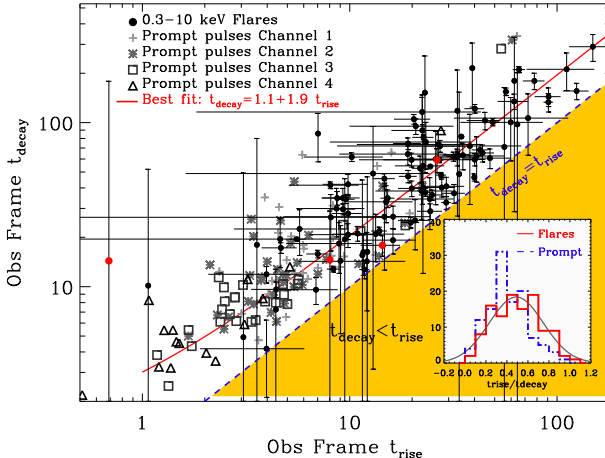


**Figure 5.** Observed decay time as a function of the rise time for our sample of X-ray flares (black and red dots correspond to flare belonging to long and short GRBs respectively) and the sample of prompt pulses from Norris et al. (2005): the different symbols refer to different BATSE energy bandpasses. Red solid line: best linear fitting for the two samples:  $t_{\text{decay}} = (1.1 \pm 0.1) + (1.9 \pm 0.1) t_{\text{rise}}$ . Blue dashed line:  $t_{\text{decay}} = t_{\text{rise}}$  locus of points. Shaded area: region of the plane for which  $t_{\text{decay}} < t_{\text{rise}}$ . No data point lies in this region. Inset: distribution of the  $t_{\text{rise}}/t_{\text{decay}}$  values for the sample of X-ray flares (red solid line) and the sample of prompt pulses of Norris et al. (2005, blue dot-dashed line). The best Gaussian fitting of the flare distribution is also shown with a solid grey line. The distribution is centered on  $t_{\text{rise}}/t_{\text{decay}} = 0.49$  with  $\sigma = 0.26$ .

thousands of seconds after the onset of the explosion. No emission episode in these two samples has  $t_{\text{decay}} < t_{\text{rise}}$ .

A trend is seen between the rise and decay times as a function of the flare peak time, reminiscent of the width-peak time correlation of Fig. 2: since the rise time is proportional to the decay time and  $w = t_{\text{rise}} + t_{\text{decay}}$  by definition, the results portrayed in Fig. 5 naturally account for the rise and decay times vs. peak time linear correlations:  $t_{\text{rise}} \sim 0.05 t_{\text{pk}}$  and  $t_{\text{decay}} \sim 0.14 t_{\text{pk}}$ .

## 4.2 Energy and spectrum

### 4.2.1 Intensity versus $t_{\text{pk}}$

In Paper I we detected an inverse correlation between the flare intensity  $A$  and  $t_{\text{pk}}$ . Moreover, it has been shown in the previous section that the flare duration  $w$  increases with  $t_{\text{pk}}$ . Therefore, flares seem to have a tendency to be equally energetic, lasting longer when the intensity is much lower.

The previous sample could cast some doubts on the correlation intensity peak time since it was heavily weighted on a few very late flares. For the early flares of that sample, the resulting correlation was not statistically significant. The present sample is restricted to flares occurring earlier than  $\sim 1000$  s in the observer frame ( $\leq 320$  s in the rest frame) where the statistics are higher. The correlation between these two quantities<sup>3</sup> is shown in Fig. 6, upper panel:

<sup>3</sup> The flare peak intensity is derived as a best fitting parame-

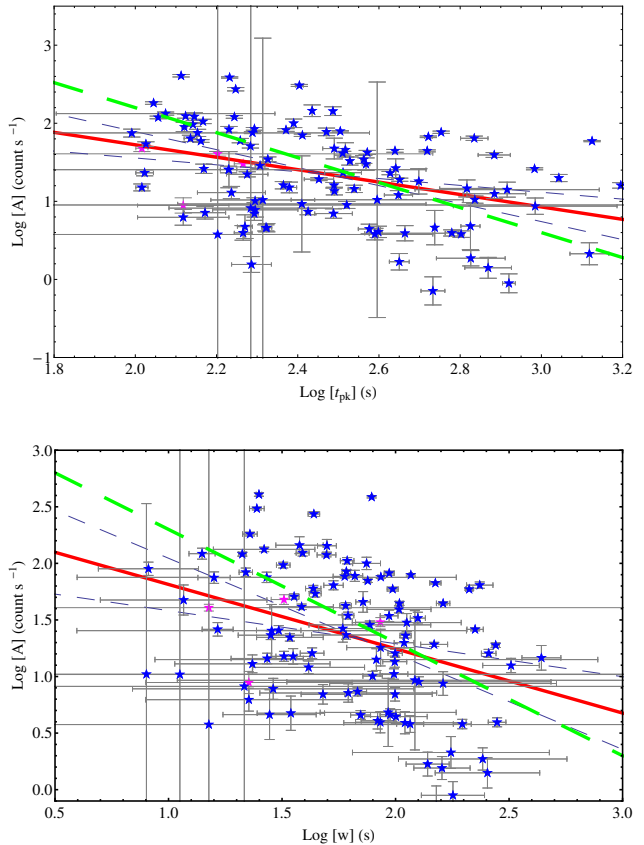


**Figure 6.** *Upper panel:* Plot of the peak intensity  $A$  of the X-ray flares as a function of the peak time  $t_{\text{pk}}$  (blue and pink dots correspond to flares belonging to long and short GRBs respectively). Red solid line: best-fitting  $A = 10^{(3.3 \pm 0.9)} t_{\text{pk}}^{(-0.70 \pm 0.01)}$ . Green dashed line: best-fitting obtained accounting for the intrinsic dispersion of the data (further details can be found in D'Agostini 2005):  $\log(A) = q + m \log(t_{\text{pk}})$ , with  $q = (5.4 \pm 0.8)$ ,  $m = (-1.6 \pm 0.4)$  and the extrinsic scatter  $\sigma = (0.55 \pm 0.07)$ . *Lower panel:* Plot of the peak intensity  $A$  of the X-ray flares as a function of the width  $w$  (blue and pink dots correspond to flare belonging to long and short GRBs respectively). Red solid line: best-fitting  $A = 10^{(2.3 \pm 0.5)} w^{(-0.6 \pm 0.3)}$ . Green dashed line: best-fitting obtained accounting for the intrinsic dispersion of the data (further details can be found in D'Agostini 2005):  $\log(A) = q + m \log(w)$ , with  $q = (3.3 \pm 0.5)$ ,  $m = (-1.0 \pm 0.3)$  and the extrinsic scatter  $\sigma = (0.55 \pm 0.07)$ .

despite the rather large errors, the correlation is evident with  $\rho = -0.3921$  ( $N = 109$ ,  $\text{nhp} = 2.9 \times 10^{-5}$ ).

A correlation also exists between  $A$  and the width  $w$  with  $\rho = -0.3442$  ( $N = 109$ ,  $\text{nhp} = 2.7 \times 10^{-4}$ ; see Fig. 6, lower panel). We find that  $A \propto w^{-0.6}$ . This correlation has the same trend to that of the prompt emission pulses (Ramirez-Ruiz & Fenimore 2000) but the power-law index for the prompt emission is remarkably different ( $A \propto w^{-2.8}$ ).

The existence of a correlation between the flare peak intensity and the flare peak time is confirmed in the rest

ter of the Norris05 profile and is defined as the excess over the underlying continuum.

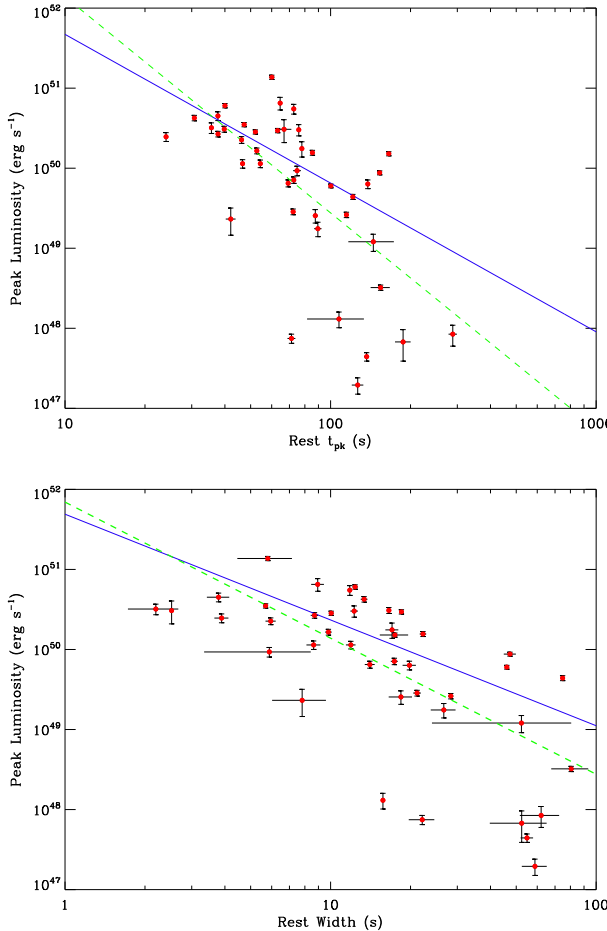


**Figure 7.** *Upper panel:* Peak luminosity vs rest frame peak time for the subsample of flares with measured redshift. The blue solid line indicates the best-fitting relation:  $L_{pk} = 10^{(49.9 \pm 0.1)} t_{pk,RF}^{(-1.9 \pm 0.1)}$ . The green dashed line indicates the best-fitting obtained accounting for the intrinsic dispersion of the data (further details can be found in D'Agostini 2005):  $\text{Log}(L_{pk}) = q + m \text{Log}(t_{pk,RF})$ , with  $q = (54.8 \pm 4.0)$ ,  $m = (-2.7 \pm 0.5)$  and the extrinsic scatter  $\sigma = (0.73 \pm 0.08)$ . *Lower panel:* Peak luminosity vs rest frame width for the subsample of flares with measured redshift. The blue solid line indicates the best-fitting power-law relation:  $L_{pk} = 10^{(48.1 \pm 0.1)} w_{RF}^{(-1.3 \pm 0.1)}$ . The green dashed line indicates the best-fitting obtained accounting for the intrinsic dispersion of the data (further details can be found in D'Agostini 2005):  $\text{Log}(L_{pk}) = q + m \text{Log}(w_{RF})$ , with  $q = (51.8 \pm 3.9)$ ,  $m = (-1.7 \pm 0.3)$  and the extrinsic scatter  $\sigma = (0.68 \pm 0.08)$ .

frame plane, as well. Fig. 7 shows the existence of a trend between the peak luminosity and the flare rest frame peak time: flares occurring later are characterized by lower peak luminosity. The best fit relation is found to be:  $L_{pk} \propto t_{pk}^{-1.9}$ . The Spearman rank coefficient is  $\rho = -0.7240$  ( $N = 43$ ,  $n_{hp} = 6.0 \times 10^{-8}$ ). The best-fitting relation is dominated by the group of bright flares for which the parameters are determined with the highest accuracy: however, Fig. 7 clearly show the presence of a group of low luminosity flares ( $L_{pk} < 10^{45} \text{ erg s}^{-1}$ ) which lies below the prediction and would indicate a much steeper relation. If we properly account for the presence of intrinsic scatter (D'Agostini 2005), the best-

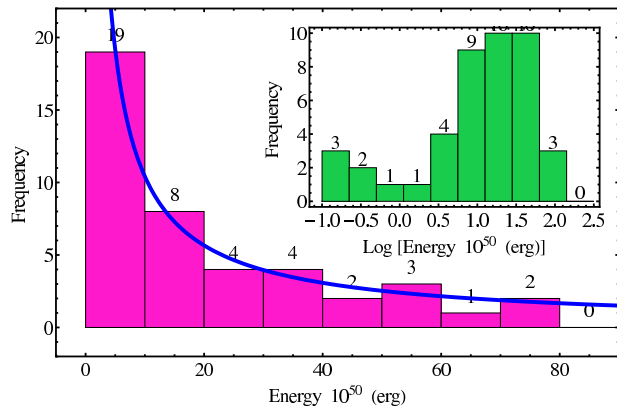


**Figure 8.** Distribution of the energy emitted in single X-ray flares of the present sample  $E_{\text{flare}}$ . *Inset:* Distribution of the logarithm of the energy to better evidence the faint tail of the distribution.

fitting relation reads:  $\text{Log}(L_{pk}) = q + m \text{Log}(t_{pk,RF})$ , with  $q = (54.8 \pm 4.0)$ ,  $m = (-2.7 \pm 0.5)$ . We note that this relation describes the evolution of the peak luminosity of single flares: the flare *mean* luminosity function can evolve differently with time. For comparison, Lazzati et al. (2008) found that the mean luminosity, averaged over a time-scale longer than the duration of the individual flares, declines as a power-law in time with index  $\sim 1.5$ .

The existence of the peak time vs. width correlation of Sec. 4.1.1 together with the result of Fig. 7, upper panel, automatically translates into a peak luminosity vs. rest frame width relation portrayed in Fig. 7, lower panel. The best fit power-law model reads:  $L_{pk} \propto t_{pk}^{-1.3}$  and  $\rho = -0.6871$  ( $N = 43$ ,  $n_{hp} = 5.0 \times 10^{-7}$ ). Accounting for the intrinsic scatter we have:  $\text{Log}(L_{pk}) = q + m \text{Log}(w_{RF})$ , with  $q = (51.8 \pm 3.9)$ ,  $m = (-1.7 \pm 0.3)$ . Flares becomes wider and less luminous as the time proceeds.

#### 4.2.2 Energy

The isotropic 0.3 – 10 keV energy of the X-ray flares of the sample can be estimated from the fluence  $S$  as:

$$E_{\text{flare}} = \frac{4\pi D_l^2}{(1+z)} S. \quad (6)$$

The distribution function of the energy emitted in each flare cannot be properly determined since the sample is not complete and homogeneous. However, from Fig. 8 we see that the average isotropic energy emitted in single X-ray flares is about  $10^{51}$  erg, 5 to 10% of the energy observed by BAT in the prompt emission. Moreover, there is a hint of a bimodal distribution of the logarithm of the energy of flares, thus revealing a possible excess of faint flares.

At high redshift we have bright flares that we do not detect at lower redshift, however, under the assumption that bright flares correlate with bright GRBs, this could be due to the smaller volume sampled at low redshift. Likewise the brightest flares occur at earlier times (peak time  $< 500$  s).

There is a trend for GRBs with fainter prompt emission to have also fainter flares. If we correlate the total isotropic energy emitted in all the flares of a single GRB in the XRT

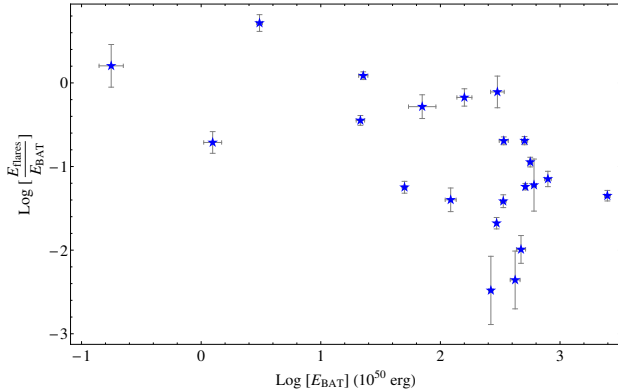


**Figure 9.** Plot of the ratio between the total isotropic energy emitted in all the flares of a single GRB  $E_{\text{flares}}$  and the total isotropic energy of its prompt emission  $E_{\text{BAT}}$  as a function of  $E_{\text{BAT}}$ . Although a correlation between these quantities is evident, its statistical significance is low due to the presence of two faint GRBs.

energy band ( $E_{\text{flares}}$ ) with the total isotropic energy of its prompt emission observed by BAT in the 15–150 keV energy band ( $E_{\text{BAT}}$ ) we find:  $E_{\text{flares}} \propto E_{\text{BAT}}^{0.6}$  (see Fig. 9). However the statistical significance is very low and driven considerably by two faint GRBs (GRB070724A and GRB060512).

#### 4.2.3 Spectral energy distribution

Except for a few cases it is very hard to measure the spectral evolution, and often the spectrum itself, of a flare because of the low SN ratio. Nevertheless, there are indications that flares have peak energies in the soft range of the X-ray spectrum,  $E_{pk} < 1$  keV (Paper II). Concerning the underlying afterglow light curve, after the steep decay the spectral index does not change considerably and  $\beta \sim 1$  (Chincarini et al. 2005). A different behaviour is observed during the steep decay, that is the phase during which we detect most of the flares: the spectrum can be very soft, up to  $\beta \sim 3$  (a beautiful example is GRB090111, Margutti et al. 2009).

An indication of the Spectral Energy Distribution (SED) during the flare event can be obtained by using the 4 sub-energy bandpasses we defined above. For each bandpass we use the  $E_{\text{eff}}$  introduced in Sec. 4.1, computed for each GRB in the source rest frame. We define the energy density  $F(E)$  in a sub-energy band as:

$$F(E)^i = \frac{4\pi D_l^2}{(1+z)} \frac{S^i}{E_{\text{eff}}^i}, \quad (7)$$

where  $S^i$  is the fluence of the flare<sup>4</sup> in the bandpass  $i$  and  $D_l^2$  is the luminosity distance.

We obtain a “characteristic” spectral index by fitting the energy density in each band for the X-ray flares fitted in all the 4 sub-energy bandpasses that results to be  $(-1.1 \pm 0.3)$  (see Fig. 10). We tentatively conclude that flares have a typical spectral index which is rather soft, although

<sup>4</sup> The fluence of a flare in each bandpass has been computed after the subtraction of the underlying continuum which therefore does not contribute to the flare energy density.

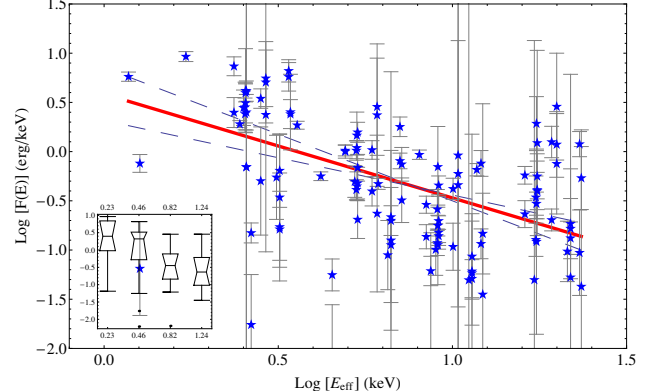


**Figure 10.** Plot of the energy density in each band for the X-ray flares fitted in all the 4 sub-energy bandpasses (blue dots). Red solid line: best-fitting  $F(E) = 10^{(0.6 \pm 0.3)} E^{(-1.1 \pm 0.3)}$ . Inset: Boxplot of the same quantities.

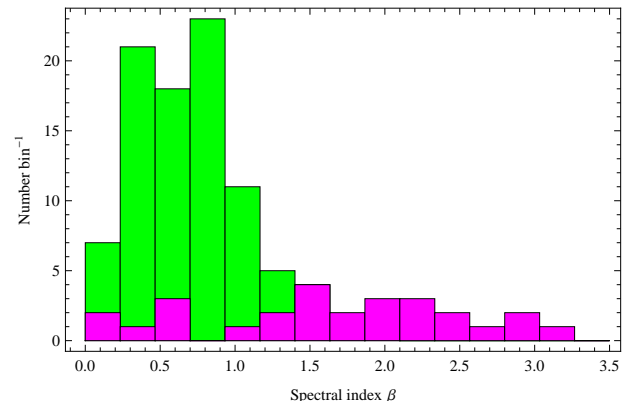


**Figure 11.** Histogram of the spectral energy indices derived from the flare SEDs (pink rectangles) compared with the indices of the spectrum integrated over the prompt emission  $T_{90}$  of the GRBs observed by BAT (green rectangles). It is evident that flares are softer, with a median 1.6, than the prompt emission (0.6). The spectral indices of the BAT GRBs are reported from Sakamoto et al. (2008) from December 2004 to July 2007, and from corresponding GCNs after.

we should note that this SED is integrated over the whole duration of the flare, therefore it is dominated by the decaying part of the light curve that is generally softer.

Flares result to be much softer than the prompt emission, as expected. This is clearly shown in Fig. 11 where we compare the histogram of the indices of the spectrum integrated over the prompt emission  $T_{90}$  of the GRBs observed by BAT with the spectral indices of the flare SEDs derived above. The median of the flare distribution is 1.6 with a standard deviation of 1.1, while the median of the BAT prompt emission distribution is 0.6 with a standard deviation of 0.4.

#### 4.2.4 Hardness ratio vs. $t_{pk}$

Fig. 12 demonstrates the presence of a softening trend during the flare emission of each event. In particular, the hard-

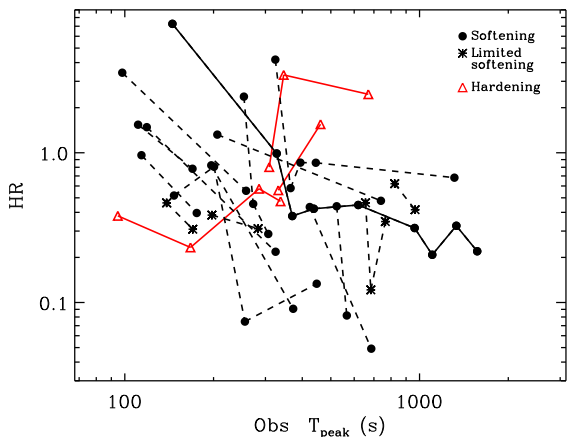


**Figure 12.** Hardness ratio evolution with peak time for the subsample of 20 GRBs containing more than one flare and for which an accurate measure of the profile parameters was possible. Solid and dashed lines connect flares belonging to the same event. Filled bullets, stars and open triangles are associated to GRBs showing a clear softening, a limited softening or a hardening with time, respectively. The black solid line connects the 11 flares from GRB051117A. A general softening trend with time is emerging.

ness ratio HR is shown as a function of the observed flare peak time for a subsample of 20 GRBs with more than one fitted flare for which an accurate measure of the flare profiles was possible. The maximum sensitivity on the softening is achieved computing the HR as the ratio of the counts in the hardest (3 – 10 keV) and in the softest (0.3 – 1 keV) energy bands as derived from the best fits. A general softening trend with time is emerging: out of 20 events, only GRB060111A, GRB070721B and GRB080319D show evidence of flare emission hardening with time. GRB051117A with 11 distinct flare episodes shows instead a consistent softening from  $\sim 200$  s to  $\sim 2000$  s post trigger. This leads us to conclude that the average energy of the arriving flares becomes softer as the burst progresses.

The phenomena of spectral evolution during the gamma-ray prompt emission is recognized to emerge in two distinct effects over both the entire, often complex light curves and the individual pulses. A trend of spectral softening on the timescale of pulses was first demonstrated by Band (1997): each pulse determines a hardening during its rise time and a softening during its decay time. At the same time, a global spectral evolution was first suggested by Norris et al. (1986) and confirmed by Ford et al. (1995). This means that, as the event progresses, the burst spectrum tends to soften with individual, evolving pulses having impressed upon them an envelope that governs a global spectral decay. Fig. 12 extends this result to the flare episodes and up to thousands of seconds after the beginning of the explosion.

## 5 DISCUSSION

Despite many observational and theoretical efforts, the origin of the GRB outflow and the role of the magnetic field are rather uncertain. While the fireball internal shock model

appears to satisfy most of the observations concerning the prompt emission, it requires various ad hoc assumptions as, for instance, the generation of a random magnetic field and efficient non-thermal particle acceleration during the collision of relativistic shells. Recent observations challenge the fireball internal shock model. Kumar et al. (2007) have, e.g., pointed out that we have no strong evidence of the reverse shock that is predicted by the fireball model. The analysis carried out by Oates et al. (2009) on the UVOT light curve of a large (27) sample of GRBs shows that the reverse shock is not the main contribution to the optical emission at early times and therefore it is not responsible for the rising optical emission. Gomboc et al. (2008) claim, however, the presence of reverse shock in GRB061126. There are, furthermore, indications that magnetic fields are rather dynamically important as shown by the polarization observed by Steele et al. (2009).

These observations specify the possibility that strong magnetic fields play a role during the acceleration of the outflow and the prompt emission (Thompson 1994; Spruit et al. 2001; Lyutikov & Blandford 2003), while any remaining magnetization at large distance can affect the interactions of the flow with the external medium. In MagnetoHydro-Dynamical (MHD) models for GRBs the flow is assumed to be launched by strong magnetic fields and is Poynting-flux dominated at the small distances. MHD acceleration of the jet leads to partial conversion of magnetic energy into kinetic energy in the flow. The efficiency of MHD acceleration remains uncertain and, therefore, model dependent. At large distance where the jet interacts with the external medium the jet may remain extremely magnetized (as in the electromagnetic model of Lyutikov & Blandford 2003) or moderately magnetized (e.g. Drenkhahn & Spruit 2002; Tchekhovskoy et al. 2008).

The parameter defining the magnetic content of a relativistic shell can be expressed by the ratio of the Poynting flux  $F_p$  to kinetic flux  $F_b$ :  $\sigma_o = F_p/F_b = B_o^2/(4\pi\gamma_o\rho c^2)$ . From this definition we have  $\sigma_o \gg 1$  for Poynting flux dominated jets while  $\sigma_o \ll 1$  in the fireball model. The interaction of the flow with the circumburst medium (the stellar wind or ISM) will generally occur at a distance of  $R \sim 10^{16}$  cm. It can be shown (Giannios 2008, and references therein) that for high magnetization the ejecta interact smoothly with the external medium and decelerate preventing the formation of a reverse shock. Numerical simulations have shown that for  $\sigma_o \sim 1$ , a reverse shock may still appear but it is generally weak (Mimica et al. 2009). Steele et al. (2009) observed in GRB090102 the early afterglow optical emission with temporal slope that is characteristic of a reverse shock. This case is interesting since they detected polarization at a 10% level. In order to reconcile the presence of a large scale magnetic field and of a reverse shock, they infer a moderate magnetization of the flow of  $\sigma_o \sim 1$ .

The present analysis of the X-ray flare properties and their comparison with the prompt emission ones should help in discriminating among different models. One fundamental question is whether the flares can originate within the internal-external shock scenario of the fireball model or they are simply due to delayed magnetic dissipation in the flow after it has powered the prompt emission (Giannios 2006).

Concerning the first possibility, we plot the variation in

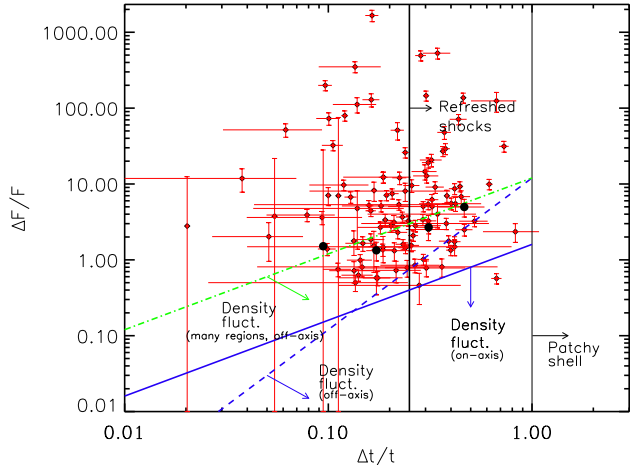


**Figure 13.** Relative variability flux ( $\Delta F/F$ ) kinematically allowed regions as a function of relative variability time-scale  $\Delta t/t$  calculated on our sample of X-ray flares (red and black dots correspond to flare belonging to long and short GRBs respectively). The three limits shown with solid, dashed and dot-dashed lines have been computed according to equations (7) and (A2) of Ioka et al. (2005).

flux during the flare  $\Delta F$  with respect to the underlying continuum  $F$  versus the duration of the flare  $\Delta t$  over the time of flare occurrence  $t$ , in analogy with the diagram presented by Ioka et al. (2005, , see Fig. 13). We calculated the ratios  $\Delta F/F$  and  $\Delta t/t$  for the flare sample and plotted over the allowed regions. The two vertical lines refer respectively to bumps due to patchy shells and to bumps due to refreshed shocks. The absence of flares with  $\Delta t/t \geq 1$  confirms previous results obtained in Paper I, outlining that flares cannot be due to the presence of patchy shells. On the contrary a rather large number of flares agrees with the refreshed shock limit. Only one flare in our sample may be related to on-axis density fluctuations while more flares are on the borderline that limits off-axis density fluctuations. This possibility cannot be ruled out and indeed a large amount of flares would originate from off-axis density fluctuations. These results are in agreement with what has been discussed previously in Paper I and they reveal that we cannot distinguish sharply among the sources of variability. However, a sizable fraction of the flares cannot be related to external shocks.

This is confirmed by the comparison of the present distribution of the ratio  $w/t_{pk}$  with the results found by Lazzati & Perna (2007) with the sample analysed in Paper I. In fact, the shortest timescale expected for the interaction with the circumburst medium is for adiabatic expansion in a wind environment: also in this case, however, assuming a spectral index  $\beta \simeq 1$  (see Sec. 4.2.3), the median value is  $w/t_{pk} \sim 0.83$ , well above the median value we found in our sample.

The indications we have seem to point toward a prolonged activity of the central engine, similar to the one producing the prompt emission. As discussed in the literature (Proga & Begelman 2003; King et al. 2005; Perna et al. 2006; Proga & Zhang 2006; Kumar et al. 2008; Lopez-Camara et al. 2009), there are several mechanisms that could keep the central engine active for a long time or reactivate it in a pseudo-random way. After the formation of

a black hole and accretion disk, accretion of the progenitor material left over by the collapse or disk instabilities could generate the activity we observe (in some cases the instability can be strong enough to generate gravitationally bound clumps within the disk and determine disk fragmentation, see Lodato 2007). Since the accretion rate during flares is much lower than during the GRB, the neutrino mechanism is not viable for powering the flares and MHD driving is favored (Barkov & Komissarov 2008).

One remarkable result we found in the present X-ray flares sample is that they have a ratio  $w/t_{pk}$  approximately constant with time (see Fig. 3). This is not expected for the internal shock model since the arrival time is not related to the conditions of the collision (see e.g. Kobayashi et al. 1997; Ramirez-Ruiz & Fenimore 2000) and in fact this is not found in BATSE prompt emission pulses, where the width remains constant throughout the GRB time history (Norris et al. 1996; Ramirez-Ruiz & Fenimore 2000). The only way to avoid this discrepancy is that it reflects a different behaviour of the progenitor generating the pulses. A positive correlation between duration and timescale in flares (see Fig. 2), as well as an anticorrelation between duration and peak luminosity (see Fig. 7, lower panel), is expected in case of gravitational instabilities leading to fragmentation of the outer disk (Perna et al. 2006). A complete explanation for the tight coupling of the evolution of the rise and decay times is, however, still missing. The analysis of the late flares sample will put more stringent constraints on this trend.

Under the assumption that the burst is produced via synchrotron emission, the internal shock model requires that the shock occurs at a distance from the center of explosion that is of the order of  $10^{17}$  cm for several bursts with inferred source Lorentz factor larger than  $\sim 1000$ . For the deceleration radius to be larger than the internal shock radius, the circumburst medium density must be extremely low. Fast variability can be reconciled with large emitting distance if the emitting material (fundamental emitters) moves relativistically within the jet (Lyutikov & Blandford 2003; Lyutikov 2006; Lazar et al. 2009; Kumar & Narayan 2009). The fundamental emitters model needs however further development. First, it is not clear how such macroscopic relativistic motions can be generated and sustained. Then, if the emitters are radiating long before their velocity points toward the observer and they continue to emit long after they move away, there is no reason for a difference the rising and decaying phase of the pulses that we found in the present sample. Furthermore, this model predicts symmetric pulses.

The asymmetry of the prompt pulses is one of the few recurrent patterns that can be distinguished among the vast range of complex GRB light-curves and the variety of GRB pulses (see e.g. Norris et al. 1996; Kocevski et al. 2003; Norris et al. 2005, and references therein). Studies on bright BATSE light curves revealed the so called GRB pulse paradigm, according to which narrower pulses tend to be more symmetric and have harder spectra (Norris et al. 1996). This paradigm has not been confirmed in the case of wide pulses (Norris et al. 2005) or single pulses (Kocevski et al. 2003): no evidence for correlation between width and asymmetry has been found for simple FRED pulses. The finding that X-ray flares which happen hundreds of seconds after the prompt emission show asymmetry values very similar to the prompt broad pulses while being charac-

terized by a larger width, carries important information on the GRB physical mechanism: it strongly indicates that the rise and the decay times of the pulses do not evolve independently from one another; instead, their evolution is tightly coupled. In the simplest shell collision scenario, the pulse rise phase is due to the shell energization while the decay phase is produced by the cooling of the energized particles and the curvature of the shell. The similarity between the asymmetry values of the prompt and flare emission would point to a similar underlying physical mechanism: in this case, our results imply that the observed rate at which the shell becomes active to produce the flare emission is dependent on the decay timescale and hence the curvature of the shell. This would produce flares with a temporal profile similar to the prompt emission but stretched in time, as the time proceeds, as observed.

Flares are not necessarily the result of late central engine activity, but may be produced in the decelerating phase of the flow. High  $\sigma_0$  flows can be prone to MHD instabilities during their interactions with the circumburst medium. The instabilities can result in energy release in localized regions through magnetic reconnection. In this picture, the presence of multiple flares, often observed in GRBs, simply corresponds to multiple reconnection regions and indeed it may be possible that dissipation in one region triggers instabilities and magnetic dissipations in nearby regions (Giannios 2006). The analysis by Giannios (2006) shows that the isotropic equivalent energy emitted in a single flare  $E_{\text{flare}}$  and produced by a single reconnection event is limited and related to the ratio  $w/t_{pk}$  by the relation:

$$E_{\text{flare}} \leq 5\epsilon \left( \frac{w}{t_{pk}} \right)^3 \frac{E_{FS}}{\alpha^2}, \quad (8)$$

where  $E_{FS}$  is the isotropic energy of the forward shock,  $\epsilon \sim 0.1$  the fraction of the Alfvén speed of the magnetic reconnection in a strongly magnetized plasma,  $\alpha$  a parameter with typical values 4 in a constant density medium and 2 in the presence of stellar wind. The flare energy is therefore a rather strong function of the ratio  $w/t_{pk}$  observed. For the XRT flares we derived  $w/t_{pk} \sim 0.23$  with a standard deviation 0.14 that would call for flares having a small fraction of the energy in the forward shock (which can be some 10 times the observed energy in the prompt emission). The flares we observe are not in contradiction within the errors with this relation. The dimensions of the reconnection region implies that fast evolving flares are less energetic than the smoother ones. In the present sample we do not have a large enough flare range of the ratio  $w/t_{pk}$  to test this effect and we find that within errors we have the same average energy. This effect will be better tested in the work in progress on late flares. It remains to be seen whether this model can quantitatively reproduce the observed decrease of the energy of the flares as function of time after the burst.

The BATSE sample reveals two types of prompt emission: prompt emission showing many overlapping short pulses (as for instance GRB991216) and prompt emission presenting a few rather wide pulses easily distinguishable and showing spectral lags. In agreement with the frequency distribution derived by Quilligan et al. (2002) the number of long lag pulses increases for GRBs detected toward the sensitivity of the BATSE threshold while bright GRBs are characterized by many short overlapping spikes (we use the

words spikes and pulses as synonymous). This also implies that the distribution function of GRBs, similarly to the one of many classes of objects, increases toward the faint end and that the number of bright GRBs is very rare. The present analysis of the X-ray flares sample possibly indicates that X-ray flares belong to the class of GRBs that dominate the tail of the distribution function.

Any model put forward to explain the GRB phenomena has to account for a some kind of memory of the central engine testified by Fig. 12: this is able to produce distinct episodes of emission -flares- where each flare determines a relative hardening with respect to the previous emission, but with an average energy which becomes softer as the burst progresses.

## 6 SUMMARY AND CONCLUSION

The main result of this work is that each flare seems to retain a memory of the previous events, so that, as time progresses, each flare is weaker and softer than the preceding one. In particular with this new sample of flares we confirmed all the findings of Paper I. Furthermore, thanks to the analysis in 4 XRT bands and to the increased number of GRBs with redshift, we were able to show the following:

- the width of flares decreases with energy:  $w \propto E^{-0.5}$ , with a power-law index that is comparable to what has been determined for the prompt emission spikes;
- flares are asymmetric, with a rise to decay ratio  $t_{\text{rise}}/t_{\text{decay}} = 0.49$  similar to prompt emission spikes. No flare is found with  $t_{\text{rise}}/t_{\text{decay}} > 1$  ;
- both the rise time and the decay time of each flare linearly evolve with time. Their evolution is such that the rise-to-decay ratio is constant with time, implying that both time scales are stretched of the same factor;
- the width linearly evolves with time:  $w \sim 0.2 t_{pk}$ . This, together with the previous point is one of the key feature that strongly distinguishes the flare emission with respect to the prompt phase;
- the flare peak intensity decreases with time: on average, late time flares have lower peak intensities. However, we caution that the relation is highly dispersed;
- the mean isotropic flare energy of the sample is about  $10^{51}$  erg and the flare mean SED is a power-law with spectral index  $\sim 1.1$ . As expected, the flares are much softer than the prompt emission;
- the last key point is the presence of global softening: in multiple-flare GRBs, the flares follow a softening trend which causes later time flares to be softer and softer.

The conclusion is that while we are making significant progress in our characterization of the properties of flares and their relation to the prompt emission spikes and prompt emission energy, at the moment there is no satisfactory model explaining their origin, evolution and energetics.

## ACKNOWLEDGMENTS

The anonymous referee is acknowledged for constructive criticism. This work is supported by ASI grant SWIFT I/011/07/0, by the Ministry of University and Research of

Italy (PRIN MIUR 2007TNYZXL), by MAE and by the University of Milano Bicocca (Italy).

## REFERENCES

- Band D. L., 1997, *ApJ*, 486, 928  
 Barkov M. V., Komissarov S. S., 2008, *MNRAS*, 385, L28  
 Barthelmy S. D., Barbier L. M., Cummings J. R., et al., 2005a, *Space Science Reviews*, 120, 143  
 Barthelmy S. D., Chincarini G., Burrows D. N., et al., 2005b, *Nat*, 438, 994  
 Borgonovo L., Frontera F., Guidorzi C., Montanari E., Vettere L., Soffitta P., 2007, *A&A*, 465, 765  
 Briggs M. S., Paciesas W. S., Pendleton G. N., et al., 1996, *ApJ*, 459, 40  
 Burrows D. N., Hill J. E., Nousek J. A., et al., 2005a, *Space Science Reviews*, 120, 165  
 Burrows D. N., Romano P., Falcone A., et al., 2005b, *Science*, 309, 1833  
 Butler N., Ricker G., Atteia J., et al., 2005, GRB Coordinates Network, 3570, 1  
 Cavallo G., Rees M. J., 1978, *MNRAS*, 183, 359  
 Chincarini G., Moretti A., Romano P., et al., 2005, ArXiv Astrophysics e-prints  
 Chincarini G., Moretti A., Romano P., et al., 2007, *ApJ*, 671, 1903  
 Costa E., Feroci M., Frontera F., et al., 1997, *IAU Circ.*, 6572, 1  
 D'Agostini G., 2005, ArXiv Physics e-prints  
 Daigne F., Mochkovitch R., 1998, *MNRAS*, 296, 275  
 Dezalay J., Barat C., Talon R., Syunyaev R., Terekhov O., Kuznetsov A., 1992, in American Institute of Physics Conference Series, edited by W. S. Paciesas & G. J. Fishman, vol. 265 of American Institute of Physics Conference Series, 304–309  
 Djorgovski S. G., Frail D. A., Kulkarni S. R., Bloom J. S., Odewahn S. C., Diercks A., 2001, *ApJ*, 562, 654  
 Drenkhahn G., Spruit H. C., 2002, *A&A*, 391, 1141  
 Evans P. A., Beardmore A. P., Page K. L., et al., 2009, *MNRAS*, 397, 1177  
 Falcone A. D., Burrows D. N., Lazzati D., et al., 2006, *ApJ*, 641, 1010  
 Falcone A. D., Morris D., Racusin J., et al., 2007, *ApJ*, 671, 1921  
 Fenimore E. E., in 't Zand J. J. M., Norris J. P., Bonnell J. T., Nemiroff R. J., 1995, *ApJ*, 448, L101+  
 Fishman G. J., Meegan C. A., Wilson R. B., et al., 1994, *ApJS*, 92, 229  
 Ford L. A., Band D. L., Matteson J. L., et al., 1995, *ApJ*, 439, 307  
 Gehrels N., Chincarini G., Giommi P., et al., 2004, *ApJ*, 611, 1005  
 Gehrels N., Sarazin C. L., O'Brien P. T., et al., 2005, *Nat*, 437, 851  
 Giannios D., 2006, *A&A*, 455, L5  
 Giannios D., Mimica P., Aloy M. A., 2008, *A&A*, 478, 747  
 Gomboc A., Kobayashi S., Guidorzi C., et al., 2008, *ApJ*, 687, 443  
 Greiner J., Krühler T., McBreen S., et al., 2009, *ApJ*, 693, 1912  
 Groot P. J., Galama T. J., van Paradijs J., et al., 1997, *IAU Circ.*, 6584, 1  
 Hill J. E., Burrows D. N., Nousek J. A., et al., 2004, in Society of Photo-Optical Instrumentation Engineers (SPIE) Conference Series, edited by K. A. Flanagan & O. H. W. Siegmund, vol. 5165 of Presented at the Society of Photo-Optical Instrumentation Engineers (SPIE) Conference, 217–231  
 Hurley K., 1989, in Cosmic Gamma Rays and Cosmic Neutrinos, 337–379  
 Hurley K., Sari R., Djorgovski S. G., 2002, ArXiv Astrophysics e-prints  
 Ioka K., Kobayashi S., Zhang B., 2005, *ApJ*, 631, 429  
 King A., O'Brien P. T., Goad M. R., Osborne J., Olsson E., Page K., 2005, *ApJ*, 630, L113  
 Klebesadel R. W., Strong I. B., Olson R. A., 1973, *ApJ*, 182, L85+  
 Kobayashi S., Piran T., Sari R., 1997, *ApJ*, 490, 92  
 Kocevski D., Ryde F., Liang E., 2003, *ApJ*, 596, 389  
 Kouveliotou C., Meegan C. A., Fishman G. J., et al., 1993, *ApJ*, 413, L101  
 Krühler T., Greiner J., McBreen S., et al., 2009, *ApJ*, 697, 758  
 Kumar P., McMahon E., Panaitescu A., et al., 2007, *MNRAS*, 376, L57  
 Kumar P., Narayan R., 2009, *MNRAS*, 395, 472  
 Kumar P., Narayan R., Johnson J. L., 2008, *MNRAS*, 388, 1729  
 Lazar A., Nakar E., Piran T., 2009, *ApJ*, 695, L10  
 Lazzati D., Perna R., 2007, *MNRAS*, 375, L46  
 Lazzati D., Perna R., Begelman M. C., 2008, *MNRAS*, 388, L15  
 Lodato G., 2007, *Nuovo Cimento Rivista Serie*, 30, 293  
 Lopez-Camara D., Lee W. H., Ramirez-Ruiz E., 2009, ArXiv e-prints  
 Lyutikov M., 2006, *MNRAS*, 369, L5  
 Lyutikov M., 2009, ArXiv e-prints  
 Lyutikov M., Blandford R., 2003, ArXiv Astrophysics e-prints  
 Margutti R., Sakamoto T., Chincarini G., et al., 2009, *MNRAS*, 400, L1  
 Mazets E. P., Golenetskii S. V., Ilyinskii V. N., et al., 1981, *A&AS*, 80, 119  
 Meegan C. A., Fishman G. J., Wilson R. B., et al., 1992, *Nat*, 355, 143  
 Meszaros P., Rees M. J., 1993, *ApJ*, 418, L59+  
 Mimica P., Giannios D., Aloy M. A., 2009, *A&A*, 494, 879  
 Moretti A., Campana S., Mineo T., et al., 2005, in Society of Photo-Optical Instrumentation Engineers (SPIE) Conference Series, edited by O. H. W. Siegmund, vol. 5898 of Presented at the Society of Photo-Optical Instrumentation Engineers (SPIE) Conference, 360–368  
 Norris J. P., Bonnell J. T., Kazanas D., Scargle J. D., Hakkila J., Giblin T. W., 2005, *ApJ*, 627, 324  
 Norris J. P., Cline T. L., Desai U. D., Teegarden B. J., 1984, *Nat*, 308, 434  
 Norris J. P., Nemiroff R. J., Bonnell J. T., et al., 1996, *ApJ*, 459, 393  
 Norris J. P., Share G. H., Messina D. C., et al., 1986, *Advances in Space Research*, 6, 19  
 Nousek J. A., Kouveliotou C., Grupe D., et al., 2006, *ApJ*, 642, 389

- Oates S. R., Page M. J., Schady P., et al., 2009, MNRAS, 395, 490
- O'Brien P. T., Willingale R., Osborne J., et al., 2006, ApJ, 647, 1213
- Paciesas W. S., Meegan C. A., Pendleton G. N., et al., 1999, ApJS, 122, 465
- Perna R., Armitage P. J., Zhang B., 2006, ApJ, 636, L29
- Piran T., 1999, Phys.Rep., 314, 575
- Piran T., 2004, Reviews of Modern Physics, 76, 1143
- Proga D., Begelman M. C., 2003, ApJ, 592, 767
- Proga D., Zhang B., 2006, MNRAS, 370, L61
- Quilligan F., McBreen B., Hanlon L., McBreen S., Hurley K. J., Watson D., 2002, A&A, 385, 377
- Ramirez-Ruiz E., Fenimore E. E., 2000, ApJ, 539, 712
- Rees M. J., Meszaros P., 1992, MNRAS, 258, 41P
- Rees M. J., Meszaros P., 1994, ApJ, 430, L93
- Romano P., Campana S., Chincarini G., et al., 2006a, A&A, 456, 917
- Romano P., Moretti A., Banat P. L., et al., 2006b, A&A, 450, 59
- Sakamoto T., Barthelmy S. D., Barbier L., et al., 2008, ApJS, 175, 179
- Spruit H. C., Daigne F., Drenkhahn G., 2001, A&A, 369, 694
- Steele I. A., Mundell C. G., Smith R. J., Kobayashi S., Guidorzi C., 2009, Nat, 462, 767
- Tchekhovskoy A., McKinney J. C., Narayan R., 2008, MNRAS, 388, 551
- Thompson C., 1994, MNRAS, 270, 480
- van Paradijs J., Groot P. J., Galama T., et al., 1997, Nat, 386, 686
- Vaughan S., Goad M. R., Beardmore A. P., et al., 2006, ApJ, 638, 920
- Vedrenne G., 1981, Royal Society of London Philosophical Transactions Series A, 301, 645
- Villasenor J. S., Lamb D. Q., Ricker G. R., et al., 2005, Nat, 437, 855
- Zhang B., Fan Y. Z., Dyks J., et al., 2006, ApJ, 642, 354